PROGNOSTICS HEALTH MANAGEMENT AND DAMAGE RELATIONSHIPS OF LEAD-FREE COMPONENTS IN THERMAL CYCLING HARSH ENVIRONMENTS

Except where reference is made to the work of others, the work described in this thesis is my own or was done in collaboration with my advisory committee. This thesis does not include proprietary or classified information.

Handattu Madhura Hande

Certificate of Approval:

Jeffrey C. Suhling Quina Distinguished Professor Mechanical Engineering	Pradeep Lall, Chair Thomas Walter Professor Mechanical Engineering
Roy W. Knight Assistant Professor Mechanical Engineering	Joe F. Pittman Interim Dean Graduate School

PROGNOSTICS HEALTH MANAGEMENT AND DAMAGE RELATIONSHIPS OF LEAD-FREE COMPONENTS IN THERMAL CYCLING HARSH ENVIRONMENTS

Handattu Madhura Hande

A Thesis

Submitted to

the Graduate Faculty of

Auburn University

in Partial Fulfillment of the

Requirement for the

Degree of

Master of Science

Auburn, Alabama
May 10, 2008

PROGNOSTICS HEALTH MANAGEMENT AND DAMAGE RELATIONSHIPS OF LEAD-FREE COMPONENTS IN THERMAL CYCLING HARSH ENVIRONMENTS

Handattu Madhura Hande

Signature of Author

Date of Graduation

VITA

Handattu Madhura Hande, daughter of Mr. H. Ramadeva Hande and Ms. H Sharadha Hande, was born on November 22, 1978, in Karnataka, India. She has graduated in 2000 with a Bachelor of Engineering degree in Mechanical Engineering from Manipal Institute of Technology, Mangalore University, Karnataka, India. She has worked for General Electric-India Technology Centre for 4 years starting from March 2001 to August 2005 as a Research Engineer. In the pursuit of enhancing her academic qualifications, she joined the M.S. Program at Auburn University in the Department of Mechanical Engineering in Fall 2005. Ever since she enrolled for the M.S. program at Auburn University, she has worked for Center for Advanced Vehicle Electronics (CAVE) as a Graduate Research Assistant in the area of harsh environment electronic packaging reliability.

PROGNOSTICS HEALTH MANAGEMENT AND DAMAGE RELATIONSHIPS OF LEAD-FREE COMPONENTS IN THERMAL CYCLING HARSH ENVIRONMENTS

Handattu Madhura Hande

Master of Science, May 10, 2008
(B.E., Manipal Institute of Technology, 2000)

193 typed pages

Directed by Pradeep Lall

There has been a growing interest in the area of health monitoring of electronics in order to predict the failure and provide warnings. Existing Prognostics Health Management methodologies are very reactive in nature and unable to estimate the residual life. The presented methodology helps in evaluating the reliability of the component in its actual life cycle environment. Also, the developed techniques are applied to the pre-failure space of the electronics system, in which no macro-indicator of failure such as crack or delamination exists.

In this thesis, the prognostics health management and damage relationships for lead-free devices under thermal cycling harsh environments have been studied. The presented methodology eliminates the need for estimation of prior-damage. The procedures have been developed using leading indicators of failure like solder microstructural coarsening. Failure data has been collected for 95.5Sn4.0Ag0.5Cu lead-free solder alloy joints in area array components mounted on FR-4 printed circuit boards. A technique for the determination of prior damage history has been presented using non-linear least squares based interrogation techniques. The presented method uses the Levenberg-Marquardt Algorithm. The utilized test vehicles include various area-array packaging architectures which are subjected to cyclic thermo-mechanical stresses over the range of -40º C to 125 º C.

In addition, the developed procedure has been further extended to various kinds of lead-free alloys like SAC105, SAC305 and SAC307 which are subjected to thermal cyclic load from -55ºC to 125ºC. Damage proxies have been investigated and correlated to solder-interconnect damage. A mathematical relationship has been developed to compute the residual life.

ACKNOWLEDGEMENTS

The author would like to thank her advisor Dr. Pradeep Lall, and other committee members for their invaluable guidance and help provided during the course of this study. The author acknowledges and extends gratitude for financial support received from the National Science Foundation, and the NSF Center for Advanced Vehicle Electronics (CAVE).

Author would like to express her deep gratitude and gratefulness to her parents H. Ramadeva Hande and H. Sharadha Hande for their enduring love and immense moral support. Author would like to thank her husband Chandrakant Naik Tari for being a constant source of inspiration and motivation and also for family members Mamatha and Manoj. The author wishes to acknowledge her colleagues for their friendship, help and all the stimulating discussions.

Style manual or journal used: Guide to Preparation and Submission of Theses and Dissertations

Computer software used: Microsoft Office 2003, Minitab 13.1, Ansys 10.0, Matlab 7.0.1, Microsoft Visual Studio 2005, National Instrument Image Analysis Software

TABLE OF CONTENTS

LIST OF FIGURES

LIST OF TABLES

CHAPTER 1

INTRODUCTION

1.1 Electronic Packaging

In today's world electronics components are available everywhere. Ever-increasing customer demand for comfort, safety, economy, and functionality makes the electronics industry one of the most fascinating and dynamic industries in the world. This industry has many technology areas; one of which is Electronic Packaging. Electronic Packaging means embodiment of electronic devices and establishment of electrical interconnection among the devices for some useful application. Various electronic devices used in any electrical circuit include integrated circuit (IC) chips, resistors, diodes, capacitors, transistors, transformers etc. Electronic Packaging provides environmental protection, mechanical support, and electrical connection for the proper and efficient functioning of these devices.

Electronic packaging has various levels of hierarchy in their connection as shown in the Figure 1.1. The bare chip fabricated from the silicon wafer is referred as the zeroth level of electronic packaging. The first level is packaging of the bare chip or the silicon die. This involves the encapsulation and interconnection at the chip level. Usually ceramic and plastic (epoxy) mold is used for encapsulation of the chip. The technologies used for the interconnection at this level include wire bonding, tape automated bonding and flip-chip solder bumps. The second level of packaging comprises assembly of the first level packaged components on the printed circuit board (PCB).

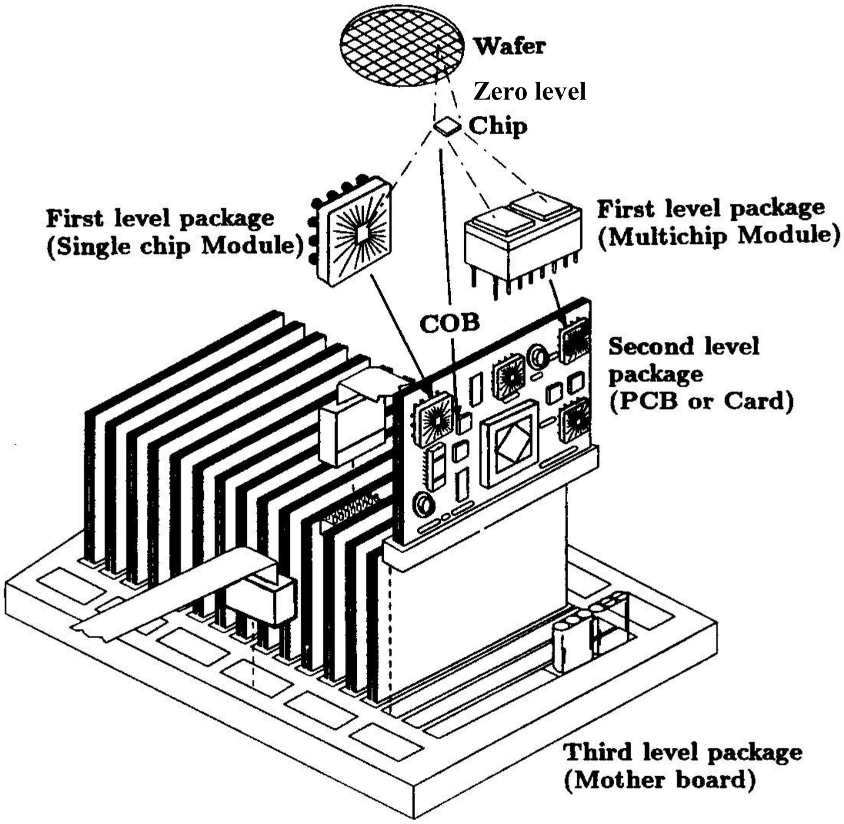

Figure 1.1- Various levels in electronic packaging [ME6310 Course Notes]

The technologies used for this purpose are plated through hole (PTH) and surface mount technology (SMT). The third level of packaging consists of mounting and connecting of the various PCBs as in case of a mother board assembly. Finally, the fourth level of packaging consists of the system level packaging and shielding of the whole system with an appropriate form of an outer shell. Once all the components are appropriately packaged in form of an electronic product, then it is ready to use. In the current work, an effort is being made to estimate the reliability of these packages in its actual life cycle environment

1.2 Reliability of second level interconnection

Reliability of second level interconnection in electronic packaging is a major concern in the electronic industry. These interconnections are made up of either solder joints or solder leads. Failure of this interconnection happens either due to wear-out or overstress. The prediction of reliability requires the understanding of the actual failure mechanism, the interaction of the stresses due to the loading and the strength of the entire assembly bonded by dissimilar materials.

The primary failure mechanism of solder joints is ductile fatigue fracture, which is caused by the generation of strains in the solder joints due to temperature changes in shipping, storage or operation. This causes the materials to expand and contract at different rates depending on their coefficient of thermal expansion. This temperature cycling results in internal stresses, which in turn causes the solder to creep. Creep is a time-dependent plasticity, which occurs in metals when they are subjected to temperature above half of its melting temperature or commonly known as homologous temperature.

Over many cycles, the creep leads to ductile fatigue damage, manifesting itself as microvoids in the solder, which grow and coalesce into macro-cracks that slowly propagate through the joint over the course of its lifetime, ultimately resulting in failure of joints. Other failure mechanisms are possible depending on the applied external conditions. For instance, if the device was subjected to vibration or dropped on to the floor, then the sudden acceleration may cause a brittle failure. In this thesis, ductile fatigue failure of solder joints is considered in order to develop the damage prediction model.

In order to have better reliability of solder joints, it is very important to select the right material for the joints. Traditionally, eutectic tin-lead (63Sn37Pb) has been widely used as one of the materials in electronic packaging due to its low melting temperature and good wetting behavior on other substrates. But the restriction of the use of hazardous substances in electrical and electronic equipment has been implemented since July 1st 2006 by European Union. This legislation mandates the electronic industry to introduce the lead-free solder alloys replacing the traditional tin-lead solder. There are various types of lead-free alloys present in the market. Sn-Ag-Cu is the leading candidate amongst them as of today. In this thesis, the thermo-mechanical reliability of 95.5Sn4.0Ag0.5Cu has been studied and an attempt has been made to study the microstructure variations in various lead-free alloys like Sn1.0Ag0.5Cu, Sn3.0Ag0.5Cu, Sn4.0Ag0.5Cu and Sn0.3Ag0.7Cu, when it has been subjected to thermal cycling loads.

Most electronic devices are expected to last for many years of use. It is unfeasible for companies to perform field tests due to the time and cost involved. Instead, accelerated tests are used which impose much harsher conditions on the joints, causing it to fail in a shorter time period and allowing a judgment to be made on the products reliability. The most popular accelerated test is thermal cycling test. Modeling is also a useful tool and has been used to supplement or replace accelerated tests, particularly in the early design stages. There are many methods including the analytical method, the finite element method and a damage mechanics based method, however, there is no clear-cut answer to judge which is the best method. The analytical method is very simple to implement but not able to capture the complete physics. The damage mechanics based methods require considerably more effort both in implementation and computational cost as well as their predictive capabilities are unproven, however, they promise to provide the most accurate predictions in future. The constitutive law and fatigue law class of methods (encompassing FEA) are very popular, providing more accurate predictions with fewer restrictions than other methods. In this thesis, constitutive law and fatigue law based methods, which use Finite Element Analysis to predict the component life have been used for reliability analysis.

There are various new kinds of interconnections exist in the market e.g. Polymer core solder ball, Copper reinforced columns etc. These interconnections outperform the conventional solder balls by 2 to 3 times in terms of thermal fatigue life. The polymer core interconnection is more reliable than the normal solder ball because the elastic modulus of this solder ball is much lower than normal solder ball that makes it to withstand more stress during thermal cycling. The copper reinforced solder column interconnections adds redundancy without significant increase in stiffness and also the failure mechanism near taper of the eutectic filet is abated by the copper reinforcement allowing the component to continue functioning long past when the high-lead core has cracked. In this thesis, the thermo-mechanical reliability of polymer core solder ball and the copper reinforced columns using finite element approach has been investigated.

1.3 Prognostics Health Management of electronics

There has been a growing interest in monitoring the ongoing health of electronic products and systems in order to predict failures and provide warning to avoid catastrophic failure. Electronic health is the extent of degradation or deviation from its expected normal condition. Prognosis is a process or method which will allow interrogation of the material state in complex systems and subsystems to determine the remaining useful life prior to repair or replacement. Presented Prognostics Health Management (PHM) methodology helps to predict the reliability of electronic components in its actual life cycle condition.

Prognostics Health Management methodology concepts exist for mechanical systems for in-situ assessment of the system state and is well established. Health Management application areas include fatigue crack damage in mechanical structure such as those in aircraft, surface ships, civil infrastructure, railway structures and power plants. But it is very difficult to detect and inspect the wear and degradation in electronic systems when compared to mechanical systems due to complex and tiny size of the structures. However electronic systems are integral to the functionality of most systems today, and their reliability is often critical for overall system reliability.

Some of the current existing PHM methodologies for electronic systems are Built-In-Self-Test (BIST), Fuses and Canaries. BIST circuits, which include onboard hardware and software diagnostic, have been used for error detection and fault location. Fuses have been used to provide advance warning of failure in electronics due to specific wear out failure mechanism as well as it is used to sense the abnormal conditions like voltage transient, critical temperature limit and to make adjustments to restore normal condition. Canaries are pre-calibrated cells which are located with the actual circuitry on the same chip experience similar stresses as the actual components. This leads to same damage mechanisms and is designed to fail faster by scaling the stress to avoid the catastrophic failure of actual components. But all these methodologies are very reactive in nature and provide very limited insight into the remaining useful life of the electronic components. PHM methodology presented in this thesis differs from the state-of-art diagnostics and resides in the pre-failure-space of the electronic system; in which no macro-indicator of failure such as cracks or delamination exists.

The existing methodology allows the prediction of time-to-failure for a pristine material under known loading conditions based on relationships such as the Paris' power law, the Coffin-Manson relationship and S-N diagram. But in reality, these components experience drastic changes in the ambient conditions. Therefore, a time-temperature history of the electronic system ambient would be extremely helpful in using life prediction models and computing life. Continuous capture of time-temperature history would put immense demands on existing system function. In this thesis, a mathematical approach has been presented to calculate the prior damage in electronics subjected to cyclic thermo-mechanical loads. This methodology obviates the need for quantification of prior stress history and helps in accurate prediction of remaining useful life. Methodologies using leading indicators of failure like solder micro structural coarsening to compute the residual life has been presented. Prior damage history has also been determined using non-linear least square method based interrogation techniques. This prognostication methodology was first developed for leaded solder alloy components. In this thesis it has been extended to various lead-free solder alloy components. Numerical methods are also developed to investigate the prior stress history for future usage.

1.4 Thesis Layout

In this thesis, Chapter 2, which is the literature survey, discusses the evolution of electronic packaging technology, issues and technical challenges faced by electronic industry today. Reliability analysis and various methods used to analyze the reliability of electronic package have been discussed. Evolution of lead-free solder alloy for second level interconnection and various combinations of lead-free alloys exists today and their reliability has been discussed. New ways of forming the second level interconnections and their impact on reliability compared to existing second level interconnections have been researched. Different prognostics health management techniques are being used in the electronic industry and pros and cons of these techniques have been reviewed.

Chapter 3 is based on the thermo-mechanical reliability of various ball grid array packages like plastic-BGA (Ball Grid Array), flex-BGA, tape-array BGA and chip-array BGA. Also the material models and method to estimate the material parameter for Anand's Viscoplastic model to represent solder creep behavior in ANSYS has been discussed. The results obtained from finite element simulation are correlated to the experimental results. Finally, the method of creating a finite element model for a new type of interconnect like polymer core solder ball and copper reinforced column grid array to investigate the reliability in their early design stage has been discussed.

Leading indicators of failure for lead-free solder alloys have been discussed in Chapter 4. This chapter also includes details of the test vehicle used for this study and methodology used to investigate the prior damage history using leading indicators of failure. Solder micro-structural coarsening effect on solder interconnect damage and also methodology to quantify the coarsening effect when it has been subjected thermal cycling has been discussed. The damage proxies have also been correlated to the solder interconnects damage using inelastic strain energy density from finite element models.

Chapter 5 and 6 discuss the interrogation of system state to investigate the prior damage using Levenberg Marquardt's Algorithm. Chapter 5 outlines the detailed methodology to estimate the prior damage using solder micro-structural coarsening data. This coarsening data obtained in the neighborhood of prognostication time is used to fit the equation using non-linear least square method in order to investigate the prior damage and subsequently find out the residual life left for future usage. The result obtained using this algorithm has been correlated to experimental data to validate the methodology for 95.5Sn4.0Ag0.5Cu alloy components. Chapter 6 covers the application of developed methodology for various lead-free alloy components. Finally, Chapter 7 includes the conclusion of the presented methodologies and discusses the scope for future work.

CHAPTER 2

LITERATURE REVIEW

2.1 Evolution of electronic package

The present method of manufacturing conventional electronic assemblies has essentially reached its limit as far as cost, weight, volume and reliability is concerned. Surface mount technology (SMT) makes it possible to produce more reliable assemblies at reduced weight, volume and cost. The surface mount concept is not new but it has its roots in relatively old technologies such as flat packs and hybrids. Electronic assembly originally used point-to-point wiring and no substrate at all. In the 1950's, surface mount devices called flat packs were used for high reliability military applications. They can be considered the first surface mount packages to be mounted on printed circuit boards. However the flat-pack devices had to be mounted too close to the board surface, requiring gold plated leads, which were very costly and that needed discrete soldering. In 1960's, flat packs were replaced with Dual Inline Packages (DIP), which were easier to insert and could be wave soldered in mass. Another significant contribution to today's SMT lies in the hybrid technology which became popular in the 1960's. They feature surface mount devices soldered inside a through-hole or surface mount ceramic package body. Today's SMT also has its roots in extensive development work done in the United States for military applications. For example, to shrink package size for larger pin counts, the military needed hermetically sealed devices with leads on all four sides. This led to the development of leadless ceramic chip carriers (LCCCs) in the late 1960's. But these packages required a very expensive substrates with matching coefficient of thermal expansion to prevent solder cracking. While the electronic industries in the United States were preoccupied with developing substrates for LCCCs for a very limited market, the Japanese and Europeans were responding to a much wider consumer market and they invented Small Outline Integrated Circuits (SOIC). Also in early 1970's, the Japanese started building calculators using plastic quad packs, which are similar to flat packs but had surface mountable leads on all four sides and bent down like gull wing or J leads. These leads are susceptible to bending and damage during handling and shipping. Even though the quad packs provide space savings because of their smaller size compared with their through-hole counter parts, the fragile gull wing leads require special handling to prevent lead bending. With this continued emphasis on faster, smaller and lighter electronic systems and also rapid increase in the number of transistors according to the Moore's Law, fine pitch packages came in to existence. The decrease in the package pitch and increase in the lead count causes complex board assembly processes, shipping and handling problems and lead coplanarity. Ball Grid Array (BGA) technology has evolved to overcome the above problems in packaging technology. It provides much better manufacturing yield and also it is much easier to place, print and solder a 1.5 mm pitch BGA package than a 0.4 mm pitch high density quad flat pack. Also, a BGA package with 1.5 mm ball pitch takes even less real estate than a 0.4 mm pitch high density quad flat pack above 300 pins and also maintains a body size of around 35mm even at 500 pins [Prasad 1997]. Figure 2.1 shows the schematic representation of

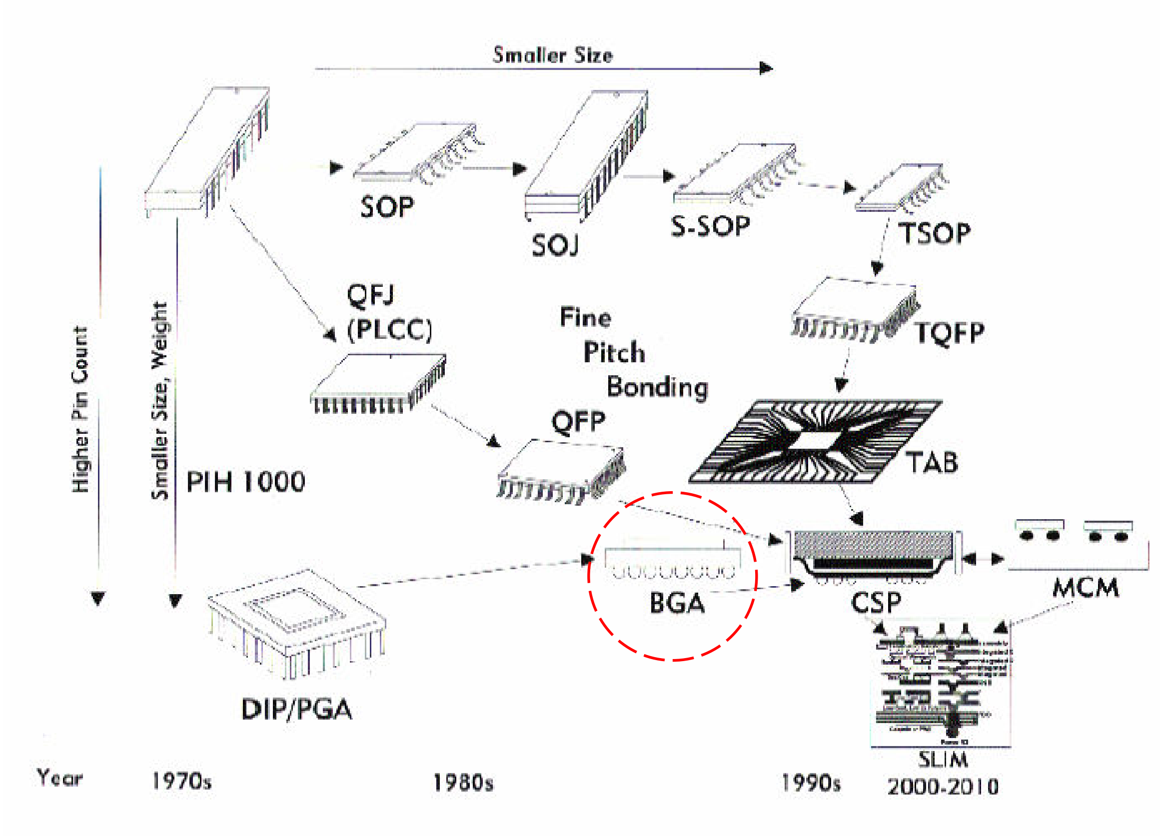

Figure 2.1 - Evolution of electronic package and size reduction and increase in pin count [ME6310 Course Notes]

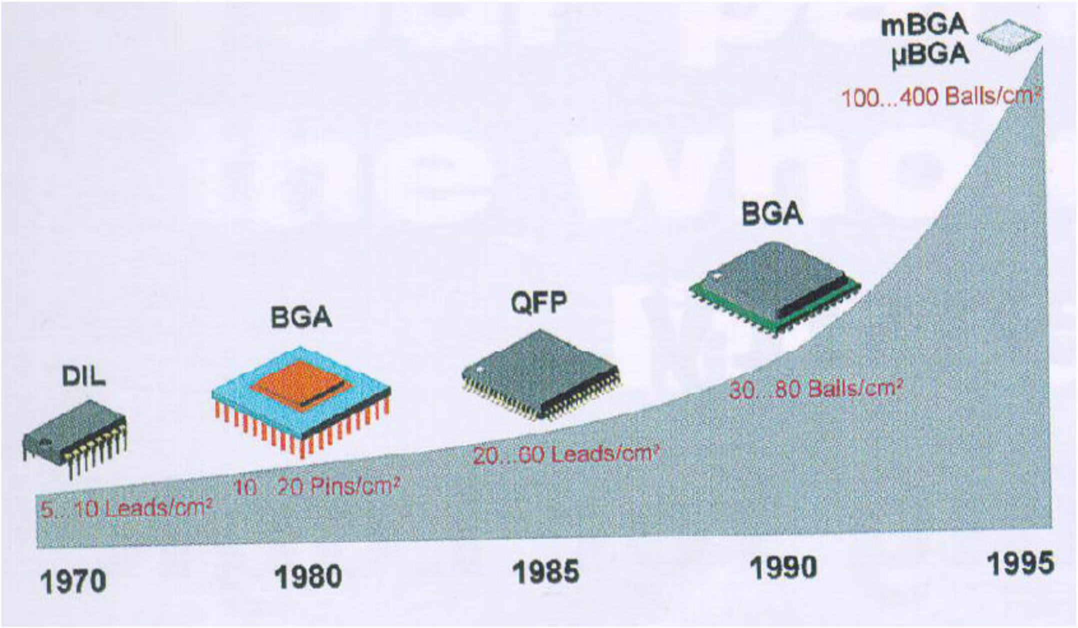

Figure 2.2 - Evolution of electronic package with year [ME6310 Course Notes]

evolution of electronic packages and also locates BGA technology amongst all packages. Figure 2.2 shows their evolution with time.

2.2 Reliability of BGA package

Reliability of BGA is a major concern in the electronic industry. In through-hole technology, the way package has been soldered to the board gives an added mechanical strength to the joints. But in SMT, surface mount lands provide both mechanical and electrical connection therefore reliability of solder joints, becomes a major concern. There are various types of BGA packages, amongst which Ceramic and Plastic BGA package are very popular. A ceramic package is less reliable compared to a plastic package because of CTE (Coefficient of Thermal Expansion) mismatch between substrate and glass epoxy board is more in ceramic package when compared to plastic package. Increase in pin count with Plastic Ball Grid Array package has made them more desirable to use in automotive applications like engine, transmission etc. These modules are exposed to under-hood environment and also typically reliability specifications include the ability to survive a certain number of thermal cycles.

Research has been done to understand the reliability of PBGA package by considering the effect of body size, die size, substrate thickness, stiffness of die adhesive, printed wiring board thickness, type of pad and type of substrate etc. In the early investigation by Lindley, et al. [1995], it was suggested that PBGA packages would fail to meet the reliability requirement for use in the automotive environment. Several investigators [Mawer 1999, Syed 1996] have demonstrated that the properly designed larger BGAs (e.g. 23, 27 9and 35 mm body size) can be robust performers and meet the solder joint reliability design requirements for under-hood controllers. Syed, et al. [1996] tested 23mm components, and examined several parameters including the BT substrate thickness, solder pad size, perimeter vs. full arrays and solder ball pitch. He has found that BGAs with perimeter arrays and thicker (0.76mm) BT substrates could comfortably satisfy automotive reliability specifications. Mawer, et al. [1999] examined several 23 and 27 mm BGA configurations, and found that they have the most satisfactory automotive reliability requirements. Most of their work focused on 27 mm BGA parts with a 0.56 mm BT substrate thickness, 1.27 mm ball pitch and Solder Mask Defined (SMD) pads. In a limited number of exploratory experiments, they demonstrated that improved reliability could be realized with Non Solder Mask Defined (NSMD) pads on the BT substrate and also concluded that a more fine pitch 17mm BGA can also meet most automotive requirements although with minimal margin. Also, some of the Motorola's solder joint fatigue data shows that smaller chip size is more reliable than larger chip size, 90Pb/10Sn is more reliable than 63Sn/37Pb solder ball, taller solder joint is more reliable than shorter ones and also high stiffness die adhesive is less reliable than low stiffness die adhesive. Thompson, et al. [1999] observed that a thin polyimide tape substrate provided better reliability than a BT substrate. Yee, et al. [1996] investigated the influence of pad geometry on BGA solder joint reliability. Larger solder pads enhance BGA life significantly due to better adhesion with the solder. Smaller body size BGAs due to their smaller ball size and pitch reduces standoff and closer proximity of the perimeter solder balls to the edge of the semiconductor die e.g. Chip-array BGAs. At last but not the least, the effect of surface finish used on copper interconnection pad, which will protect it from environment to prevent oxidation, otherwise it causes poor adhesion with solder and hence reduces the solder joint life. It has been observed by Langan, et al. [1996] that the Hot Air Solder Leveling (HASL) surface finish printed circuit board yields very good reliability. Bradley, et al. [1996] examined the solderability of Organic Protective Coatings (OPC) and various metallic plating chemistries as alternatives to traditional HASL.

Thermal fatigue life prediction of a fine pitch package is a major concern for the electronic packaging industry, which has driven research efforts to develop effective models that are capable of predicting crack initiation and propagation under thermal fatigue loads. There are various modeling methods available, for example analytical method, constitutive law and fatigue law method and damage mechanics based methods [Ridout 2006]. The analytical methods proposed by Engelmaier [1991] are simple to implement but with many caveats restricts its use in certain situations. The constitutive law and fatigue law methods are very popular, providing the accurate predictions with fewer restrictions than analytical method. The damage mechanics based methods require considerable more effort both in implementation and computational cost and their predictive capability is currently unproven [Ridout 2006].

In under-hood environments, solder joint failure occurs as crack initiations followed by crack propagation through the bulk of solder joint. Darveaux, et al. [2000] proposed a model which correlates the in-elastic strain energy density obtained from finite element simulation to the crack initiations and propagations. Crack growth measurements are conducted by slicing the fine pitch packages at some particular level of cycling for crack initiation and rate of crack propagation. Numerical solution models were created for the packages used in experimental measurements and loaded with thermal loads similar to those applied experimentally. Failure prediction model has been developed by correlating the experimental measurements with numerical simulations. The inelastic behavior of solder is captured in this method using Anand's constitutive model [Anand 1982]. Several finite element based analysis methodologies have been proposed for solder joint fatigue life by many researchers e.g. Zahn et al. [2002], Engelmaier et al [1984], Darveaux et al. [1994], Dasgupta et al. [1992], and Syed [1995]. All these models require proper representation of solder behavior. In some cases researchers used eutectic SnPb material parameter for other alloys. Some researchers have written standard procedure to estimate the material parameters for Anand's viscoplastic model in order to represent it in ANSYS from material characterization data [Pang 2000, Rodgers 2005].

2.3 Reliability of lead-free solder

As it is been discussed earlier, type of solder material used for interconnections effects the solder joint reliability. Increasing global concern about the environment is bringing the regulatory and consumer pressure on the electronics industry in Europe and Japan to reduce or completely eliminate the use of lead in products. This transition from a technology using SnPb for electronic interconnections to new lead-free technology is a challenging and demanding task for the companies. It not only has an impact on material supply, process equipment and conditions but also on reliability. Components have to withstand higher soldering temperatures typically 20-35°C higher and the solder joint should have at least the same life time.

Engelmaier [2003] already mentioned possible appearing problems with lead free solder joint reliability. Lead free solders have creep rates up to 100 times slower than the creep rates of standard SnPb solders. The implication of this is that the meaningful reliability tests cannot be accelerated too much and also that it can be used in consumer goods like cell phones but definitely not for high-reliability applications. In published literature [Bartelo 2001, Chalo 2001, Schubert 2003], the results depicts that there are no general conclusions about the trend in life time for conversion from SnPb to SnAgCu. The main conclusion is probably that trend is very dependent on the package type as well as on the applied loading conditions such as T_{min}, T_{max}, dwell and ramp-up time. Lead free solder materials are more creep resistant at high temperatures resulting in higher life time under similar stress conditions for the solder joint. However the lead free solder materials have a higher elastic modulus, which can result in much higher stress conditions for certain packages. And also few researchers have shown that the SnAgCu alloys appear to often outperform SnPb when used in leaded components and PBGA applications. However, for very stiff components with high CTE mismatch with the substrate (CBGA), the solder joint reliability is poorer.

Recently, a number of papers have been published on the constitutive equation for creep deformation for SnAgCu alloy for different compositions. Wiese, et al. [2003] studied the creep behavior of bulk, PCB sample, and Flip Chip solder joint samples of 95.5Sn4.0Ag0.5Cu solder and identified two mechanisms for steady state creep deformation for the bulk and PCB samples. They attributed these to climb controlled and combined glide behavior and represented steady state creep behavior using the double creep power law model. Zhang, et al. [2003] studied the single lap shear specimen of the

Sn3.9Ag0.5Cu solder alloy. They generated data on the test results and modeled the steady state creep behavior using hyperbolic sine function claiming power law bread-down at high value of stress. Morris et al. [2003] used double power law constitutive model to represent creep data on single lap shear specimens of Sn3.0Ag0.5Cu solder joints. But these models do not unify the creep and plastic deformation. Anand's model is more robust because this is an example of unified model which combines the creep and plastic deformation. Since lead-free solder alloy is still evolving and there are various combination of SAC alloys has been studied by researcher. The Anand's model material parameters were not available for the lead-free solder alloys used in this thesis. There was a need for an algorithm to estimate the material parameter in order to simulate the solder creep behavior from material characterization data. Amagai, et al. [Amagai 2002] presented the results for 95.75Sn3.5Ag0.75Cu and 98.5Sn1.0Ag0.5Cu but neglected to include one of the nine required constants. Kim, et al. [Kim 2003] updating the work by Amagai, et al. [Amagai 2002] have indeed published all nine constants for 98.5Sn1.0Ag0.5Cu but not for other lead-free alloys. There was no data available for Anand's model to represent in ANSYS for 95.5Sn4.0Ag0.5Cu lead free solder alloy. Ma, et al. [Ma 2007] published the tensile test data for 95.5Sn4.0Ag0.5Cu alloy at different strain rates and temperatures which can be used to fit the Anand's model to obtain the nine constants required to model it in ANSYS.

The material properties of lead free solder are dependent on temperature and strain rates. Pang, et al. [Pang 2003] found that the mechanical properties of Sn3.8Ag0.7Cu solder alloy will decrease with an increase in temperature and with lower strain rate. Ma, et al. [Ma 2007] found the same thing for Sn4.0Ag0.5Cu solder alloy for the aged sample, using a very thin rectangular sample instead of dog-bone type sample.

2.4 Reliability of polymer core ball and copper reinforced column interconnect

BGA package style uses the solder ball as electrical interconnects between package and application boards. Solder balls are rigid and tend to fracture under thermal fatigue and/or shock loading. Metalized polymer spheres (MPS) offer a more compliant interconnect compared to solder balls thereby increasing the thermal cycling fatigue life. A reduction in thermal and electrical performance may be expected for MPS interconnects as a result of its higher thermal and electrical resistance. Studies done on polymer stud grid array (PSGA) showed at least 3x more improvement in thermal cycling reliability [Vandevelde 1999]. But PSGA packages incur a larger initial cost associated with tooling and injection mold process, where as, MPS interconnects can be directly applied to existing BGA style package with no extra tooling cost. Thermal cycling testing on MPS interconnects by Yoon, et al. [Yoon 2001], Aguirre and Movva, et al. [Aguirre 2004] showed a 2-3x times improvements in second level interconnect reliability when compared to a Sn/Pb/Ag solder alloy. Sekisui [Sekisui 2005] has done the thermal reliability test on various ball grid array packages and found that there is 3x times improvement in fatigue life compared to conventional solder balls. The reason being this package outperform the conventional architecture is stress applied at solder joint during thermal cycling, which is in part dependent on elastic modulus of interconnect materials. Solder is a metal with high modulus of elasticity of approximately 32 GPa. Polymer core interconnects have much lower modulus of elasticity, approximately 5-9 GPa [Galloway 2005].

BGA is rapidly becoming the industry standard for high lead-count microelectronics packaging. As this revolution in packaging takes place, the industry is accepting a compromise in thermal cycling reliability. A perimeter-leaded device, such as a Plastic Quad Flat Package (PQFP), with flexible gull-wing leads, can be subjected to thermal cycles without encountering stresses due to the CTE mismatch between the component and the board. BGA packages on the other hand, are connected with a rigid structure of solder spheres that provides very little compliance between the component and the board. The temperature differential, as well as the differences in CTE between the component and the board will lead to stresses in the solder joints. A successful solution to the BGA compromise is to utilize a flexible column in place of the solder spheres. This gives more robust design for thermal cycling in two ways, first, leads are designed to have a lower stiffness and second, they have higher standoff distance between component and board. The solder column technology has been available for over 20 years. There are various types of columns. Winslow et al. [Winslow 2005] explains the methodology to convert the ball grid array to column grid array and also has shown the constructional details of copper reinforced columns. A long-term temperature cycle study by Lockheed Martin [Clifford 2004] shows a significant performance improvement of the reinforced column over other type of columns like wire column and solder column interposer. Winslow et al. [Winslow 2005] also conducted the temperature cycle test from -10 ºC to 125 °C on ceramic ball grid array and column grid array and showed that there is significant increase in the thermal fatigue life of column grid array compared to ball grid array. Another long-term reliability test performed by an un-disclosed company on ceramic ball grid array and ceramic column grid array with reinforced column showed around 5x increases in reliability. Many researchers have done a finite element analysis on column grid array packages to find out the thermal fatigue failure [Sinha 1997, Master 1995, and Ingalls 1998]. But there is no finite element model available for copper reinforced column grid array.

2.5 Prognostics Health Management of electronics

Methodologies for prognostication and health monitoring can significantly impact the electronic reliability for applications in which even minimal risk of failure may be unbearable. The current state of the art methodology in managing the reliability is geared towards the development of life-prediction models for un-aged pristine materials under known loading conditions based on relationships such as the Paris' Power Law [Paris 1960, Paris 1961], Coffin Manson Relationship [Coffin 1954] and S-N diagrams. Since electronics have become the integral part of the system, reliability of these electronics affects the overall system reliability. Therefore, there is a need for methods or processes which will allow interrogation of complex systems and sub-systems to determine the remaining useful life prior to repair or replacement. This capability of material or system state is called "prognosis". There is a scarcity of methods which will enable the estimation of reliability in its actual life cycle conditions and also determination of damage state, when the prior stress histories are not accurately known.

Prognostics Health Management (PHM) methodology exists for many mechanical systems. Examples include, aircraft engines, which start and stop quite frequently and run at high speeds, a model-based method has been used for the on-line identification of cracks in a rotor while it is passing through its flexural critical speed [Sekhar 2003]. Detection of surface corrosion has been used to reduce the maintenance required, and trigger preventive repair for increased aircraft availability and significantly reduced cost of ownership. Crack modeling approach in beams has been used to demonstrate the structural HM using low frequency vibration. Simple models of crack flexibility based on beam elements are adequate [Friswell 2002]. Optical fiber based sensor systems have been used on concrete structures to evaluate their performance for health monitoring [Fernando 2003]. Monitoring bridge performance has been done to answer questions on the performance of existing bridges, refine techniques needed to evaluate different bridge components, and develop approaches that can be used to provide a continuous picture of a bridge's structural integrity using structural health monitoring [DeWolf 2002]. Transducers along with a wireless data acquisition system can enable the possibility of achieving long distance monitoring [Kok 2005]. These techniques help in detection of damage of bridges or building to avoid the economic and social effect of aging and deterioration [Chang 2003]. In railway industry, wayside detection systems monitor critical parameters relating to the condition of in-service railway vehicles. [Barke 2005].

Wear and degradation in electronics is very difficult to detect and inspect compared to most other mechanical systems and structures due to the complex and tiny structure. Built-In-Self Test (BIST) circuit, which includes onboard hardware and software diagnostics, has been used for error detection and fault location [Drees 2004]. BIST is a methodology that embeds additional functionality in the product to give it the ability to test and diagnose itself with minimal interaction from external test equipment

[Chadramouli 1996, Hassan 1992, Williams 1983, Zorian 1994]. BIST controllers are typically used for reactive failure detection to output failure data that can be correlated to show exactly when the failure occurred. This data can then be interpreted by diagnostic software to analyze the cause of failure. Several studies conducted [Drees 2004, Allen 2003, Gao 2002, Rosenthal 1990] have shown that BIST can be prone to false alarms and can result in unnecessary costly replacement, re-qualification, delayed shipping, and loss of system availability.

Fuses and Canaries have been used to provide advance warnings of failure in electronics due to specific wear out failure mechanism [Vichare 2006] .Fuses within circuits and thermostats; can be used to sense the abnormal conditions like voltage transients, critical temperature limit and to make adjustments to restore normal condition [Ramakrishnan 2000]. Canary devices like pre-calibrated cells which are located with the actual circuitry on the same chip experience similar stresses as the actual component. This leads to the same damage mechanism. But these cells are designed to fail faster by scaling the stress which is been experienced to avoid the catastrophic failure of the actual component and also can be used to find the time to failure of actual products [Mishra 2002, Anderson 2004]. However, replacement of fuses and canaries impacts the maintenance, repair and part replacement making it difficult to integrate these systems with host systems. In addition, fuses provide limited insight into the remaining useful life prior to fuse-failure.

An electronic component operating in a harsh environment is subjected to both temperature variations as well as aging for a finite duration during use-life. Therefore, a time-temperature history of the electronic system ambient would be extremely helpful in using life prediction models and computing life. Continuous capture of time-temperature history would put immense demands on the existing system function. Previously, Lall, et al. [Lall 2006] have developed leading indicators of failure for leaded solder, which will enable the interrogation of material state and determination of residual life before appearance of macro-indicator of failure. In this methodology, proxies like the phase growth rate of solder interconnects, normal stress at chip interface, and interfacial shear stresses, have been experimentally identified as indicators to failure and mathematical relationships have been developed for computation of residual life based in terms of these damage proxies. This health monitoring framework will facilitate quick assessment of system state and potential for failure of critical electronic systems.

The solder microstructure coarsening effect thermal fatigue life has been reported previously by several researchers. Morris, et al. [1991, 2003] reported that the thermal fatigue of Sn63/37Pb solder was characterized by microstructural coarsening in the interface volume. Pang et al. [2001] reported that the microstructural coarsening due to thermal cycling aging had a major impact on the fatigue strength of solder joints. Frear, et al analytically studied the microstructural evolution of solder and suggested that solder grain size could be used as an important parameter for thermal fatigue life prediction. Sayama, et al. [Sayama 2003, Sayama 1999] examined the changes in microstructure occurring in the Sn63/37Pb chip resistor solder joints during thermal cycling. A power law type relation has also been investigated between the number of cycles to crack initiation and the average increase in the α-Pb phase growth parameter. Bangs and Beal [Bangs 1978], Wolverton [Wolverton 1987] and Tribula et al. [Tribula 1989] have shown that during thermal fatigue of eutectic and high lead solders, grain coarsening has been observed and the fatigue failure initiates in the coarsened region. The grain growth rate per unit time is found to increase with increasing strain rate. Callister [Callister 1985] found that after re-crystallization is complete, the strain free phases will continue to grow if the metal specimen is stored at an elevated temperature. The process of the particle growth induced by volume diffusion was theoretically analyzed by Lifshitz, et al. [Lifshitz 1961], Ardell [Ardell 1972] and Speight [Speight 1968] studied independently and proposed a phase diffusion theory, which states that when phase boundary diffusion dominates, then average phase size to the fourth power increases proportional to time. Senkov and Myshlev [Senkov 1986] extended the theory to the phase growth processes of a superplastic alloy and validated the theory in that of Zn/Al alloy. Dutta, et al.[Dutta 2003] represented the total vacancy concentration due to grain coarsening at any location within the solder joint at any instant of time has been written as the sum of the equilibrium vacancy concentration and vacancy concentration under applied instantaneous strain rate.

Since lead-free solder alloys are becoming more and more popular because of legislation, many researchers are investigation effect of grain coarsening on these alloys. It was found that SnAgCu solders consist of primary dendrites/grains of β-Sn, and a eutectic micro constituents comprising fine Ag_3Sn and Cu_6Sn_5 particles in β. Previously Lall, et al. [Lall 2006] investigated the solder microstructural coarsening effect using experiment and analytical methods on BGA packages, in order to prognosticate the electronic system. Very few package architecture has been considered for this study. It was necessary to identify the leading indicators of failure, which solder-microstructural coarsening in various package architecture using same alloys, which has been used previously [95.5Sn4.0Ag0.5Cu] in order to come up with an empirical relationship. Also there was a need for a methodology to interrogate the system state without knowing the prior damage history. There are a lot of Pb-free alloys in the market like Sn1.0Ag0.5Cu, Sn3.0Ag0.5Cu and Sn0.3Ag0.7Cu; all these have different creep behavior because creep behavior depends strongly on microstructural constituent [Dutta 2007]. Concentration of Ag and Cu in these alloys effect the creep behavior of solder and also the solder micro-structural coarsening rate is varied. In this thesis, an effort has been made to prognosticate these alloy components to estimate the prior damage when it has been subjected to variable stress history to compute the residual life.

CHAPTER 3

THERMO-MECHANICAL RELIABILITY OF VARIOUS INTERCONNECTS UNDER THERMAL CYCLING HARSH ENVIRONMENT

3.1 Introduction

One of the major goals of solder joint reliability modeling in the electronics industry is to be able to understand its stress-strain behavior and then predict its reliability in accelerated tests. In addition to numerical simulation using finite-element analysis (FEA), the solder fatigue failure mechanism can be characterized by low cycle fatigue testing. During a thermal cycling test, solder materials are typically subjected to temperature above half of its melting point also known as homologous temperature, therefore, the elastic-plastic-creep and viscoplastic constitutive models have to be considered in order to describe the inelastic deformation behavior of the solder joint. Since the failure mechanism for solder under thermal cycling is creep-fatigue, the number of cycles to fatigue failure can be correlated to a fatigue failure parameter called inelastic strain energy density obtained from the finite-element (FE) simulation.

There are two major steps in solder joint reliability modeling. First, a suitable solder constitutive equation has to be incorporated into the FE model. The stress-strain results from the FE model are extracted by averaging the inelastic strain energy density as a fatigue parameter. Then, a solder fatigue model is needed to calculate the number of cycles to fatigue failure using the failure parameter extracted from the FE model results.

In this thesis, thermo-mechanical stress-strain calculations for many solder interconnects have been presented. First, thermo-mechanical reliability of lead-free component in various ball grid arrays interconnects like plastic, tape-array, flex-tape and chip array ball grid array package under thermal cycling load from -40°C to 125°C has been considered. The life obtained in this conventional study has been used to compare the life obtained from prognostication study in a later chapter. Secondly, thermo-mechanical reliability of various solder interconnects like polymer-core and copper reinforced column solder balls have been studied using finite-element and fatigue law approach.

3.2 Lead-free component reliability

Increasing global concern about the environment is bringing regulatory and consumer pressure on the electronics industry in Europe and Japan to reduce or completely eliminate the use of lead (Pb) in products. The transition from a technology using SnPb for electronic interconnections to a new lead-free technology is a challenging and demanding task for the companies. It has an impact not only on material supply, process equipment and conditions but also will bring about a change in reliability. Components have to withstand higher soldering temperatures (typically 20 to 35°C higher) and the solder joints should have at least the same life time. A leading-indicator based methodology to prognosticate the electronics has been presented using SnPb solder joint [Lall 2006], but in this thesis it has been extended to lead-free solder components. A Reliability study of lead-free component has been performed on similar test board with same number of packages and package architectures as the one used for prognostics study so that life time obtained in reliability study can be used to compare the life estimated during leading indicator based prognostics study. The lead-free solder alloy used for this study is 95.5Sn4.0Ag0.5Cu. The study is done using both finite-element and fatigue law method and also using an accelerated thermal cycling test. There are many factors contributing to the accuracy of the FE model and fatigue life prediction results. One of the factors affecting the accuracy of the FE model results is the solder constitutive model. The constitutive relations used for this study is Anand’s viscoplastic model and also an algorithm has been written to estimate the material parameter to represent this model in ANSYS accurately by curve fitting the material characterization data for the 95.5Sn4.0Ag0.5Cu alloy.

3.2.1 Test Vehicle Description

Component analyzed include I/O counts in the range of 64 to 676 I/O, pitch in the range of 0.5 to 1 mm and package size in the range of 6mm to 27 mm. The test board contains three each of the following package architectures: 7mm CABGA, 6mm TABGA, 10 mm TABGA, 16 mm FlexBGA, 15mm PBGA and 27mm PBGA package architecture. The BGAs have the solder ball made up of 95.5Sn4.0Ag0.5Cu solder alloy. The substrates used were ImAg finished high temperature glass epoxy laminate (FR4-06). All the pads on the board were non-solder mask defined (NSMD) and have an ImAg finish. All the BGAs were daisy chained so that resistance monitoring could be done easily during the thermal cycling test. The component test matrix for this study is shown in Figure 3.1 and Table 3.1.

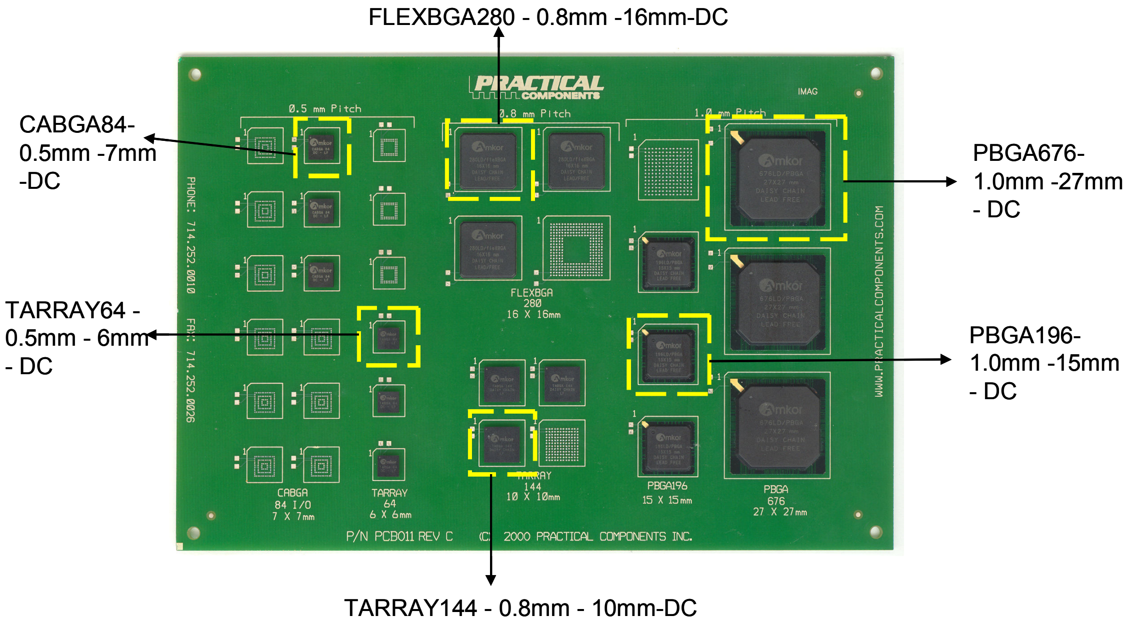

Figure 3.1- Test board used for thermo-mechanical reliability study

Body Size	Package	Ball Count	Ball Pitch (mm)	Die Thickness (mm)	BT Thickness (mm)	Die size (mm)	BT Pad Type	Ball Diameter (mm)
6 mm	TABGA	64	0.5	0.36	0.36	4	NSMD	0.32
7 mm	CABGA	84	0.5	0.36	0.36	5.4	NSMD	0.48
10 mm	TABGA	144	0.8	0.36	0.36	7	NSMD	0.48
15 mm	PBGA	196	1	0.36	0.36	6.35	SMD	0.5
16 mm	FlexBGA	280	0.8	0.36	0.36	10	NSMD	0.48
27 mm	PBGA	676	1	0.36	0.36	6.35	SMD	0.63

Table 3.1- Component test matrix design

3.2.2 Reliability Testing

Thermal cycling (-40°C to 125°C) of the assembled test boards was performed in a single chamber system. The thermal cycle duration was 2 hours, with a 30 minutes dwell at each extreme and a 5.5 °C/min ramp. The temperature profile has been shown in Figure 3.2. A total of 10 boards were used for the study, with 3 packages of each type on each board. The boards were placed vertically in the chamber. Monitoring of the various daisy-chain networks was performed throughout the cycling. Failure of a daisy-chain network was defined as the point when the change in the resistance becomes 20% higher than the initial resistance.

3.2.3 Thermal Cycling Results

For those components with sufficient failures after 3000 cycles, the resulting failure data were statistically analyzed using two parameter Weibull models. The standard parameters in such an approach are the Weibull Slope β, and the Characteristic Life ή, which is the number of cycles required to fail 63.2% of the samples from a particular leg of the test matrix. From these values for a particular BGA configuration, the cumulative failures after any number of thermal cycles can be predicted. When comparing these values with the one obtained during finite element analysis, we have used the value of $N_{1\%}$, the number of cycles necessary to cause 1% of the parts in a sample set to fail. For electronic component, thermal cycling failure phenomenon governed by the Weibull distribution, the percentage of failed component is given by:

$$F(N) = 1 - e^{\left[\frac{N}{\eta}\right]^{\beta}} \qquad 3.1$$

Where F(N) is the fraction of parts failing(CDF), N is the number of thermal cycles(time), ή is the Weibull characteristic life or scale parameter, and β is the Weibull slope or shape parameter. The relation can be inverted to solve for the number of thermal cycles in terms of the failure fraction:

$$N = \eta\left[\ln\left(\frac{1}{1-F(N)}\right)\right]^{1/\beta} \tag{3.2}$$

When comparing the various component reliabilities in this study, the value of $N_{1\%}$ (number of cycles necessary to cause 1% of the parts in a sample set to fail) has been utilized. For 1% failure (F=0.01) becomes

$$N_{1\%} = \eta[0.0100503]^{1/\beta} \tag{3.3}$$

The measured failure data for various package architectures has been analyzed and plotted using WinSmith Weibull commercial software, which calculates the best-fit values of η and β for a set of failure data. Equation 3.3 was then used to calculate the $N_{1\%}$ values. Weibull plots for the various BGA parts are shown in Figure 3.3 and Figure 3.4. Extensive failure analysis has been performed on the similar samples subjected to thermal cycling and samples were removed at an interval of 250 cycles and cross-sectioned to check for failure. It is found that thermal cycle fatigue cracks were typically found to initiate at the top of the solder joint (BT), in the high strain regions in the corners. Crack growth would proceed across the entire joint, near but not at the BT pad interface. In some cases, solder joint cracking occurred simultaneously at the both the top and bottom of the solder joint. Figure 3.5 and Figure 3.6 shows few examples of failure analysis done for this test matrix.

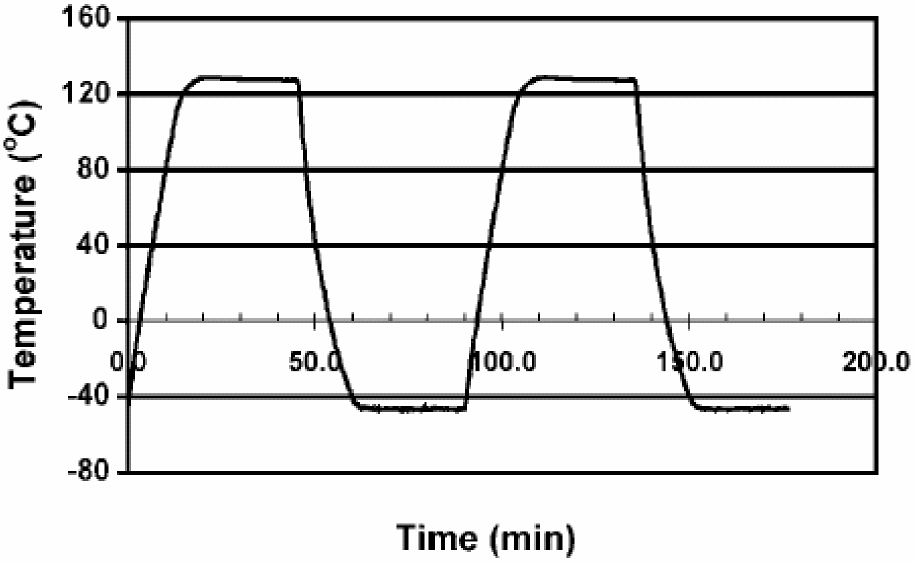

Figure 3.2 - Chamber thermal profile

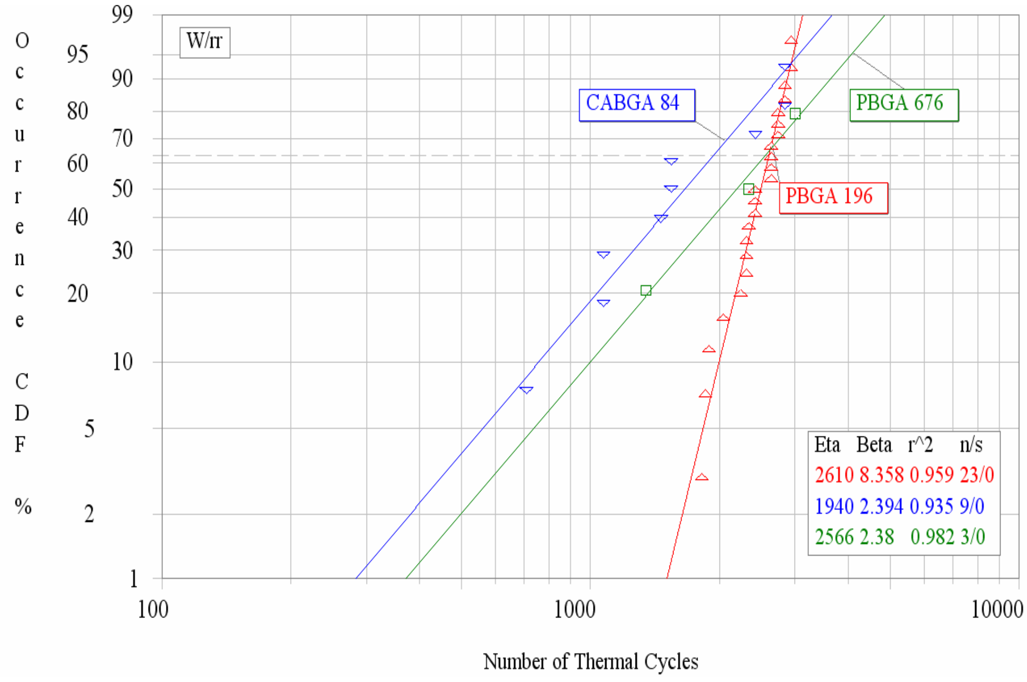

Figure 3.3 - Weibull plot for PBGA and CABGA packages

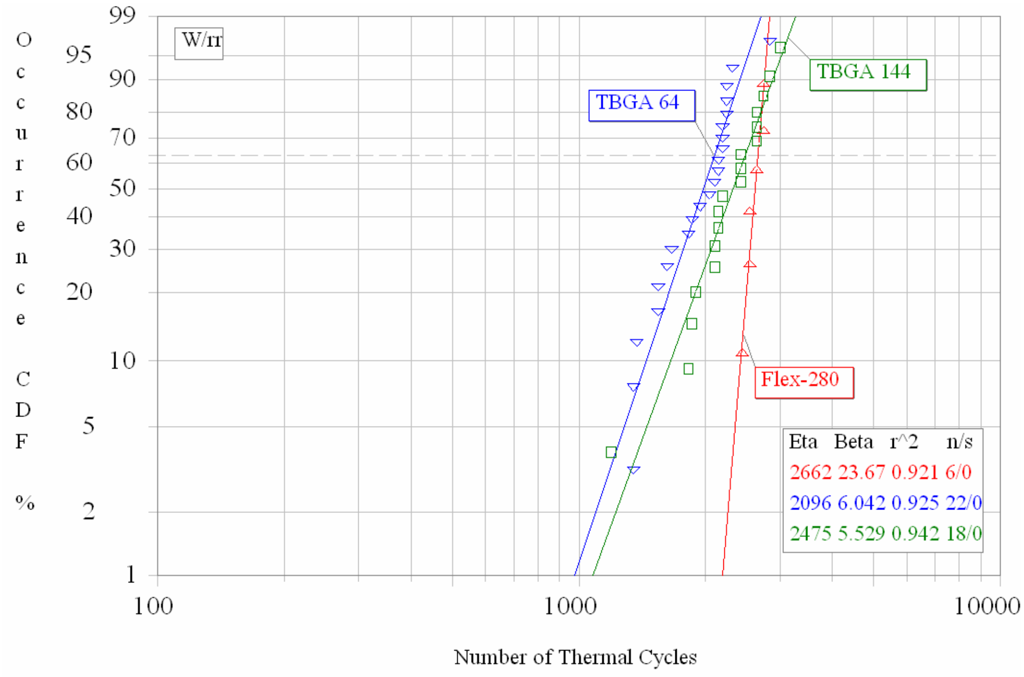

Figure 3.4 - Weibull plot for Tape array BGA and Flex BGA packages

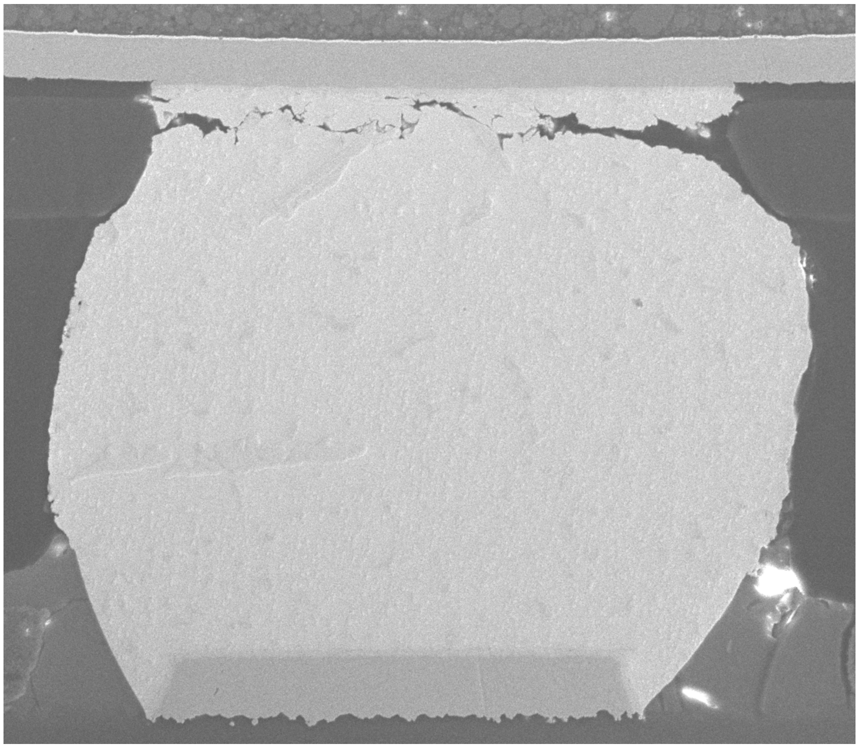

Figure 3.5 - Typical Solder Joint Failure in 7mm Tape array BGA

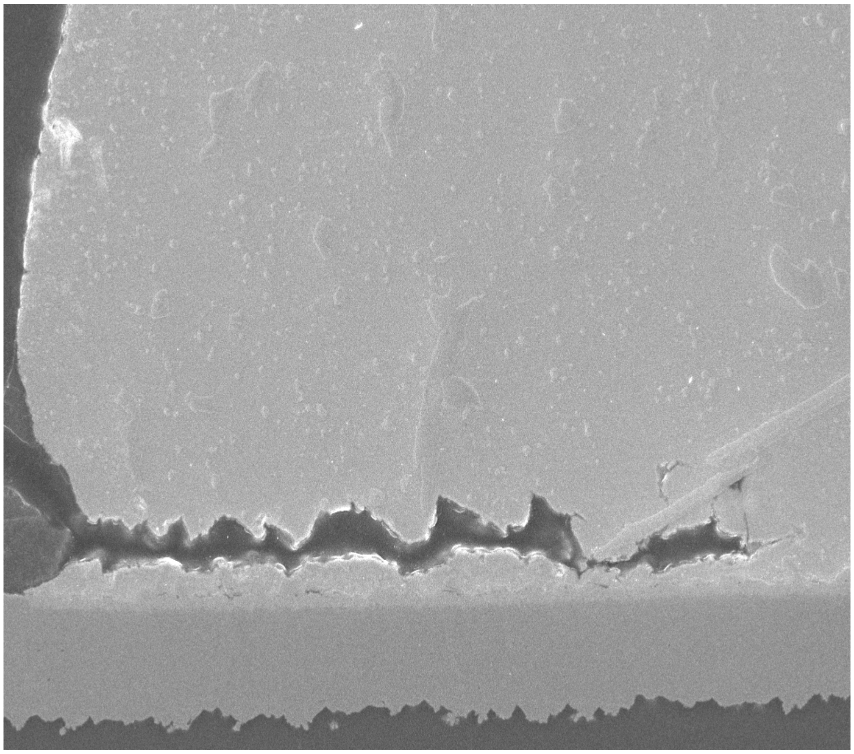

Figure 3.6 - Typical Solder Joint Failure in 16mm Flex BGA

3.2.4 Material Model

Most failure physics approaches to fatigue life modeling of electronic component solder joints require the estimation of either stress or strain or plastic work from a finite element model. The finite element technique requires the user to provide key information on the material properties and boundary conditions for the model before it can be implemented successfully. In particular, the stress-strain behavior of solder is extremely complex, being temperature and rate-dependent and must be well understood. For solder, two constitutive models tend to predominate: unified and non-unified. Non-unified models partition the inelastic deformations into two groups: time-independent or plastic and time-dependent or creep. The unified models also differentiate between elastic and inelastic strain but unify creep and plastic deformations into a single inelastic term which is expressed in terms of internal state variables [Zhang 2003]. The Anand's model is an example of such a unified Viscoplasticity model, used widely in the finite element analysis of solder interconnects. In this study viscoplastic behavior of solder has been captured using Anand's model and the rest of the material in the package has been modeled as either linear or orthotropic materials. Table 3.2 shows the material properties used for this study.

3.2.5 Anand's Viscoplastic Model

Anand [1982] developed constitutive equations for the rate-dependent deformation of metals at high temperature (i.e. in excess of a homologous temperature of $0.5T_m$). Although aimed at hot working of steels and other structural metals, it has been adopted successfully to represent the viscoplastic behavior of solders. The model proposed by Anand and subsequently developed by Brown, et al. [1989], unifies the creep and rate-independent plastic behavior of the solder by making use of a flow equation and an evolution equation [Zhang 2003]. The necessary equations are as follows:

Flow Equation

$$\dot{\varepsilon}_{\mathrm{p}} = \mathrm{A}\exp\left(-\frac{\mathrm{Q}}{\mathrm{R}\Theta}\right)\left[\sinh\left(\xi\frac{\sigma}{\mathrm{s}}\right)\right]^{1/\mathrm{m}} \qquad 3.4$$

Evolution Equation

$$\dot{\mathrm{s}} = \left\{\mathrm{h}_0\left(\left|\mathrm{B}\right|\right)^{\mathrm{a}}\frac{\mathrm{B}}{\left|\mathrm{B}\right|}\right\}\dot{\varepsilon}_{\mathrm{p}} \qquad 3.5$$

Where

$$\mathrm{B} = 1 - \frac{\mathrm{s}}{\mathrm{s}^*} \qquad 3.6$$

And

$$\mathrm{s}^* = \hat{\mathrm{s}}\left[\frac{\dot{\varepsilon}_{\mathrm{p}}}{\mathrm{A}}\exp\left(\frac{\mathrm{Q}}{\mathrm{R}\Theta}\right)\right]^{\mathrm{n}} \qquad 3.7$$

The flow equation is similar in form to that used to describe steady-state secondary creep but with the addition of an internal state variable defined as the deformation resistance, s, which depends on the temperature and rate-dependent strain history of the material. Note that $\dot{\varepsilon}_p$ is the inelastic strain rate and is the sum of creep and time-independent plastic strain rates. The first part of the equation is an Arrhenius Law-type term which captures the temperature dependence of the creep process. The second part of the equation, the hyperbolic sine term, describes the stress dependence of the inelastic strain rate. It is this term which includes the state variable. The evolution equation, in the context of solder behaviour, mainly captures the strain hardening effect through the hardening coefficient $h_\circ$. The assumed relationship between the stress of the model and the deformation resistance variable is

$$\sigma = cs \tag{3.8}$$

Where, by definition,

$$c = \frac{1}{\xi}\sinh^{-1}\left[\left(\frac{\dot{\varepsilon}_p}{A}\exp\left(\frac{Q}{R\Theta}\right)\right)^m\right] \tag{3.9}$$

3.2.6 Anand's Model Parameter Estimation

The estimation of the model parameter for iron and aluminum and iron alloys is presented by Brown, et al. [1989] and Amagai, et al. [2002] presented some what limited description of the procedure for solder alloys, but the latter neglects to include the initial deformation resistance term $s_\circ$. The method presented by Brown, et al. [1989], has been used to develop an algorithm to fit the equation with the experimental data. The steps followed in the algorithm are as follows.

3.2.6.1 Estimation of A, m, n, Q/R and $\hat{s}/\xi$

The steady-state saturation may be derived from the evolution equation 3.4 and equation 3.7 as

$$\sigma^* = \frac{\hat{s}}{\xi}\left(\frac{\dot{\varepsilon}_p}{A}\exp\frac{Q}{R\Theta}\right)^n \sinh^{-1}\left[\left(\frac{\dot{\varepsilon}_p}{A}\exp\frac{Q}{R\Theta}\right)^m\right] \tag{3.10}$$

Constant stress tests at a range of temperature and stresses yield pairs of data points $\left(\sigma^*, \dot{\varepsilon}_p\right)$ when steady state conditions are established. Saturation stress is estimated from Figure 3.7 when the curve reaches steady state for each temperature at a particular strain rate. Figure 3.8 shows the strain rate vs. saturation stress at different temperatures [Ma 2007]. Using a nonlinear fitting procedure with the measured data points, the terms A, m, n, Q/R and $\hat{s}/\xi$ may then be estimated in equation 3.10.

Levenberg Marquardt Algorithm, a non-linear curve fitting procedure has been developed to fit the $\left(\sigma^*, \dot{\varepsilon}_p\right)$ shown in Figure 3.8 to equation 3.10 to estimate the A, m, n, Q/R and $\hat{s}/\xi$ terms in the equation. Curve fitting procedure is iterated to many initial guesses because convergence of the algorithm depends on initial guesses. In order to get the global minima, a design space has been decided for each unknown parameter by researching Anand's constant for different kinds of SAC alloys in the literature. The initial guess array has been generated using the random number generator option available in MINITAB$^{\text{TM}}$, using uniform distribution. These numbers are given as arrays to LM Algorithm, which had generated almost total of 100000 iterations. The output from each of the iterations is written to a file along with root mean square error. The final answer is picked out of several iterations based on the one that has least root mean square error. The resulting fit is indicated in the plot of strain rate as a function of saturation stress in Figure 3.9.

3.2.6.2 Estimation of a, h_o and σ_o

The second part of the fitting procedure looks at the influence of plastic strain hardening on the evolution of the deformation resistance, captured by the following equation, which comes from restating the evolution equation 3.5 in terms of the slope of the stress-strain curve:

$$\frac{d\sigma}{d\varepsilon_p} = ch_o\left(1 - \frac{\sigma}{\sigma^*}\right)^a \qquad 3.11$$

This equation applies to isothermal, constant true strain rate tests and the experimental data shown in Figure 3.7 may again be used for fitting its parameters. If the experimental data is noisy, as is often the case, this equation can be difficult to curve fit. An alternative approach is to integrate it to give the following:

$$\sigma = \sigma^* - \left[\left(\sigma^* - \sigma_\circ\right)^{(1-a)} + (a-1)\left\{\left(ch_\circ\right)\left(\sigma^*\right)^{-a}\right\}\varepsilon_p\right]^{1/(1-a)} \qquad 3.12$$

Performing the integration introduces an extra parameter, $\sigma_\circ$ the initial stress value. As earlier, a nonlinear fitting procedure is used to evaluate the parameter a, $\sigma_\circ$ and h_o, where ‘a’ must be greater than unity. A total of 27 isothermal test data as shown in Figure 3.10 to Figure 3.12 [Ma 2007] were used to fit the equation. MATLAB^{TM} code is written to read the data for each test and fit the data to equation 3.12. Curve fitting procedure is repeated with varying initial values in the trust region. For each test the output value has been written to the file. Final values of a, $\sigma_\circ$ and h_o are found by averaging the value for all the tests.

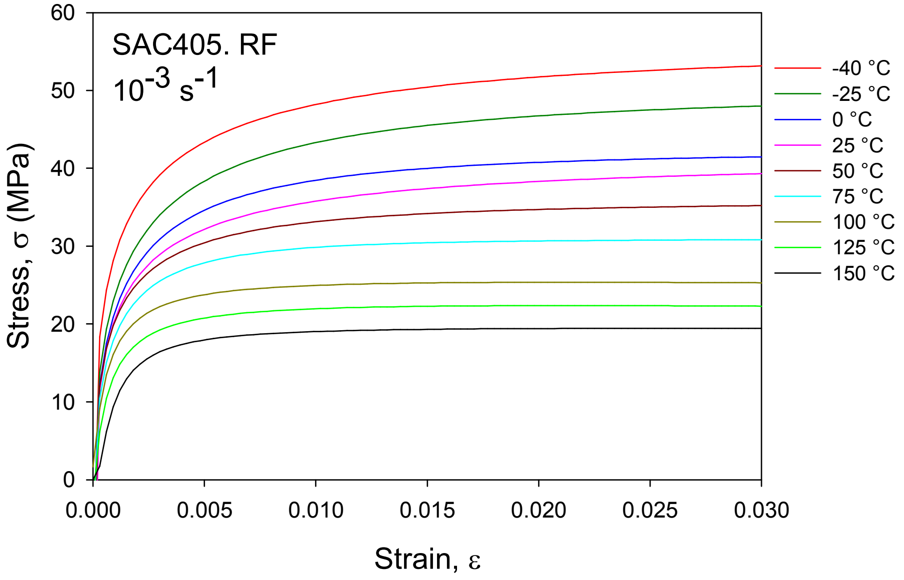

Figure 3.7 - Stress vs. strain plot for SAC405 at different temperatures [Ma 2007]

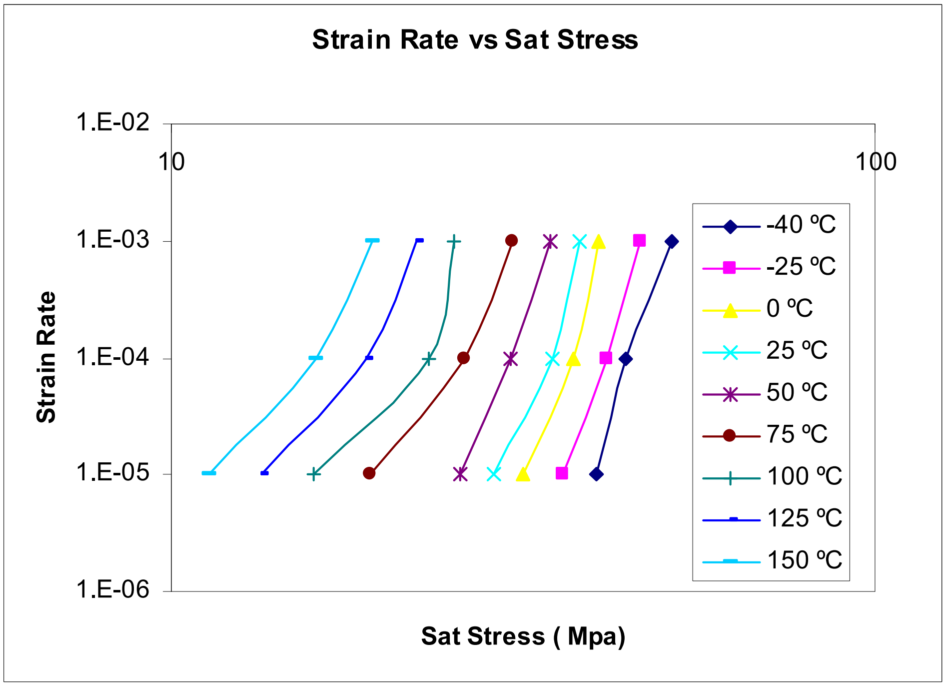

Figure 3.8 - Strain rate vs. Sat stress at different temperatures for SAC405 [Ma 2007]

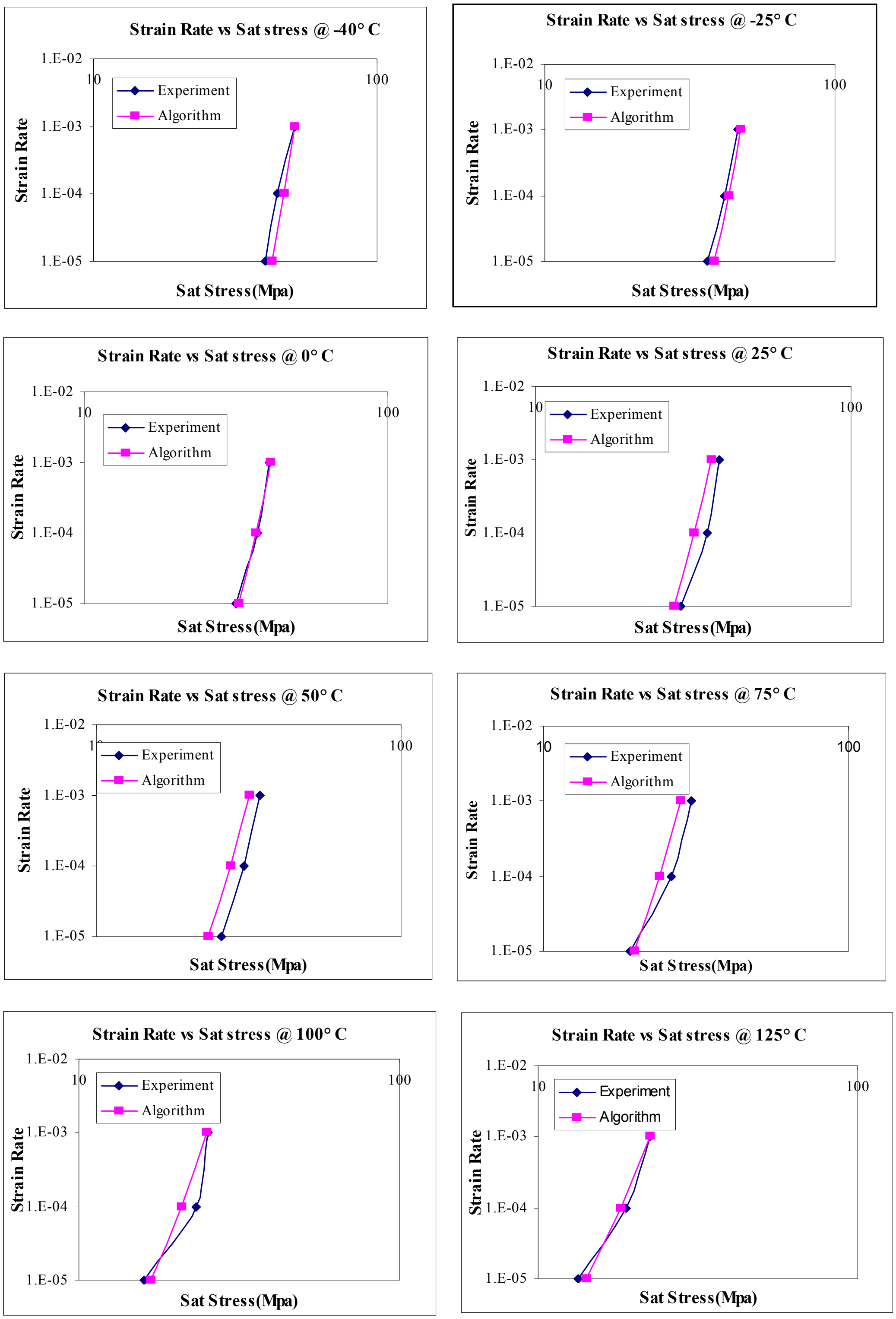

Figure 3.9 - Comparison plot of strain rate vs. saturation stress at a range of temperature for SAC405 from algorithm and experimental data [Ma 2007]

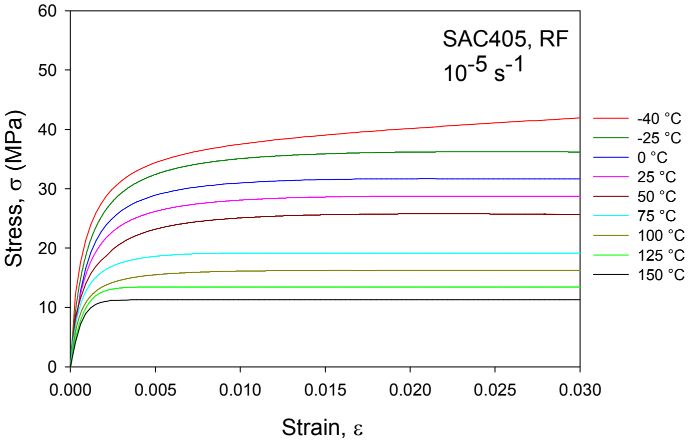

Figure 3.10 - SAC 405 tensile test data for strain rate 10^{-5} at various temperatures [Ma 2007]

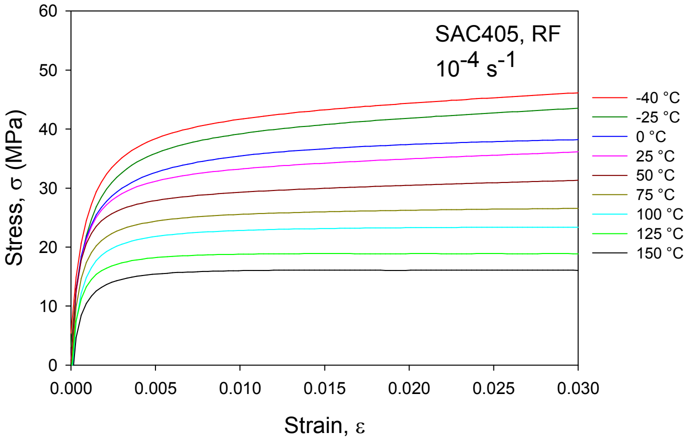

Figure 3.11 - SAC 405 tensile test data for strain rate 10^{-4} at various temperatures [Ma 2007]

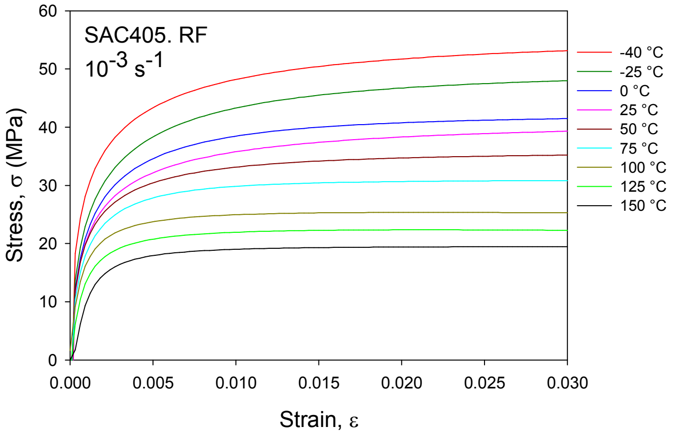

Figure 3.12 - SAC 405 tensile test data for strain rate 10^{-3} at various temperatures [Ma 2007]

3.2.6.3 Estimation of ξ, $\hat{s}$ and $s_\circ$

Some final mathematical steps are required to estimate the remaining parameters. Using values of A, m, n and the ratio of Q/R determined earlier, the value of ξ is selected from equation 3.9, for c<1 for each test. In equation 3.9, the product of c and ξ for each test was found first. From the literature, we have the range for ξ value. For each ξ value, c has been calculated and written to a file. The iterations for which c < 1 for each test have been isolated and the c and ξ value have been averaged for the final answer.

The value $\hat{s}$ is then determined from the ratio of $\hat{s}/\xi$ and ξ found earlier. Finally the value of $s_\circ$ for each test is determined by dividing the initial stress value $\sigma_\circ$ estimated earlier by the corresponding value of c (noting that $\sigma_0 = cs_0$). A value of $s_\circ$ at a given temperature is then calculated by averaging all $s_\circ$ values obtained at that temperature. Final values of Anand's constant obtained from the algorithm is listed in Table 3.3

3.2.7 Non-linear Finite Element Model

Viscoplastic finite-element simulation methodologies were utilized to predict solder ball joint reliability. Due to complex physics that encompass this type of non-linear transient finite element analysis, only a diagonal slice of the package was modeled in order to facilitate reasonable model run time. The utilization of a diagonal slice assures the worst-case situation where the perimeter solder ball is at the furthest distance from the package center neutral point. The diagonal slice representing the finite element model is shown by two bold lines in Figure 3.13. The finite element model has been created in ANSYS^{TM} using hexahedral elements. Except for the solder joints, the rest of the materials have been modeled using SOLID45 element. Solder joint has been modeled using VISCO107 elements.

The diagonal slice model passes through the thickness of the package assembly, capturing all major components and a full set of solder joints. The use of slice model involves a choice on the part of the analyst on the boundary constraints to be applied at the slice plane; the plane is neither a free surface nor a true symmetry plane. A reasonable compromise of coupling the z-displacements of the nodes on the slice plane was chosen. This has the effect that the slice plane is free to move in the z-direction, but that the surface is required to remain planar. Boundary constraints applied to a typical slice model are shown in Figure 3.14. And also for all package in this thesis, the printed circuit board length was set to 1.5 times that of the modeled package slices length. The width of the slice model is one-half of the solder ball pitch. Also, the ball pitch is the hypotenuse of the true ball pitch because we are modeling the diagonal length of the package. [Zahn 2002]. Figure 3.16 to Figure 3.20 shows the diagonal symmetry finite element model and plastic work per volume for various BGA packages.

Material Name	E (Mpa)	Poisson's Ratio	CTE (1/K)	G (Mpa)
Mold Compound	23520	0.3	1.50E-05	
Silicon Die	162716	0.28	2.54E-06	
Die Adhesive	6769	0.35	5.20E-05	
BT Substrate	17890 (X&Z)	0.39 (XY & YZ)	12.4E-6 (X&Z)	8061 (XZ)
	7846 (Y)	0.11 (XZ)	57.0E-6 (Y)	2822 (YZ & XY)
Polyimide Tape	2415	0.24	5.00E-05	
Copper Pad	128932	0.34	1.63E-05	
Solder Mask	3100	0.3	3.00E-05	
Solder - 96.5Sn4Ag0.5Cu	54000	0.38	2.00E-05	
PCB	27924-37T (X &Z)	0.39 (XY & YZ)	14.5E-6 (X&Z)	12600-16.7T (XZ)
	12204-16T (Y)	0.11 (XZ)	67.2E-6 (Y)	5500-7.3T (YZ & XY)

Table 3.2- Material properties used to model packages on the test board

Fitted Anand Constant for 95.5Sn4.0Ag0.5Cu		
Definition	**Parameter**	**Value**
Initial Value of Deformation Resistance	So (MPa)	27.1824
Activation Energy / Boltzmann's Constant	Q/R(1/K)	8751.3
Pre-Exponential Factor	A (1/sec)	120.3158
Multiplier of Stress	ξ	9.4232
Strain Rate Sensitivity of Stress	m	0.3179
Hardening Constant	ho (MPa)	9249.56
Coefficient of Deformation Resistance Saturation Value	s-hat (MPa)	52.5172
Strain Rate Sensitivity of Saturation Value	n	0.0013
Strain Rate Sensitivity of Hardening	a	1.0523

Table 3.3 - Fitted Anand’s constant value for SAC405 estimated using algorithm

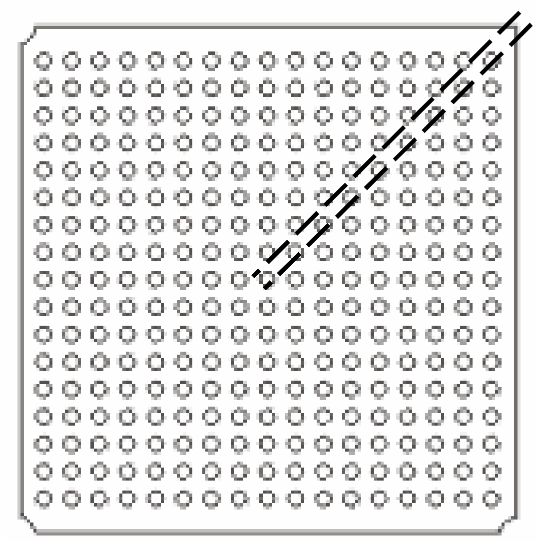

Figure 3.13 - Diagonal slice model representation for finite element model

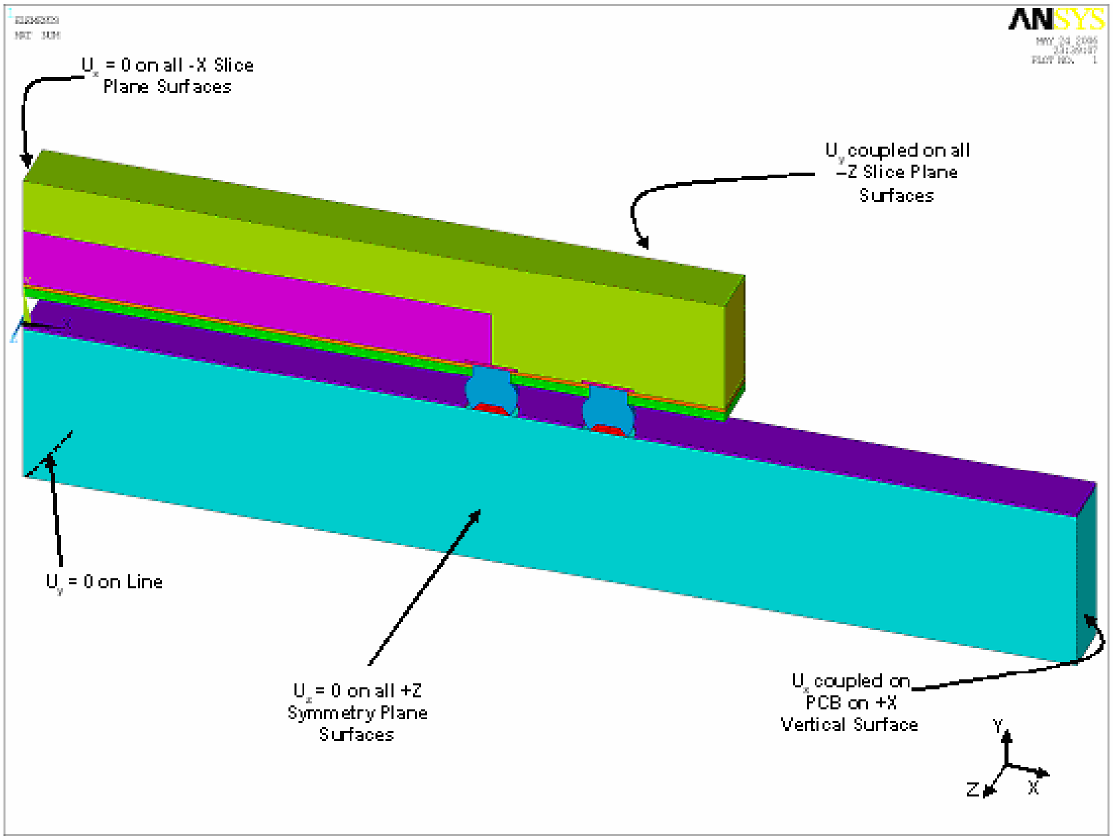

Figure 3.14 - Applied Boundary condition for the diagonal slice model

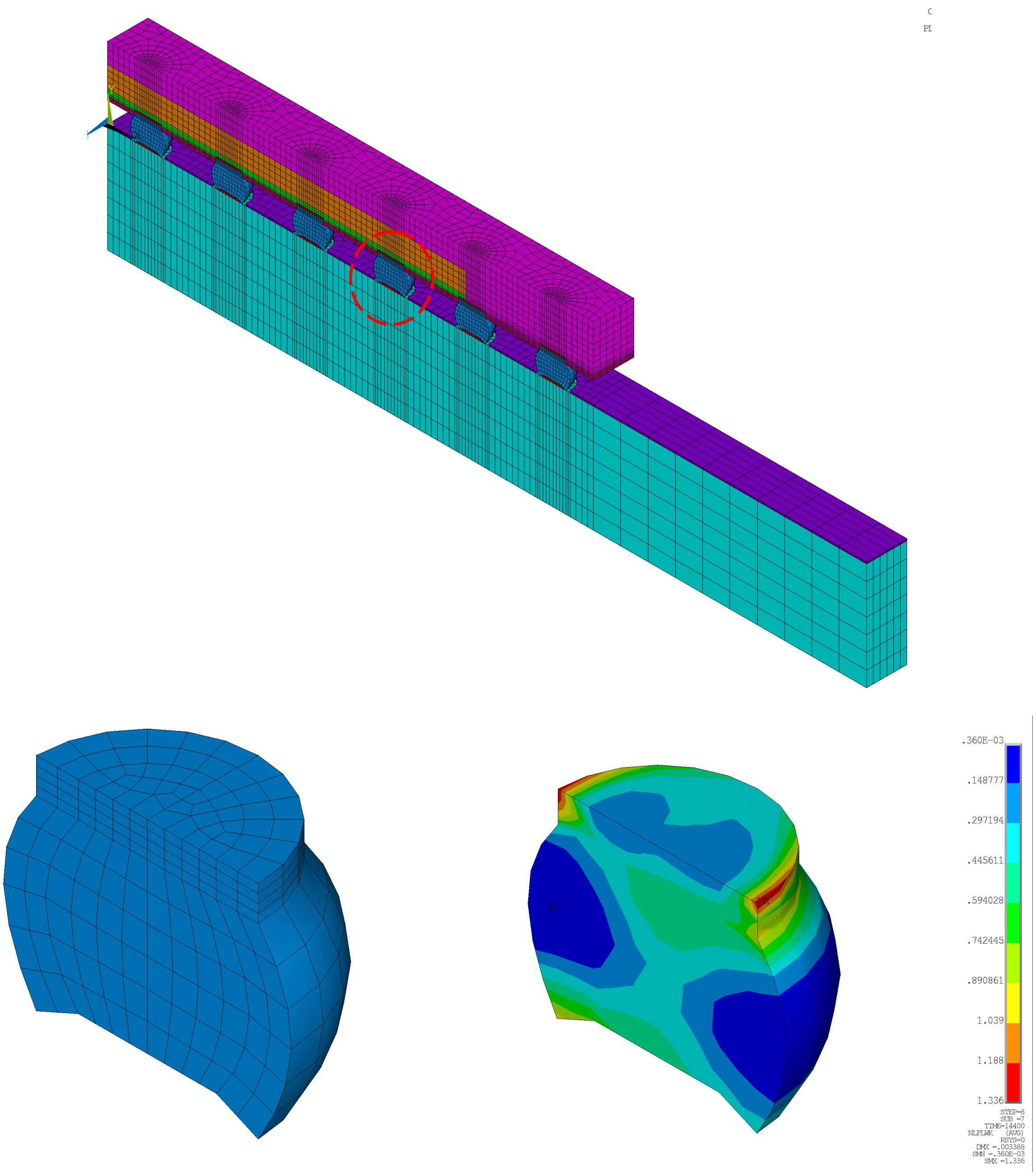

Figure 3.15 - Diagonal slice finite element model and plastic work per volume result for Tape array 144 I/O BGA

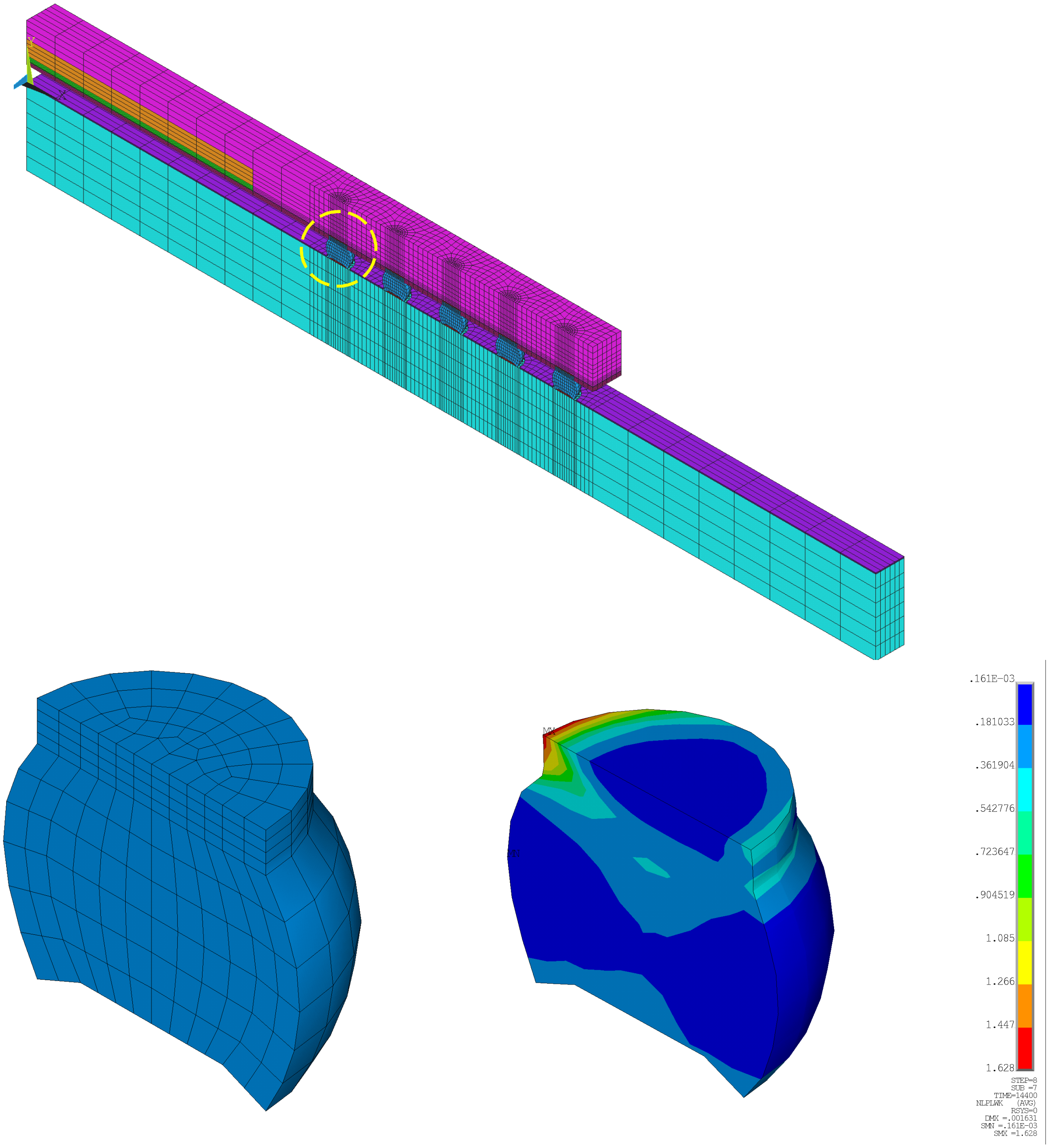

Figure 3.16 - Diagonal slice finite element model and plastic work per volume result for Flex-280 I/O BGA

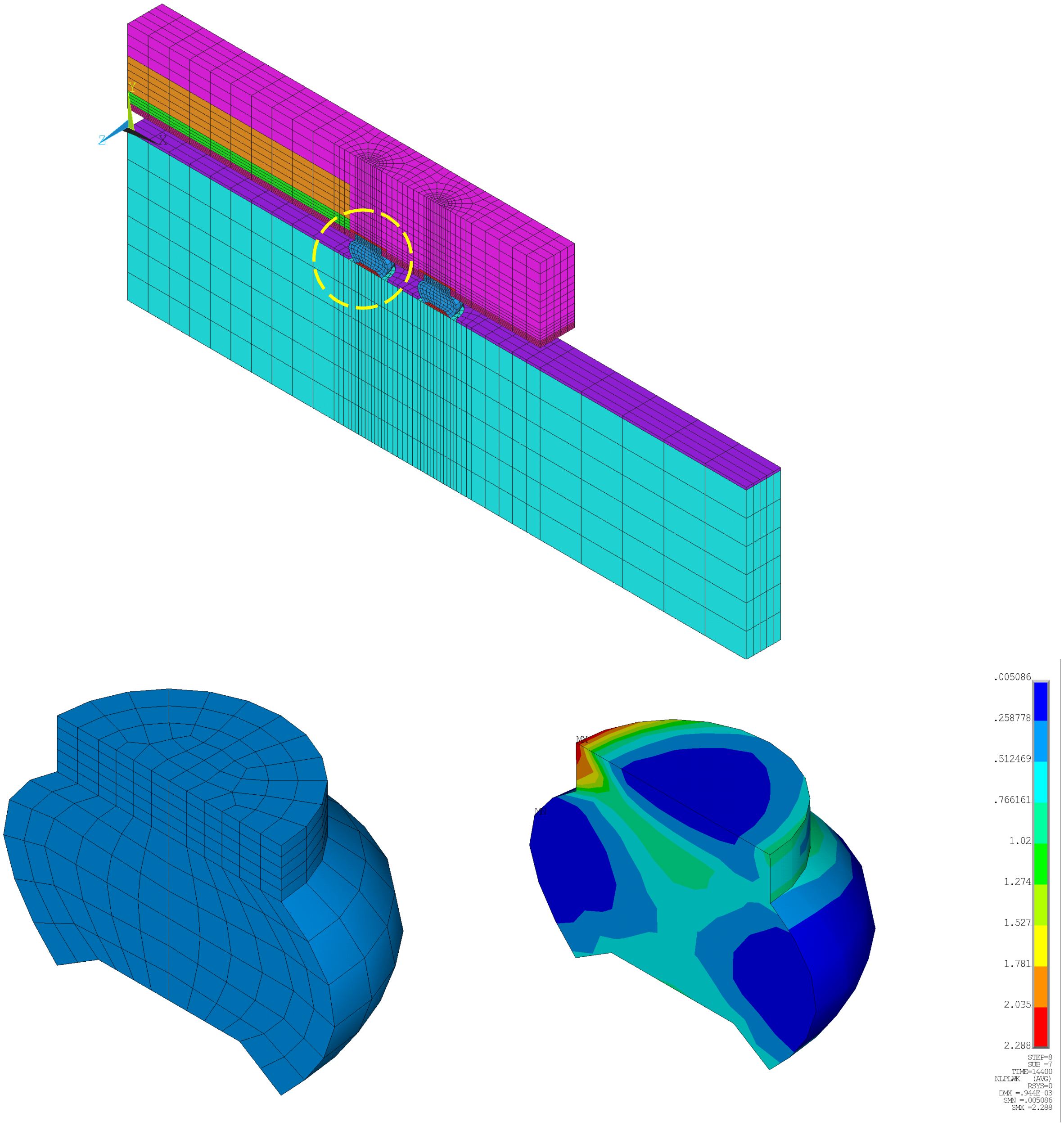

Figure 3.17 - Diagonal slice finite element model and plastic work per volume result for Tape array 64 I/O BGA

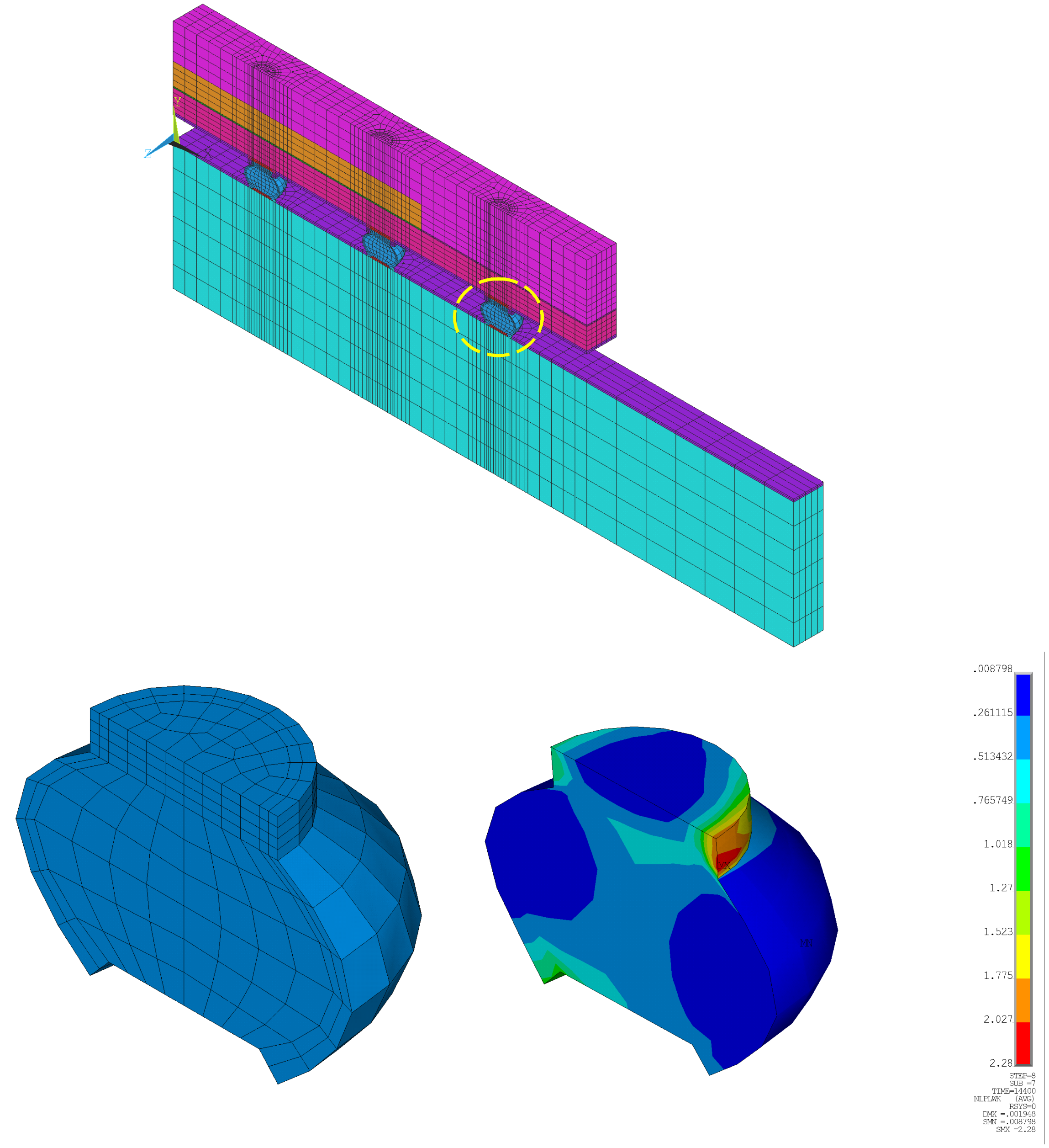

Figure 3.18 - Diagonal slice finite element model and plastic work per volume result for chip-array 84 I/O BGA

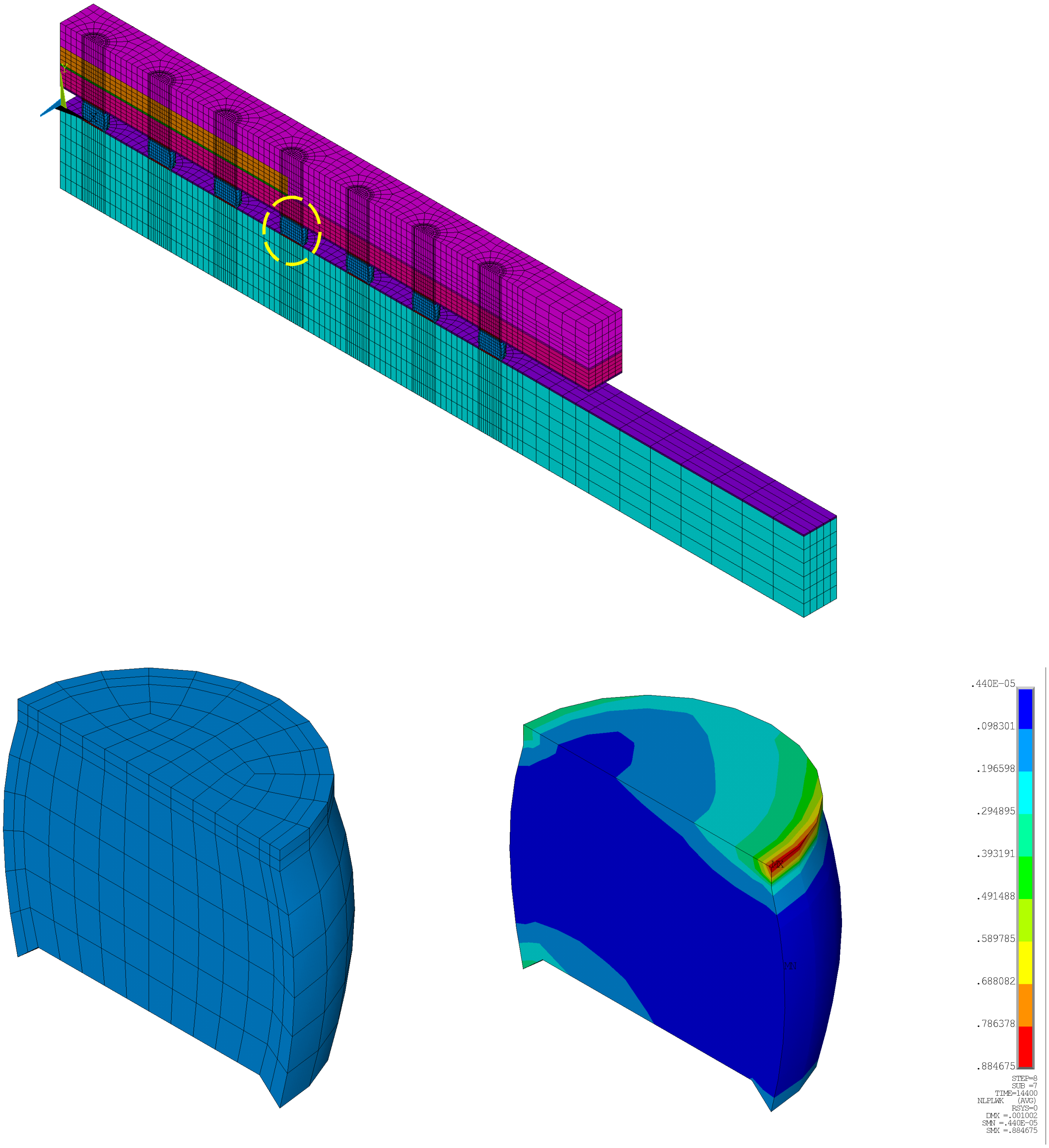

Figure 3.19 - Diagonal slice finite element model and plastic work per volume result for Plastic 196 I/O BGA

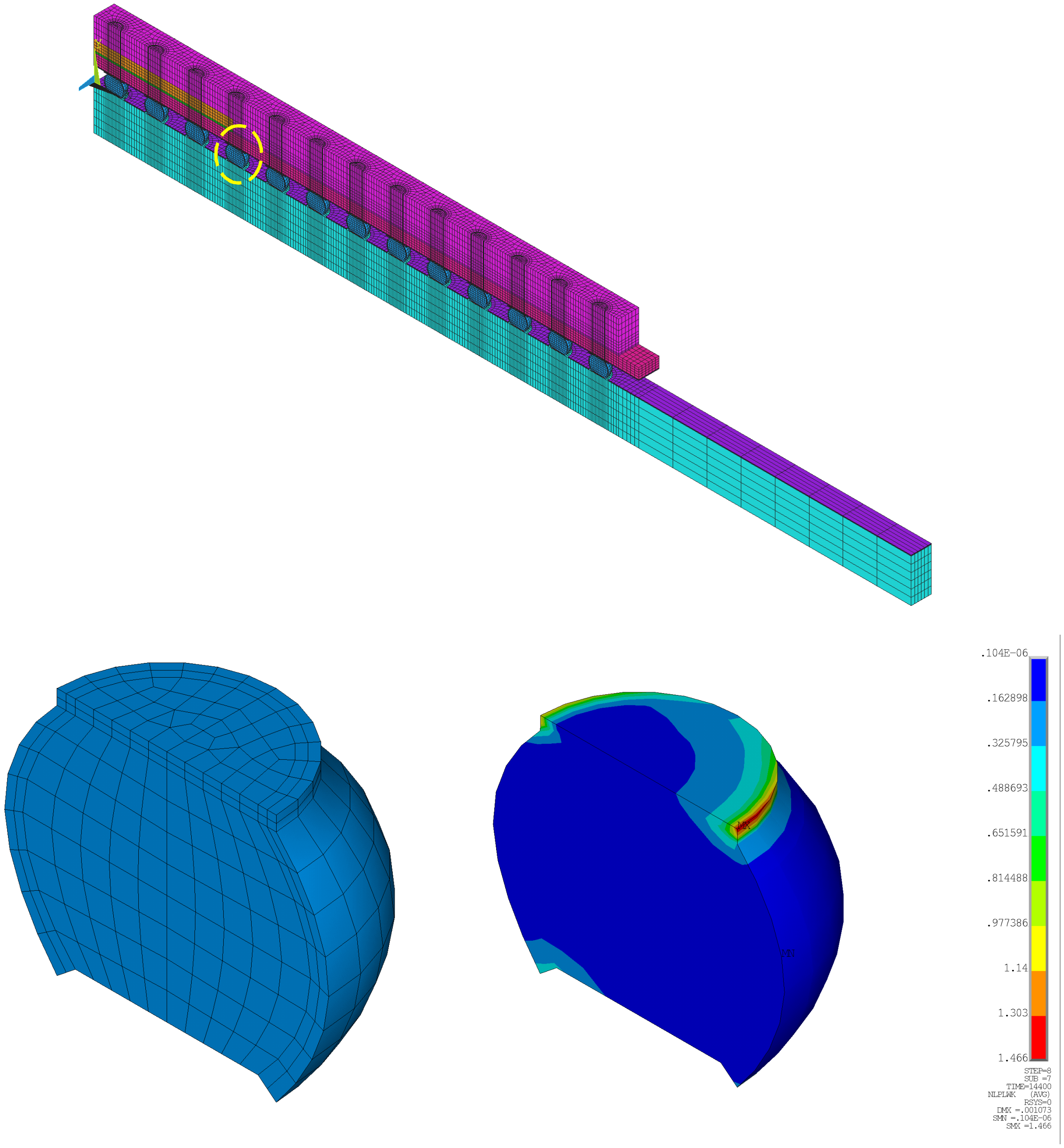

Figure 3.20 - Diagonal slice finite element model and plastic work per volume result for Plastic 676 I/O BGA

3.2.8 Solder Joint Life Prediction Model

Solder fatigue life prediction models are required for predicting the solder joint life cycle to failure. Low cycle fatigue approaches employing inelastic strain-based, or inelastic energy-based fatigue models are often used. However, there is a lack of fatigue database for lead-free solders. In this thesis, Morrow's energy-based model [Morrow 1964, Morrow 1965] which uses inelastic strain-energy to estimate the fatigue life has been used. The model predicts the fatigue life N_f in terms of inelastic strain energy density W_{avg} as shows below

$$N_f = C_1(\Delta W_{avg})^{C2} \tag{3.13}$$

Where C_1 is the material ductility coefficient and C_2 is the fatigue exponent. The inelastic strain energy density was determined from the area within the stable hysterisis loop. Zahn, et al. [2003] has already investigated the constant value C_1 as 1722.33 Cycles/Mpa^{C2} and C_2 as -0.1492 for 95.5Sn4.0Ag0.5Cu solder alloy using experiment and finite element analysis results.

The solder joint is subjected to a complex state of multi-axial stress-strain response during thermal cycling and the equivalent stress-strain concept is required to represent the multi-axial state of stresses and strains in the solder joints. From the experimental results, the interface between the solder and silicon chip is the sensitive region to failure. Solder joint fatigue failure is due to the cyclic plastic and creep strain damage leading to crack initiation and propagation. Hence the plastic work or inelastic strain energy density ΔW_{avg} is extracted as a fatigue parameter, at the top layer of the solder elements. ΔW_{avg} in the strain concentration area is very sensitive to the local mesh density. To minimize the mesh sensitivity and stress/strain singularity, element volume averaging technique is used in this modeling. In order to calculate the inelastic strain energy density, thermo-mechanical analysis has been simulated in ANSYS using the same temperature profile as in the thermal chamber. Analysis has been performed till stabilization of hysterisis loop is found for the critical solder ball. Volumetric average of inelastic strain-energy density accumulated per cycle for the critical ball where the crack propagates is given by:

$$\Delta W_{avg} = \frac{\sum_{k=1}^{N} \Delta W_k V_k}{\sum_{k=1}^{N} V_k} \tag{3.14}$$

Where ΔW_k is the plastic work per volume for each element and V_k is the volume of each element.

Once we know the ΔW_{avg}, Number of cycles to failure has been calculated using Equation 3.14 and it is compared with the experimental results. Table 3.4 shows the comparison of finite element result with experimental result. It is found that they correlate very well and finite element model can be used in the future to calculate the fatigue life. The life estimated in this study has been used to compare the life estimated during prognostication study of electronics.

Package	Weibull			Simulation		
	η	β	N1%	ΔW	η	N1%
PBGA 676	2566	2.38	371	0.1242	2351	340
PBGA 196	2610	8.048	1474	0.0871	2479	1400
FlexBGA 280	2662	23.61	2191	0.1432	2302	1894
TBGA 144	2475	5.51	1074	0.2312	2143	930
TBGA 64	2096	5.636	927	0.2616	2104	930
CABGA 84	1940	2.394	284	0.2754	2088	306

Table 3.4 - Comparison of fatigue life from experiment and empirical relationships

3.3 Reliability of Polymer core ball (Microperl SOL) and Copper reinforced column grid array

The reliability of electronic package is affected in part by the stresses experienced at the interconnect solder joints. Stresses are produced by virtue of a coefficient of thermal expansion (CTE) mismatch between package materials or by out-of-plane bending. Solder balls are rigid and tend to fracture under thermal fatigue and/or shock loading. Polymer core ball offer a more compliant interconnects compared to conventional solder balls, thereby increasing the thermal cycling fatigue life. In reality, some electronic components experience a very harsh environment such as under-the-hood applications. Normal solder balls can not be used in these applications because of repeated thermal cycling or vibration which create cracks in solder joints that will eventually cause a reduction in current carrying capacity. Therefore a polymer core solder ball has been invented to withstand such an environment because of their low elastic modulus and increased electrical connectivity. In this thesis, a study has been done to understand the thermo-mechanical reliability of polymer core ball under thermal cycling environment using finite element models and the fatigue law approach. The study is done using both ceramic and plastic ball grid array with conventional solder ball and polymer core ball interconnect and using eutectic tin-lead solder alloy.

Column grid array provides a more robust design for thermal cycling environment than ball grid array because the leads are designed to have a lower stiffness than a solder sphere and they have higher standoff distance between the component and the board. These two features enable the leads to flex with less stress as the dimensional expansion between the component and the board varies. A taller standoff will reduce the stress in the solder joint by the square of the distance between the component and the board [Cherian 1984]. Typically solder columns have a standoff height of approximately 2.2 mm and typical solder spheres will have a standoff of approximately 0.64 mm. This change in standoff reduces the stresses by a factor of 4 [Winslow 2005]. Additional reductions are achieved because the solder columns are smaller in diameter and, therefore have a lower overall stiffness. This actually provides significant improvements in second-level reliability. There are three basic types of solder column technologies in the market today, they are the wire column, the solder column interposer and the reinforced solder column. In this thesis, thermo-mechanical reliability of copper reinforced solder column has been studied using Finite-Element method. This column consists of a high-lead solid wire core spiral-wrapped with a copper ribbon. The column material is encapsulated with eutectic tin-lead solder. The advantage of this type of solder column is that the spiral copper ribbon adds redundancy without significant increase in stiffness. And also the typical failure mechanism of solder column near the taper of eutectic filet has been abated by the copper reinforcement allowing the component to continue functioning long after the high-lead core has cracked.

3.3.1 Polymer core ball [Microperl SOL^{TM}] Reliability

Polymer core balls are available in a wide range of diameters and plating thickness as shown in Figure 3.21 [Sekisui 2005]. The plastic material decomposition temperature is rated at 447°C.Thus the plastic material is able to withstand the 230 to 270°C reflow temperatures. From a mechanical standpoint, these interconnects offer an attractive means for extending the second level interconnect reliability compared to conventional solder alloys, However, a second level interconnect made from an insulating material raises several practical concerns. Mainly, will the copper plated insulating sphere meet the electrical impedance requirements while not greatly reducing the thermal performance?

In this thesis, an effort has been made to understand the thermo-mechanical reliability of these interconnects when it has been used with plastic packages and also with ceramic substrates, using finite element analysis. These polymer core solder joint failures occur by similar damage mechanisms commonly observed for standard tin-lead solder joints. Shown in Figure 3.22 [Galloway 2005] is a cross-sectioned view of failed 300μm diameter polymer core interconnects. A crack was formed near the pad interface on the package side and propagated through the solder filet. Therefore, methodology used to model the thermo-mechanical reliability model of tin-lead solder has been used.

3.3.2 Finite Element Models for Microperl SOL^{TM} with ceramic substrate

A three-dimensional diagonal symmetry slice model has been created for Microperl SOL with ceramic substrate in ANSYS for both Microperl SOL^{TM} and conventional solder ball. The dimension used for Microperl SOL^{TM} is 500/20/30μm i.e. 500 μm plastic core, 20 μm thickness copper surrounds the plastic core and 30 μm is eutectic solder thickness surrounds the copper plate. At the same time conventional solder ball is modeled with 540 μm diameter high-lead solder. Total height of the solder is 600 μm, the package dimension is 21 mm, and ball pitch is 1 mm in both the cases. The package has 400 I/O count. Table 3.5 has the material property information used for modeling the ceramic ball grid array package. A thermo-mechanical finite element analysis on these packages using the temperature profile is performed to simulate the effect in the thermal chamber with temperature varying between -40°C to 125°C. Thermal cycling is simulated until the inelastic strain energy density in the critical solder ball stabilizes. Figure 3.23 and Figure 3.24 show the finite element model and plastic work per volume for CBGA with Microperl and CBGA with conventional solder ball.

Since there were no experimental results to compare the reliability of these models, plastic work accumulated per volume vs. time and hysterisis loop accumulated for both package architectures has been compared. Figures 3.25 and 3.26 show the plastic work per volume vs. time and hysterisis loop comparison respectively. It can be concluded from the graph that there is very increase in the reliability of CBGA package with Microperl SOL^{TM} when compared to conventional solder ball.

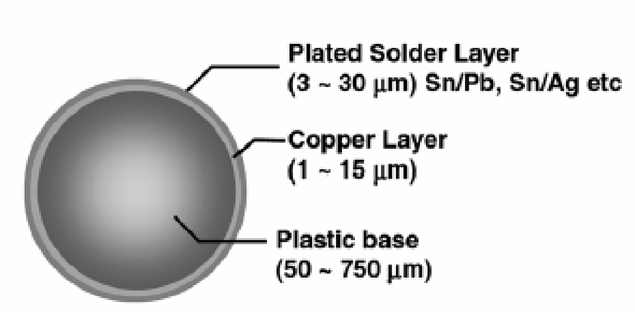

Figure 3.21 - Polymer core solder ball showing its plating layer [Sekisui 2005]

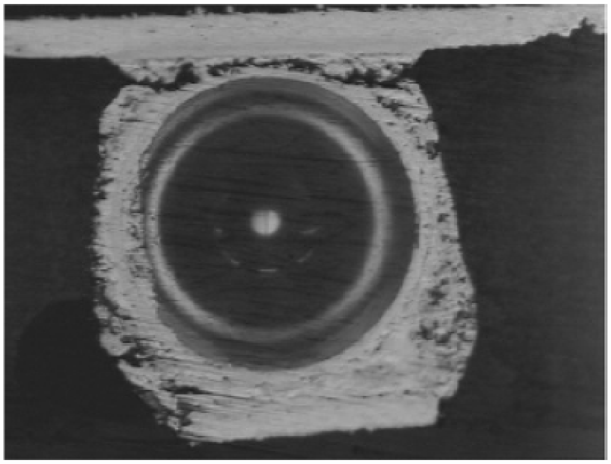

Figure 3.22 - Typical failures in the polymer core solder ball [Galloway 2005]

Material	**E(Mpa)**	**PR**	**CTE ppm/ºC**	**G(Mpa)**
Ceramic(Al203)	276000	0.3	6.7	
Solder Mask	3100	0.3	30	
Solder(63Sn37Pb)	30550	0.35	24	
HighLead(90Pb10Sn)	19000	0.316	27.6	
Copper	128932	0.34	16.3	
Plastic Core	9000	0.38	20	
PCB	27924-37T (X&Z)	0.39(XY&YZ)	14.5(X&Z)	12600-16.7T (XZ)
	12204-16T (Y)	0.11(XZ)	67.2(Y)	5500-7.3T(YZ&XY)
Anand Parameter	**Symbol**	**63Sn37Pb**	**90Pb10Sn**	
Initial Value of Deformation Resistance	So (MPa)	0.9358	4.72	
Activation Energy / Boltzmann's Constant	Q/R(1/K)	8400	76231	
Pre-Exponential Factor	A (1/sec)	4.61E+06	7073	
Multiplier of Stress	ξ	0.038	5.21	
Strain Rate Sensitivity of Stress	m	0.162	0.27	
Hardening Constant	ho (MPa)	3088.85	33884	
Coefficient of Deformation Resistance Saturation Value	s-hat (MPa)	1.04	25.75	
Strain Rate Sensitivity of Saturation Value	n	0.0046	0.019	
Strain Rate Sensitivity of Hardening	a	1.56	2.05	

Table 3.5 - Material Property used to model CBGA and CBGA-Microperl Package

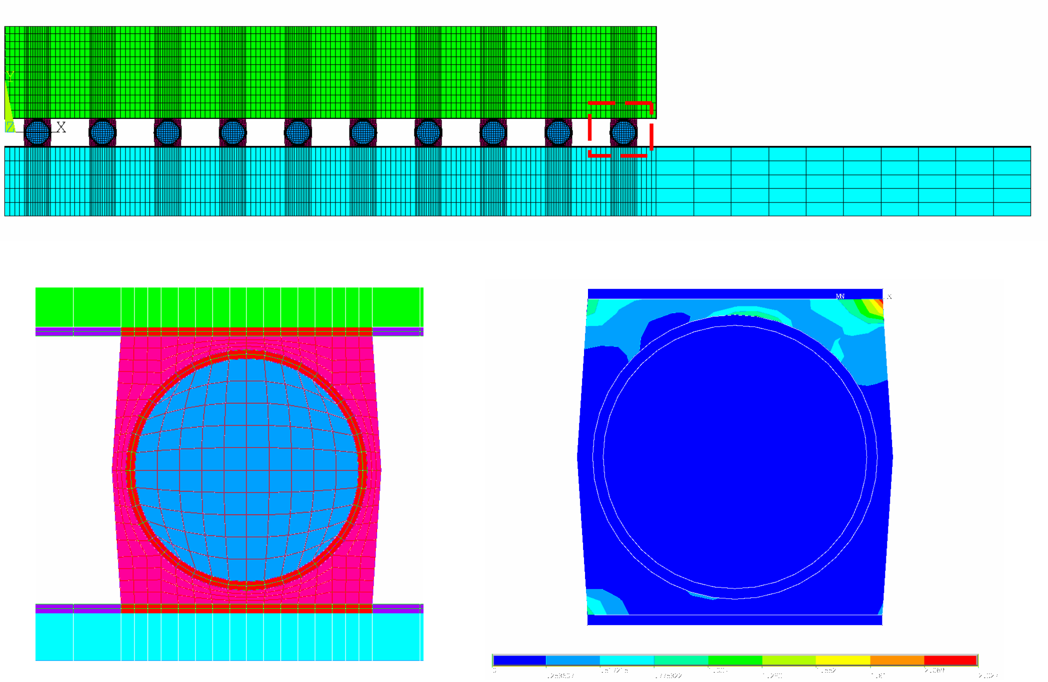

Figure 3.23 - Finite element models for CBGA package with Microperl SOL^{TM} and plastic work per volume at the corner solder ball

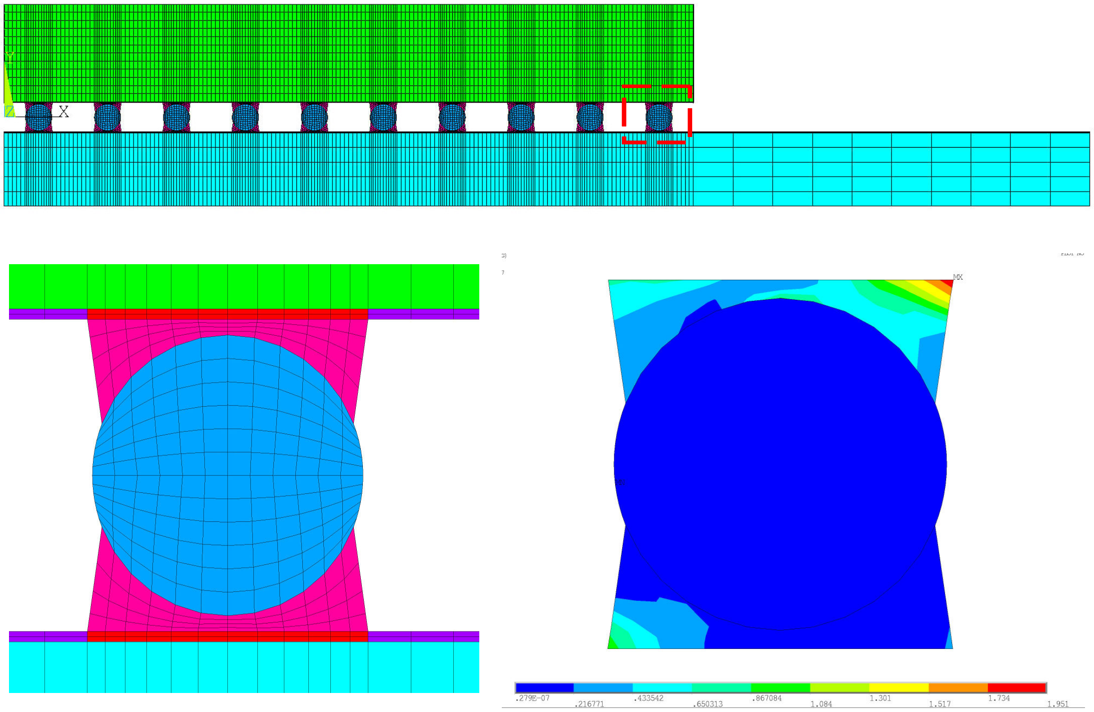

Figure 3.24 - Finite element models for CBGA package with Conventional Solder Ball and plastic work per volume at the corner solder ball

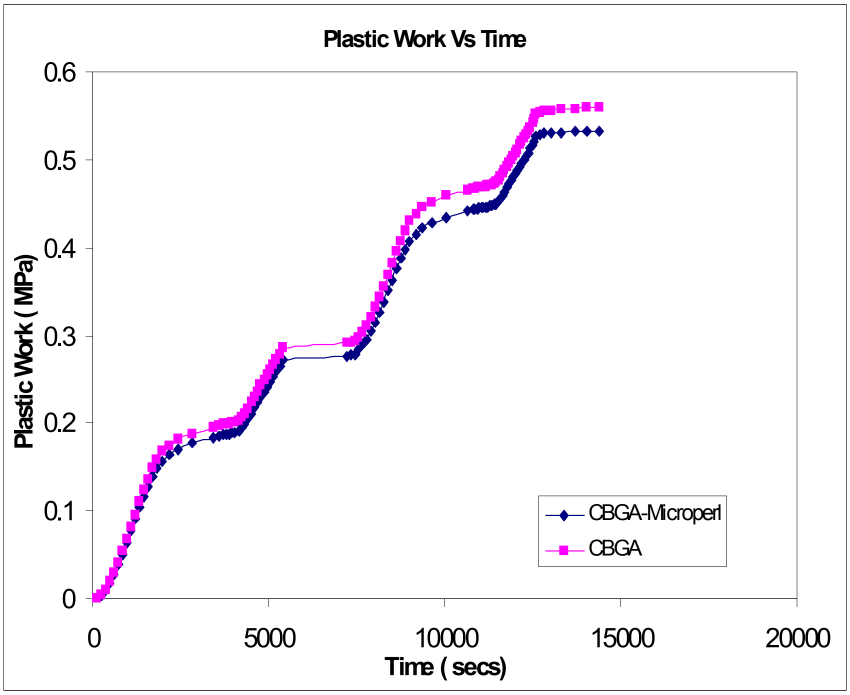

Figure 3.25 - Plastic work per volume comparison plot for Ceramic Package

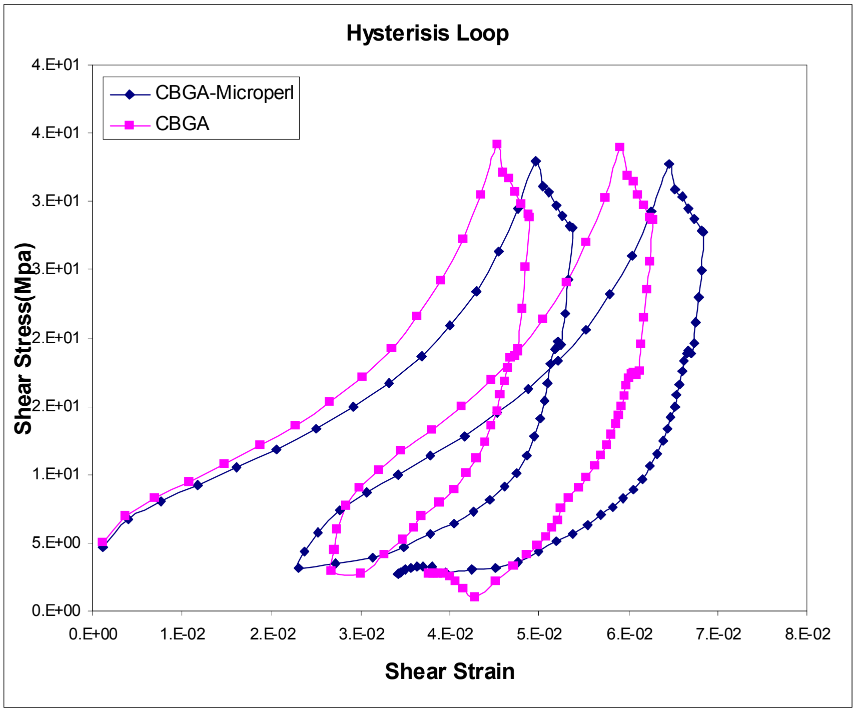

Figure 3.26 - Hysterisis Loop comparison plot for Ceramic Package

3.3.3 Finite Element Models for Microperl SOL^{TM} with Plastic package.

The same methodology has been implemented on plastic package architecture with Microperl-SOL and conventional methodology. Figure 3.25 shows the cross-sectional view of the plastic package with Microperl SOL and conventional solder ball [Sekisui 2005]. The package architecture used has 352 I/O counts with body dimension of 35mm and pitch of 1.27mm. The Microperl SOL^{TM} used in this study has 704/8/20 μm dimension, in which plastic core diameter is 704 μm, copper plate thickness surrounding the plastic core is 8 μm and eutectic solder thickness surround the copper plate is 20 μm. Figure 3.28 shows the package dimension and ball architecture. A thermo-mechanical finite element analysis has been performed on these packages using the temperature profile of -40°C to 125°C. Thermal cycling is simulated until the inelastic strain energy density in the critical solder ball stabilizes. Figures 3.29 and 3.30 show the diagonal symmetry model and plastic work per volume result for PBGA package with Microperl SOL^{TM} and with conventional solder ball.

Since there was no experimental result to compare the reliability of these models, plastic work accumulated per volume vs. time and hysterisis loop accumulated for both package architectures has been compared. Figure 3.31 and 3.32 shows the plastic work per volume vs. time and hysterisis loop comparison respectively. It can be concluded from the graph that there is slight increase in the reliability of CBGA package with Microperl SOL^{TM} when compared to conventional solder ball.

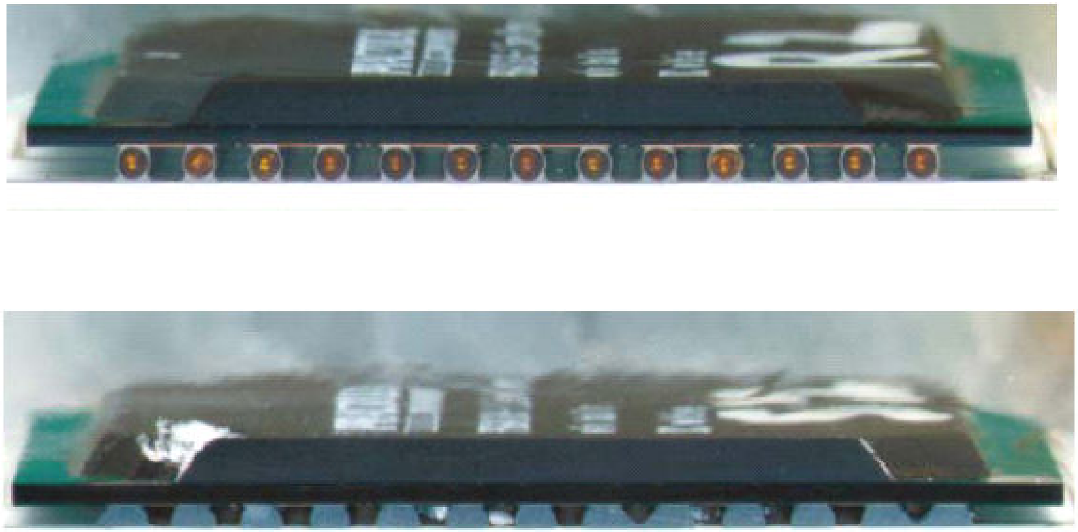

Figure 3.27 - Cross-sectional view of plastic package with Microperl-SOL and conventional solder ball [Sekisui 2005]

Package Size	35 mm
Die Size	9 mm
Pin Count	352
Pin Layout	4 rows
Ball Pitch	1.27 mm
Substrate	FR4 4 Layer
Substrate Size	1.6mm
Solder Ball	760 µm
Microperl SOL Plastic/Copper/Solder	704/8/20 µm

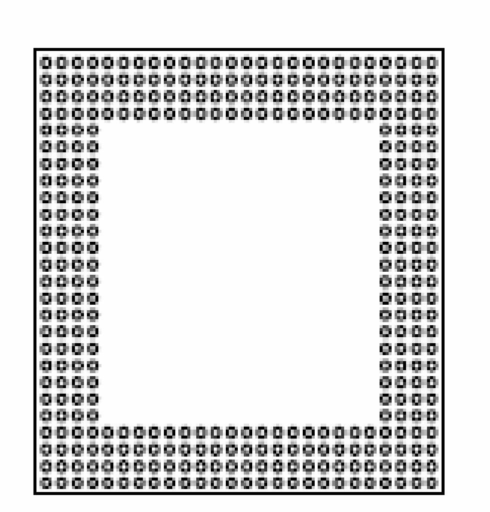

Figure 3.28 - Package Dimensions and ball layout for the PBGA package used for this study [Sekisui 2005]

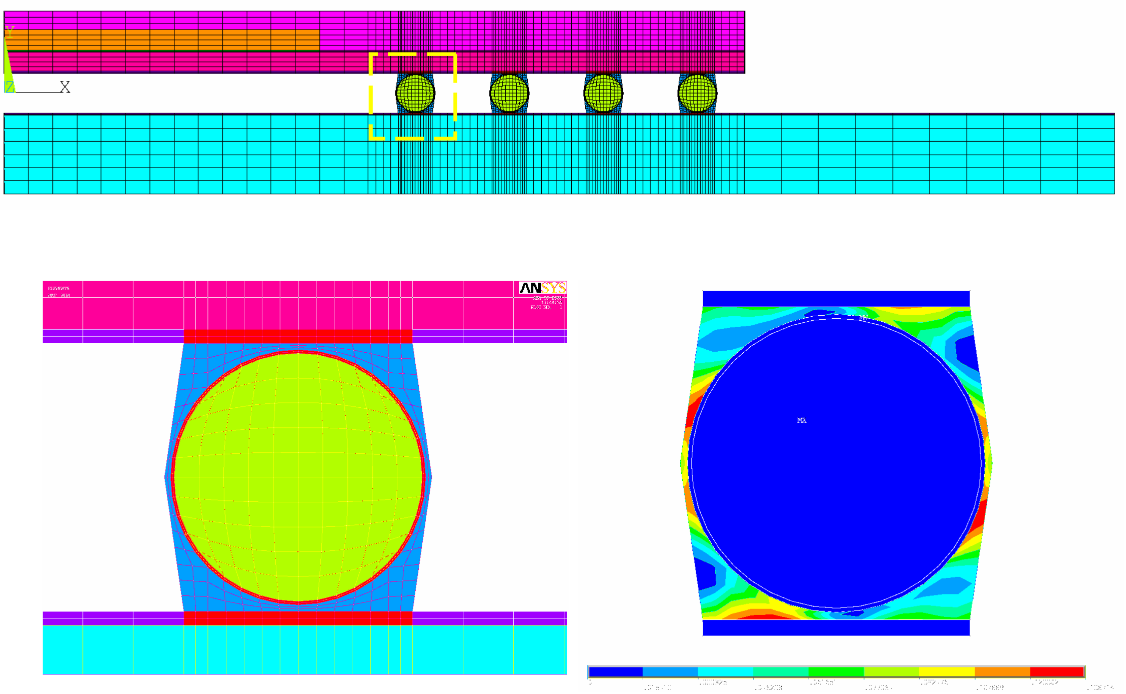

Figure 3.29 - Finite element models for PBGA package with Microperl-SOL and plastic work per volume at the corner solder ball

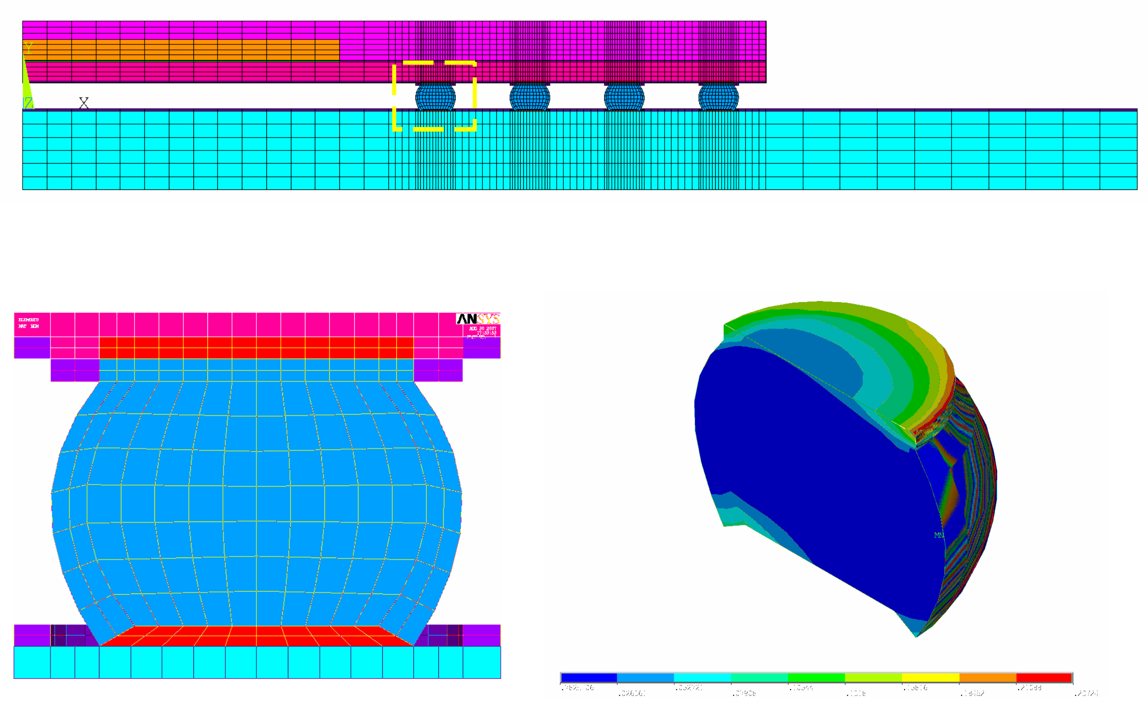

Figure 3.30 - Finite element models for PBGA package with Conventional Solder ball and plastic work per volume at the corner solder ball

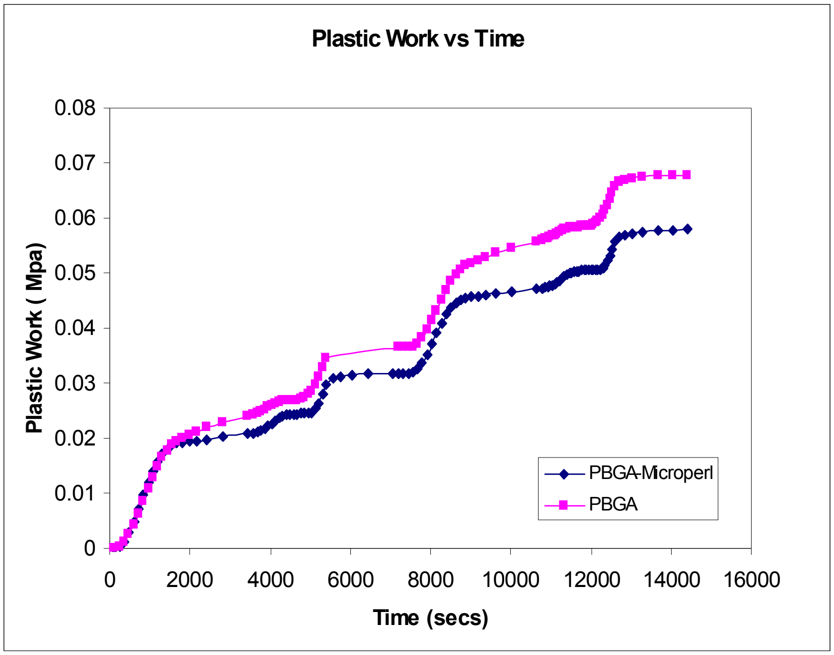

Figure 3.31 - Plastic work per volume comparison plot for Plastic Package

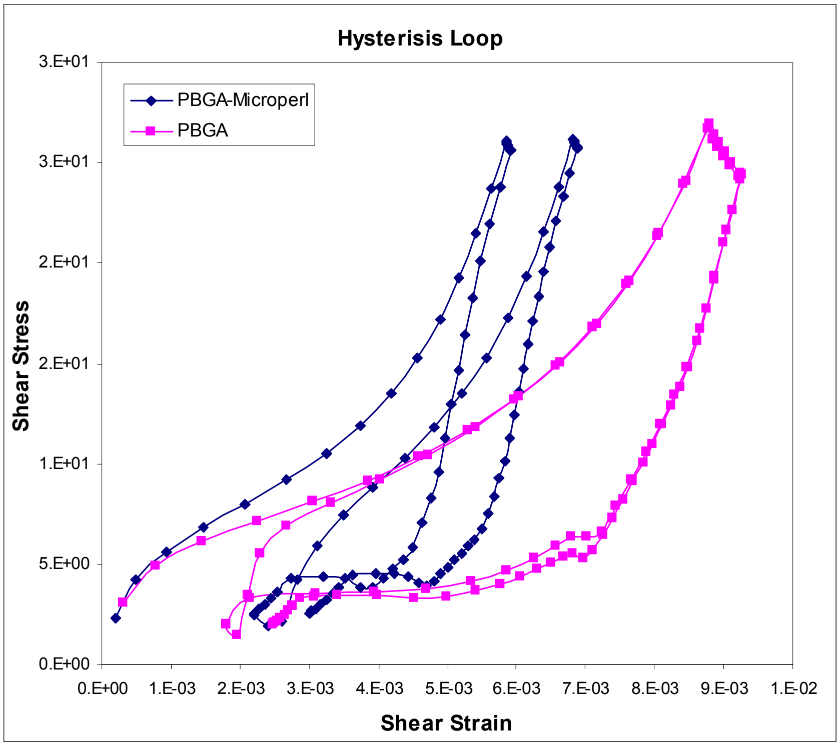

Figure 3.32 - Hysterisis Loop comparison plot for Plastic Package

3.3.4 Finite Element Model for Copper Reinforced Column Grid Array

Column Grid Array (CGA) is more reliable than Ball Grid Array because of two reasons, first, the leads are designed to have a lower stiffness than a solder sphere, and second, they have a higher standoff distance between the component and the board. There are various types of columns available in the market. Many Researchers [Sinha 1997, Master 1995, Ingalls 1998] have studied the thermo-mechanical reliability of Non-reinforced columns using experiment and finite-element analysis. In this thesis, Copper Reinforced Column Grid Array reliability using finite-element method has been studied. A finite-element model has been developed in ANSYS and temperature-cycle analysis from -40°C to 125°C has been performed. The in-elastic strain energy density from the maximum strained column to calculate the number of cycles required to initiate the crack has been extracted and has been used to calculate the crack propagation rate.

The reinforced column is a wire made by wrapping the high-lead solder wire with a tin plated copper ribbon and the wire is then passed across a wave of eutectic solder to encapsulate it. The reinforced column is shown in Figure 3.33. The cross-sectional view of the reinforced CGA is shown in Figure 3.34. The package size is 21 mm; pitch of column is 1 mm and has 400 I/O Ceramic Package. The height and diameter of the column is 87 and 15 mils respectively. The copper ribbon has rectangular cross-section and its dimensions are 12 mils height and 1 mil width. Figure 3.35 and 3.36 show the diagonal symmetry finite element model and plastic work per volume. Plastic work per volume vs. time and hysterisis loop vs. time have been plotted and the results have been compared against the CBGA package and CBGA-Microperl SOL^{TM} package results as shown in Figures 3.37 and 3.38. It is observed that the Reinforced Column has less plastic work accumulated and small area under the hysterisis loop as compared to other packages.

Figure 3.33 - Picture showing the copper ribbon spirals, the high-lead solder and column after wave soldering [Winslow 2005]

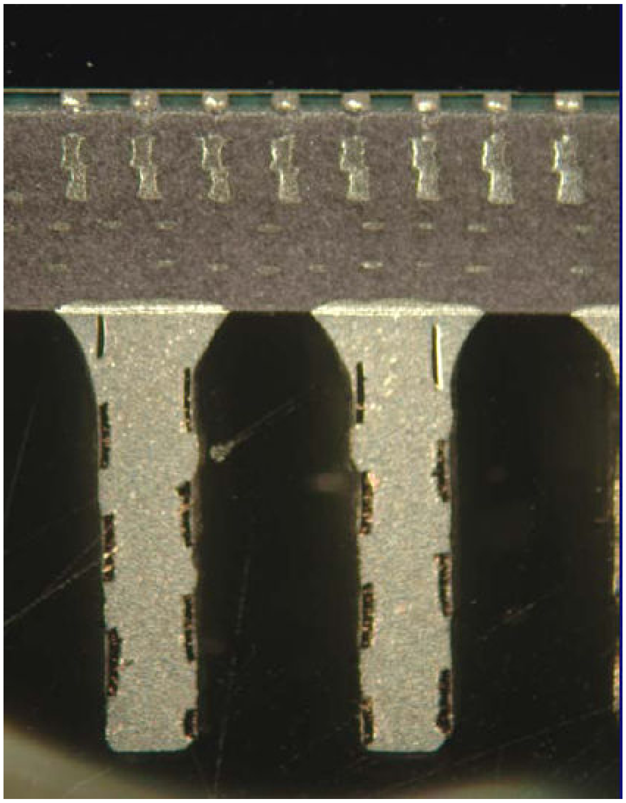

Figure 3.34 - Cross-sectional view of the copper reinforced solder column after reflow [Winslow 2005]

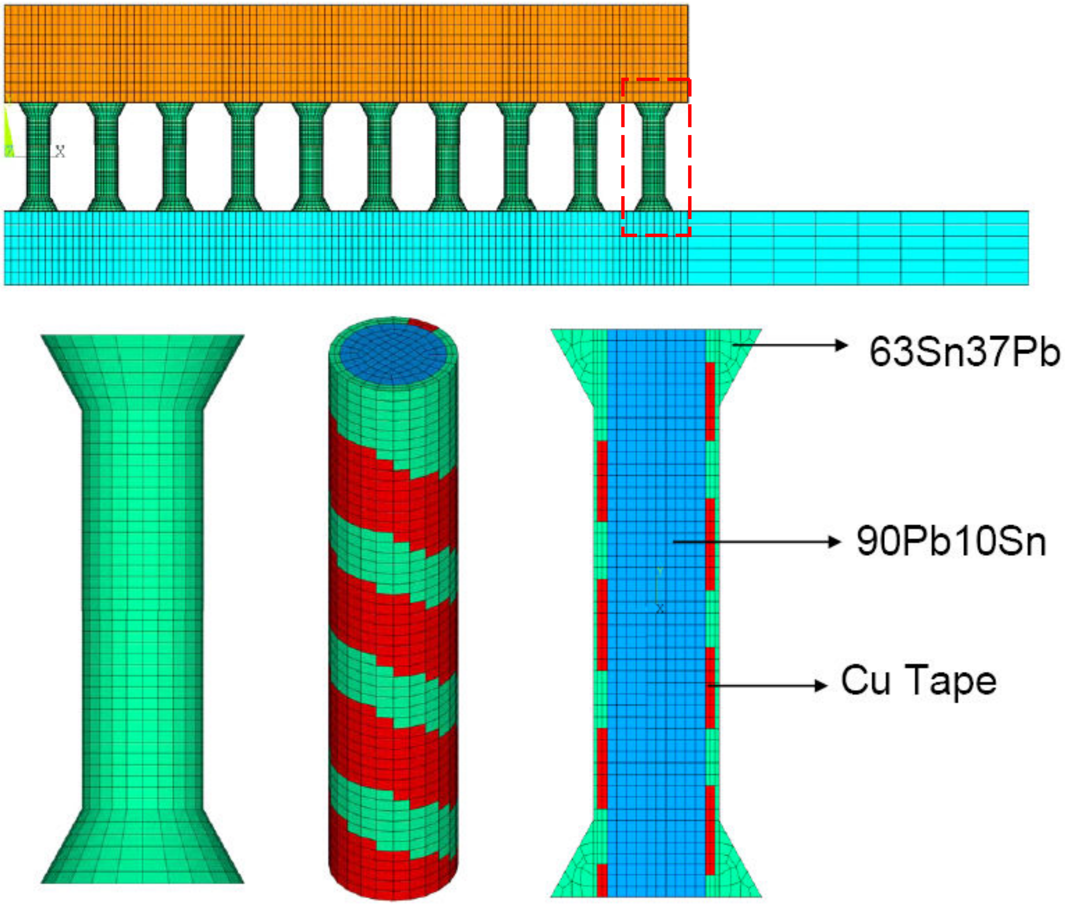

Figure 3.35 - Diagonal symmetry finite element model for copper reinforced Column Grid Array

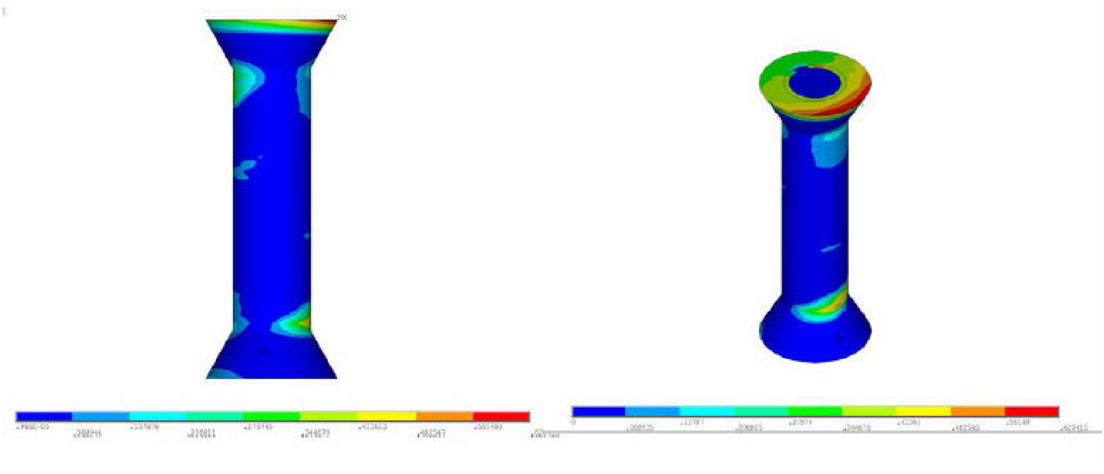

Figure 3.36 - Plastic work per volume of the maximum strained solder column

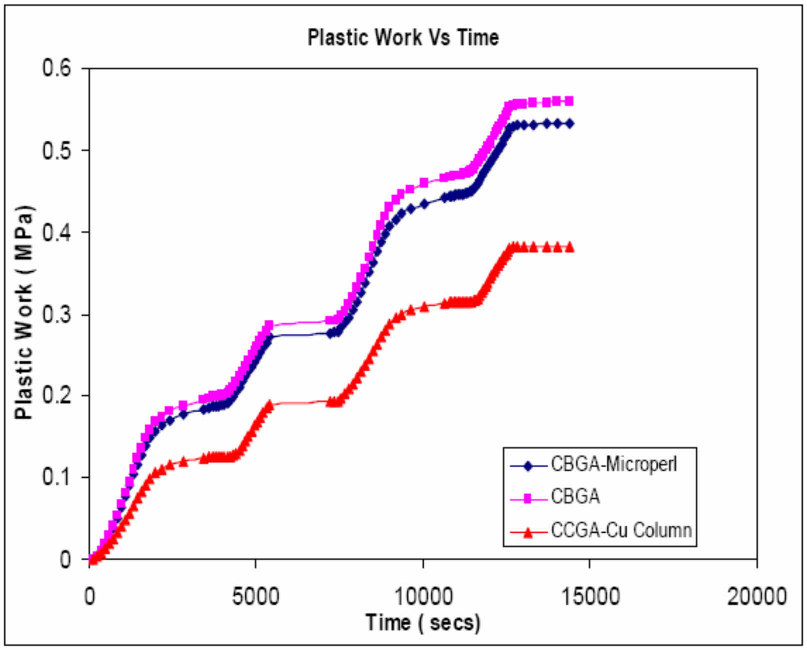

Figure 3.37 - Plastic work per volume vs. time comparison for CBGA, CBGA-Microperl, and Copper Reinforced Column Grid Array

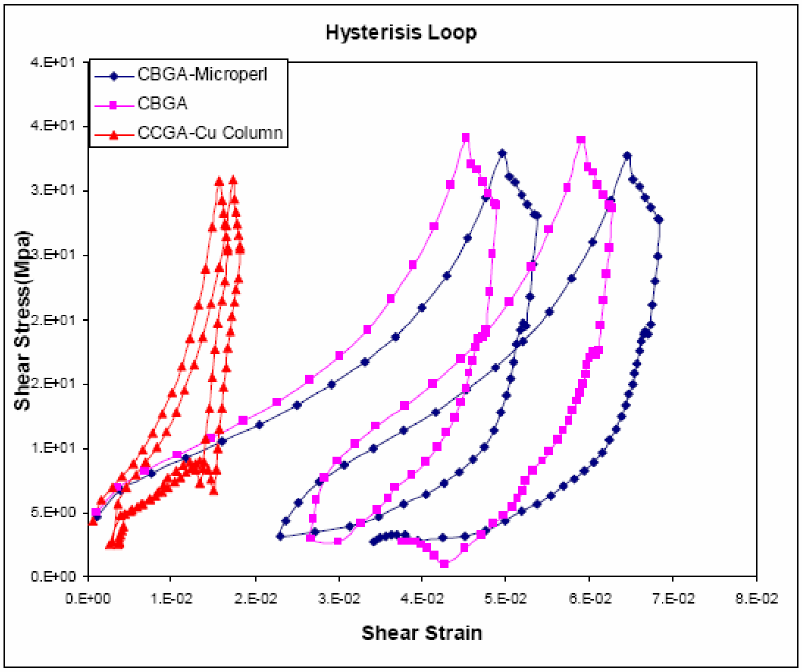

Figure 3.38 - Hysterisis loop Comparison of CBGA, CBGA-Microperl, and CCGA-Copper Reinforcement

3.3.5 Thermal Fatigue Life Prediction

Darveaux et al. [2000] developed a model to predict the crack initiation and crack propagation using in-elastic strain energy density obtained from finite element model. According to this model the crack initiation life and crack propagation rate is related by power law as shown below

$$N_i = K_1(\Delta W)^{K_2} \tag{3.15}$$

$$\frac{da}{dN} = K_3(\Delta W)^{K_4} \tag{3.16}$$

Table 3.6 shows the constants K_1, K_2, K_3 and K_4 [Lall 2003]. Since the crack growth rate is constant during the thermal cycling, the fatigue life of a joint can be calculated by adding the number of cycles to grow the cracks across the joint interface. The characteristic life can be expressed as

$$\alpha_w = N_i + \frac{a}{da/dN} \tag{3.17}$$

Where "a" is the joint diameter at the interface. Darveaux [2000] found that the maximum crack length in the population was approximately one half of the characteristic length. The characteristic crack length can be defined as the total joint diameter of the solder ball with cu pad. So it has been decided that the failure free life is approximately one half of the characteristic life.

$$N_0 = \alpha_w/2 \tag{3.18}$$

This methodology has been used to calculate the crack initiation life and crack propagation rate from finite element result for CBGA, CBGA-Microperl, PBGA, PBGA-Microperl and CCGA- Copper Reinforced packages. The result is shown in Table 3.7.

	Crack Initiation and Propagation Constant			
	K1 (Cycles/ Mpa^K2)	K2	K3 (mm/Cycles- Mpa^K4)	K4
CAVE data	14.062	-1.53	6.97E-04	0.7684

Table 3.6 - Crack Initiation and Propagation Constants [Lall 2003, Islam 2005]

Package	**ΔW (Mpa)**	**a (mm)**	**No (cycles)**	**da/dN (mm/Cycles)**
CBGA	0.2685	0.5635	105	2.54E-04
CBGA-Microperl	0.2564	0.5635	113	2.45E-04
PBGA	0.0314	0.6628	2807	4.87E-05
PBGA-Microperl	0.0261	0.6628	3725	4.23E-05

Table 3.7- Fatigue Life for BGA and BGA-Microperl

3.4 Summary and Conclusion

In this work, the reliability of Plastic Ball Grid Array, Flex-substrate Ball Grid Array, Tape-array Ball Grid Array and Chip-array Ball Grid Array with 95.5Sn4.0Ag0.5Cu solder alloy, under thermal cycling environment from -40°C to 125°C has been studied using experiment and finite-element approach. The study showed a good correlation between the experiment and finite-element method of finding out the fatigue life. The life obtained in this study has been used as a benchmark to the one obtained during prognostication study in later chapters. There is a difference in the fatigue life because of the approximation used in finite element models e.g. diagonal symmetry model to reduce the computation time, solder ball is assumed to be of the same shape throughout, intermetallic compound has been ignored in the finite element model and also the constitutive relationship is based on bulk solder material than the actual solder joint etc. Also the non-linear least square method algorithm has been developed to estimate the material parameters for Anand Viscoplastic model to be used in ANSYS for any solder alloy using their material characterization data.

The reliability of various types of second level interconnections like Ceramic Ball Grid Array, Ceramic Ball Grid Array with Microperl SOL^{TM} (Polymer core solder ball), Ceramic Column Grid Array with copper reinforced columns, Plastic packages with Microperl SOL^{TM} and conventional solder balls using finite element model and constitutive fatigue law have been investigated. Comparison of the plastic work per volume and hysterisis loop for maximum strained solder ball has also been done for all the packages. It is found that the column grid array has less plastic work per volume and small area under the hysterisis loop compared to other packages. Therefore it can concluded that it is more reliable than the other packages. Amongst Plastic packages with Microperl SOL^{TM} and conventional solder ball, Microperl SOL^{TM} shows significantly higher reliability than other packages. But in Ceramic packages the difference is very small. However the results could be verified if the experiment results were available.

CHAPTER 4

FEATURE EXTRACTION AND DAMAGE-PRECURSORS FOR PROGNOSTICATION OF LEAD-FREE ELECTRONICS

4.1 Introduction

Health Management of electronic systems requires knowledge of impending failure. Presently, acquisition of mechanical system-diagnostics has been successfully achieved for automotive applications through an elaborate system of fault codes. The state-of-art health management systems focus on detection and isolation of faults and failures, and are largely reactive in nature, limiting the scope of maintenance decisions. In this thesis, the focus is health management methodologies for electronic systems in thermal cycling harsh environment applications, based on system-level prognostication to facilitate assessment of residual life. The reliability of electronic control and safety systems in harsh environment applications, such as automotive safety systems, can be significantly impacted through development of methodologies for monitoring the degradation and understanding damage evolution to enable avoidance of system-level failures. Challenges in implementing prognostics can be attributed to the lack of understanding of the underlying component degrading mechanisms.

In this thesis, investigation of the changes of the features as well as time-evolution of physical damage and the relationship between physical damage and feature-set has been established for thermo-mechanical stresses. Damage pre-cursors based residual life computation approach for various package elements has been developed, to prognosticate electronic systems prior to appearance of any macro-indicator of damage. This is shown in Figure 4.1. In order to implement the system-health monitoring system, precursor variable or leading indicators-of-failure have been identified for various package elements and failure mechanisms. Model-algorithms have been developed to correlate pre-cursors with impending failure for computation of residual life. The correlations serve a basis for interrogation of damage-state and extraction of features quantifying underlying degradation. Examples of damage pre-cursors include phase-growth, intermetallic thickness, and patterns in interfacial stress distributions. Change in damage pre-cursors are sensed through a network of system-state monitors. Mathematical relationships have been developed for computation of residual life, based in terms of damage proxies. Use of interfacial stress variation as a prognostic parameter has been discussed in [Lall 2004[b], 2005, 2006[a,b], 2007[a,b]].

The damage precursor based damage computation approach eliminates the need for knowledge of prior operational stresses and enables health management of deployed non-pristine electronic systems under unknown prior-loading conditions. The approach is powerful, since it reduces the demands on electronic system field-usage and deployment logistics required for acquisition of prior stress histories. Use of pre-cursors for damage computation addresses the limitation of existing life-prediction models like Paris's Power Law [Paris 1960, Paris 1961], Coffin-Manson Relationship [Coffin 1954] and the S-N Diagram, which target damage estimation for known stress histories imposed on pristine materials.

Reconstruction of operational profiles is often challenging and future operational profiles are often unpredictable. In addition, it may not be always possible to characterize the operational loads under all possible scenarios (assuming they are known and can be simulated). Damage pre-cursors target fundamental understanding of underlying degradations in electronic systems, such as thermo-mechanical interconnect-fatigue, interfacial delamination of underfills etc. Once identified for specific package elements and failure mechanisms, the pre-cursors are scalable for future package architectures and for application across a broad spectrum of design.

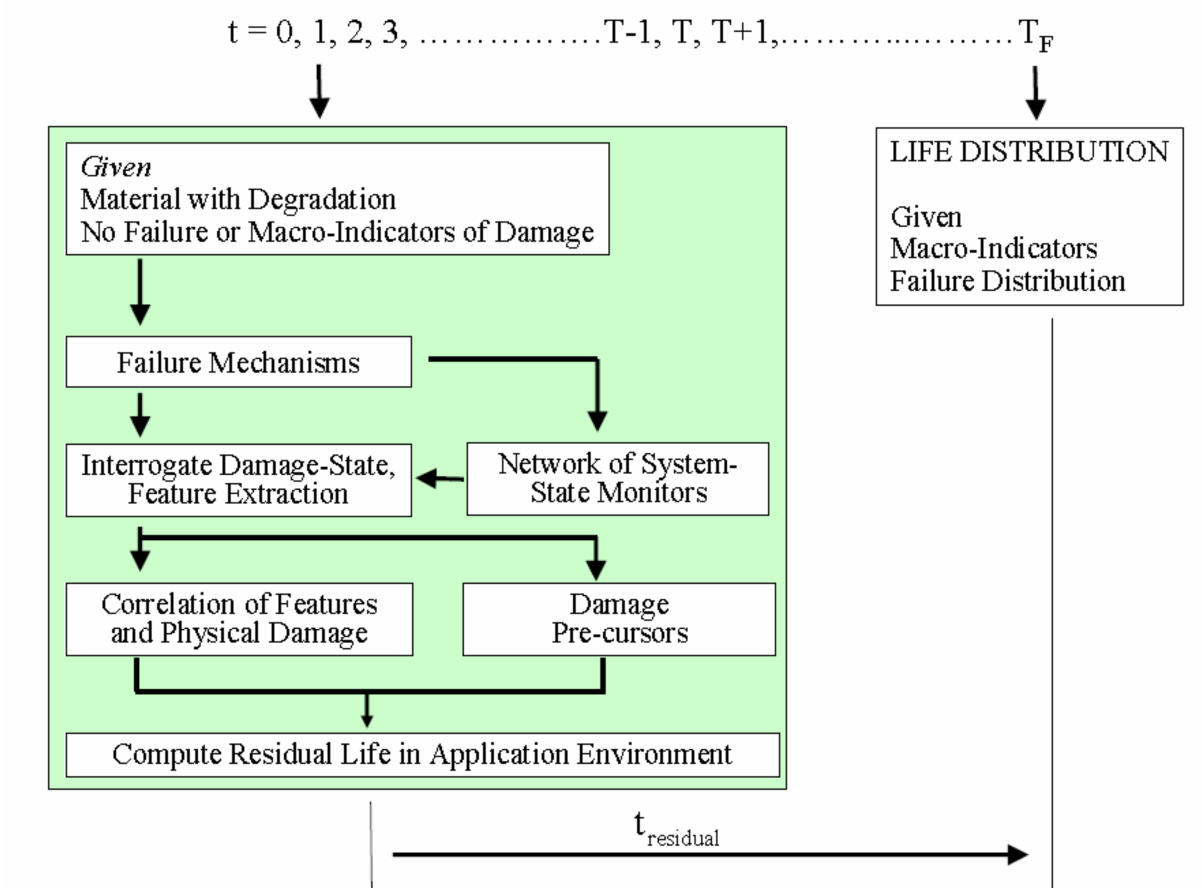

Figure 4.1: Damage pre-cursor based methodology for prognostication of electronic systems

4.2 Solder micro-structural coarsening as a leading indicator of failure

Solder micro-structural coarsening which is also know as Phase growth has been used as a leading indicator of failure in this study. Previously several researchers reported that the micro-structural coarsening impacts the solder interconnect fatigue damage. Micro-structural coarsening during thermo-mechanical deformation is attributed to the generation of excess vacancies caused by the combined effect of local hydrostatic state of stress (σ_h) and the instantaneous inelastic strain rate (ε) [Dutta 2003^{a}, 2003^{b}, 2004]. Previous researchers have examined changes in microstructure occurring in the Sn63/Pb37 and lead-free chip resistor solder joints during thermal cycling [Sayama 1999, 2003],investigated the grain-size evolution and derivatives of phase growth rate as prognostics parameter on a wide range of leaded devices in underhood applications [Lall 2005, 2006^{a,b}, 2007^{a,b}],correlated thermal fatigue with occurrence of micro-structural coarsening in the fatigue damaged region in 63Sn37Pb solder interconnects [Morris 1991, Frear 1990].Correlation of grain coarsening with thermal fatigue has also been established for high-lead solders [Bangs 1978, Wolverton 1987, Tribula 1989]

In this study, changes in solder microstructure and its derivatives have been investigated as leading indicators of failure. Quantitative metrics of changes in microstructure have been identified and relationships have been developed to represent damage progression. Data presented covers a wide range of 95.5Sn4Ag0.5Cu lead-free packaging architectures and discrete devices in extreme temperature cycling and steady-state temperature environments. The phase growth parameter has been defined as the relative change from phase-state after reflow, instead of the absolute value of phase state. The fundamental reason for selection of phase growth and its derivatives is that super plastic alloys are usually made up of fine grain structure. Therefore a considerable growth of the matrix grains and the second phase particles frequently occurs during high temperature deformation. The grain growth rate is found to increase with increasing strain rate. Callister et al. [1985] states that for many polycrystalline materials phase size varies with time according to the following relation

$$g^n - g_0{}^n = Kt \qquad 4.1$$

where *g* is the grain size at time *t*, and g_0 is the initial grain size, and *K* and *n* are time-independent constants. The value *n* generally varies between 2 and 5. The process of the particle growth induced by volume diffusion was theoretically analyzed by Lifshitz et al. [1961]. It was reveled that the variation of the average particle radius with time is

$$r^4 - r_0{}^4 = B_1 \frac{\gamma \Omega C_0 D_b}{RT} t \qquad 4.2$$

where *r* is the average particle radius, r_0 is the initial radius of an average particle, B_1 is the parameter related to the volume fraction of the particles, γ is the free energy per unit area of the phase boundary, Ω is the molar volume of the particle phase, C_0 is equilibrium solute concentration near the phase boundary. D_b is the coefficient of solute diffusion in the phase boundary. *R* is the gas constant, *T* is the absolute temperature, and *t* is time [Senkov 1986] Applied the theory of the phase growth process of a superplastic alloy and validated it for the Zn/Al eutectic alloy. They expressed the evolution of the average phase size *g* with time as shown below

$$g^4 - g_0^4 = \frac{B\delta \Omega C_0 D_b}{RT} t \qquad 4.3$$

where g_0 is the initial average phase size, B is the phase geometry parameter, δ is the phase boundary width. Dutta et. al. [Dutta 2003^a, 2003^b, 2004] represented the total vacancy concentration at any location with in the solder joint at any instant of t as the sum of the equilibrium vacancy concentration and vacancy concentration under applied instantaneous strain rate.

$$n_{total} = n_{eqlm} + n_{strn}$$
$$n_{eqlm} = \exp\left(\frac{-Q_{f,v}}{kT}\right)\exp\left(\frac{\sigma_h\Omega}{kT}\right) \qquad 4.4$$
$$n_{strn} = \exp\left(\frac{-Q_{f,v}}{kT}\right)\exp\left(\frac{\sigma_h\Omega}{kT}\right)N\dot{\varepsilon}\left[1-\exp\left(\frac{-t}{\tau_c}\right)\right]$$

Here, $Q_{f,\,v}$ is the enthalpy of formation of a vacancy, Ω is the molar volume, τ_c is the time constant associated with the decay of a vacancy following formation, and N is a constant that scales the vacancy concentration to ε. Based on Lifshitz-Wagner theory, and assuming a linear time dependence of temperature ($T=T_{min} + \beta t$) during thermal cycle [Dutta 2003^a, 2003^b, 2004] showed that the final particle size, at any time $r(t)$ can be expressed as

$$r(t) = \left\{\left[\left(\frac{B_1\gamma_s V_m C_0}{RT}\right)\overline{D}_{sol}(t + 2N\hat{\gamma}t_{hc}v_c\varphi) + r_0{}^3\right]^{1/3}\right\} \qquad 4.5$$

where,

$$\overline{D}_{sol} = \frac{\int_0^{t_{hc}} D^0{}_{sol}\exp\left[\left(\frac{\sigma_h\Omega}{k} - \frac{Q_{sol}}{R}\right)\frac{1}{T}\right]dt}{\int_0^{t_{hc}} dt} \qquad 4.6$$

And, D_{sol} is the effective solute diffusivity in the matrix, D^{0}_{sol} and Q_{sol} are the associated frequency factor and activation energy respectively, γ is the average shear-strain rate during a half cycle, and can be approximated as

$$\hat{\gamma} \approx \frac{\Delta\alpha(T_{\max} - T_{\min})}{h t_{hc}},$$

where $(T_{max} - T_{min})$ is the temperature range of the cycle, v_c is the number of thermal cycles, each with a half period of t_{hc}.

In equation 4.6, when $\hat{\gamma} = 0$, value of phase-radius, r, represents the coarsened size caused by isothermal aging only. For $\hat{\gamma} \neq 0$, the value of phase-radius, r, includes contributions caused by both static aging and strain-enhanced coarsening. Figure 4.2 shows a plot of equations 4.6 and 4.7 for a 27mm BGA solder joint with Sn95.5Ag4.0Cu0.5 solder alloy subjected to -40 to 125°C. The experimented particle coarsening slope correlates well with the model.

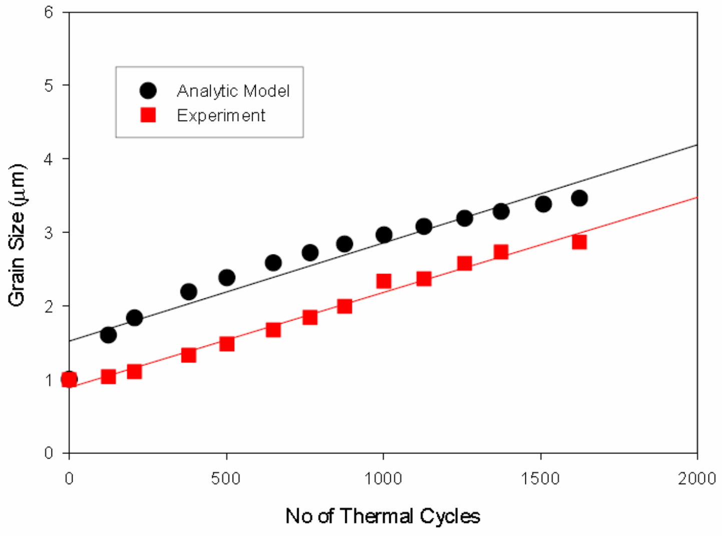

Figure 4.2: Comparison between analytical and experimental increase in the Ag$_3$Sn particle size for 388 I/O BGA lead-free solder joint subjected to -40 to 125° C.

4.3 Experimental design and phase analysis

The components analyzed include various packaging architectures such as plastic ball-grid arrays, chip-array ball-grid arrays, tape-array ball-grid arrays, flex-substrate ball-grid arrays. Ball counts are in the range of 64-676 I/O, pitch sizes are in the range of 0.5-1mm, and package sizes are in the range of 6-27 mm (Table 4.1 and Figure 4.3). The boards contain six trace layers to simulate the thermal mass of a true production board, though all functional traces were run on the topmost layer. The test vehicle comprised of 6 component architectures, 3 of each type on each test board. There were 10 such test boards. Therefore, 30 components of each type were in the test matrix. Samples were subjected to temperature cycling from -40 to 125°C. Each component was cross-sectioned, such that it yielded four Ag_3Sn phase values pertaining to the four highly strained solder ball locations for each component. These phase size values for each component type per board are averaged and presented in the graphs. The stresses were increased gradually and the samples were cross-sectioned at various levels of stress exposure length. The cross-sections were studied by a Field Emission Scanning Electron Microscope (SEM), JEOL JSM-7000F operated at an accelerating voltage of 20 kV. The pictures were taken at a magnification of 750x. All samples were imaged after polishing and etched to reveal grain structure. The quantitative measure of Ag_3Sn particle size was established from a 60μm x 45μm rectangular region selected from a back-scattered SEM image of the highest strained solder ball. The location of the examination region was identical for various samples. Grain size was averaged from various samples for each package architecture and stress exposure. The typical SEM pictures before and after the mapping of phase size using image analysis is shown in Figure 4.4.

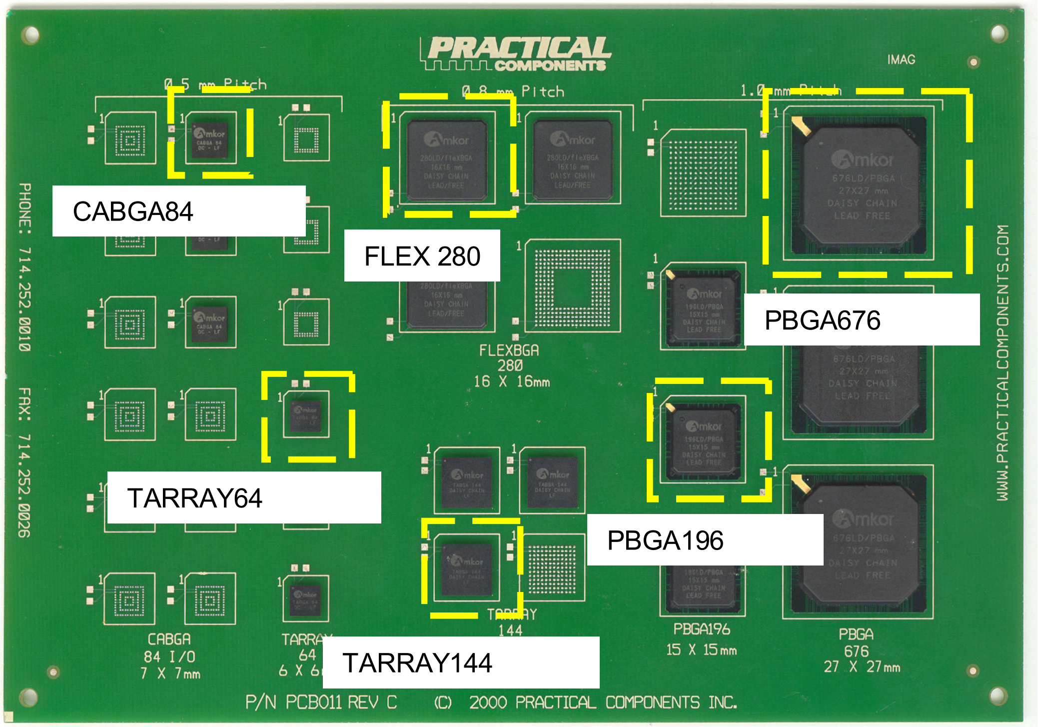

Figure 4.3: Test board used for electronic package prognostication of SAC405 alloy

Body Size	Package	Ball Count	Ball Pitch (mm)	Die Thickness (mm)	BT Thickness (mm)	Die size (mm)	BT Pad Type	Ball Diameter (mm)
6 mm	TABGA	64	0.5	0.36	0.36	4	NSMD	0.32
7 mm	CABGA	84	0.5	0.36	0.36	5.4	NSMD	0.48
10 mm	TABGA	144	0.8	0.36	0.36	7	NSMD	0.48
15 mm	PBGA	196	1	0.36	0.36	6.35	SMD	0.5
16 mm	FlexBGA	280	0.8	0.36	0.36	10	NSMD	0.48
27 mm	PBGA	676	1	0.36	0.36	6.35	SMD	0.63

Table 4.1: Package dimensions of the various BGA packages on Test board

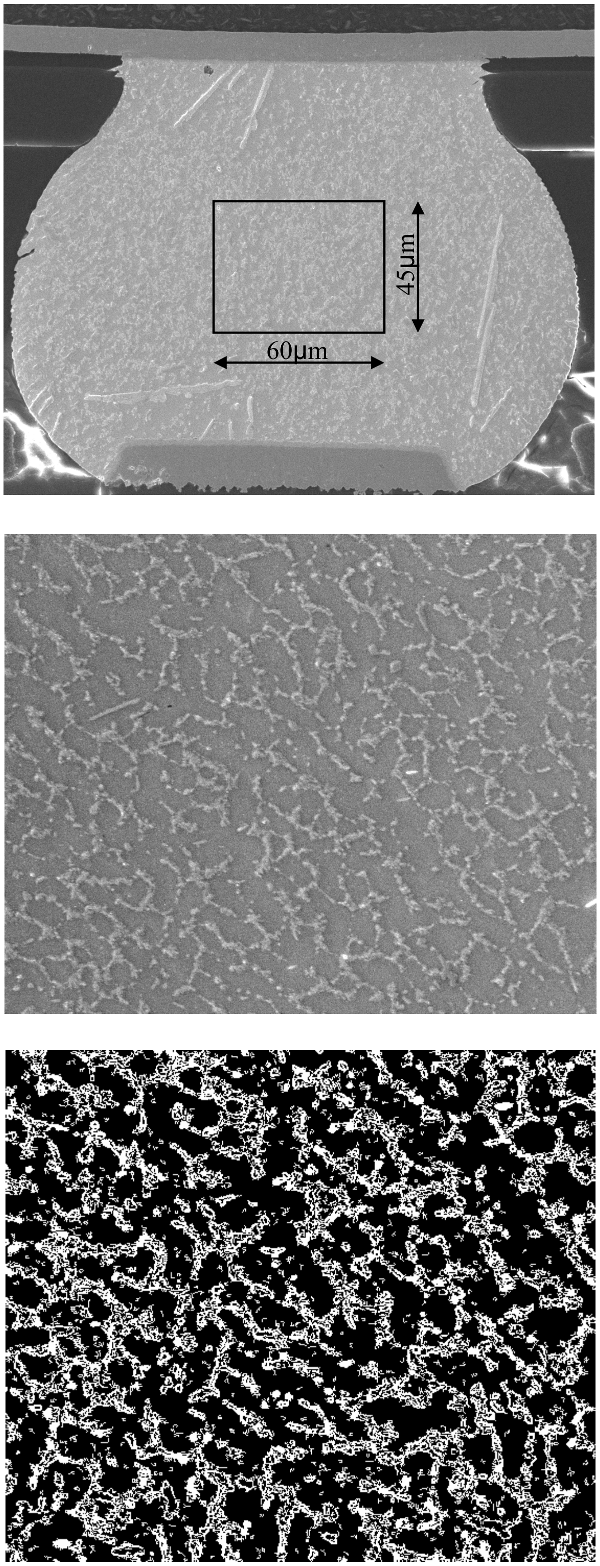

Figure 4.4: Methodology to calculate the grain size using SEM Picture and Image Analysis Software.

4.4 Determination of Damage Proxy (Phase Growth)

The average grain size “g” in the selected region is measured using Image Analysis software. The phase growth parameter S can be expressed as

$$S = g^4 - g_0^4 \qquad 4.7$$

Where, g_0 is the average grain size of the solder after reflows at zero thermal cycles. The average phase growth parameter S, changes with the cycles in thermal cycle environment and with time in steady-state temperature environment. Figure 4.5-4.6 show the SEM backscattered images exhibiting examples of Ag_3Sn phase growth process in the 676 I/O, 280 I/O BGA solder balls at different levels of thermal cycle. Most of the SnAgCu solder is comprised of the Sn-phase, so that the growth rate of tin and Ag_3Sn intermetallic particles are significant. Since Ag atoms have a higher diffusion rate in the molten solder, they can diffuse out of the way and thus allow the Sn dendrites to grow. Particles of Ag_3Sn grow either into spheres or needle shaped structures. Since tin cannot anticipate the shape of the Ag_3Sn intermetallic particles, they have to grow ahead of the tin phase [Islam 2005].

The average phase growth parameter S measured under thermal cycling and thermal aging for each individual component has been plotted versus cycles in Figure 4.7-4.12. The phase growth data in this study indicates that phase growth rate stays fairly uniform during the thermal cycle tests. Since an electronic system may have variety of material sets and packaging architectures, the linearity of phase size growth depicts the validity of phase growth as a proxy for damage progression. The damage progression can thus be tracked in various devices based on damage proxies. This is consistent with the stabilization of the hysterisis loop that is observed in thermal fatigue simulations.

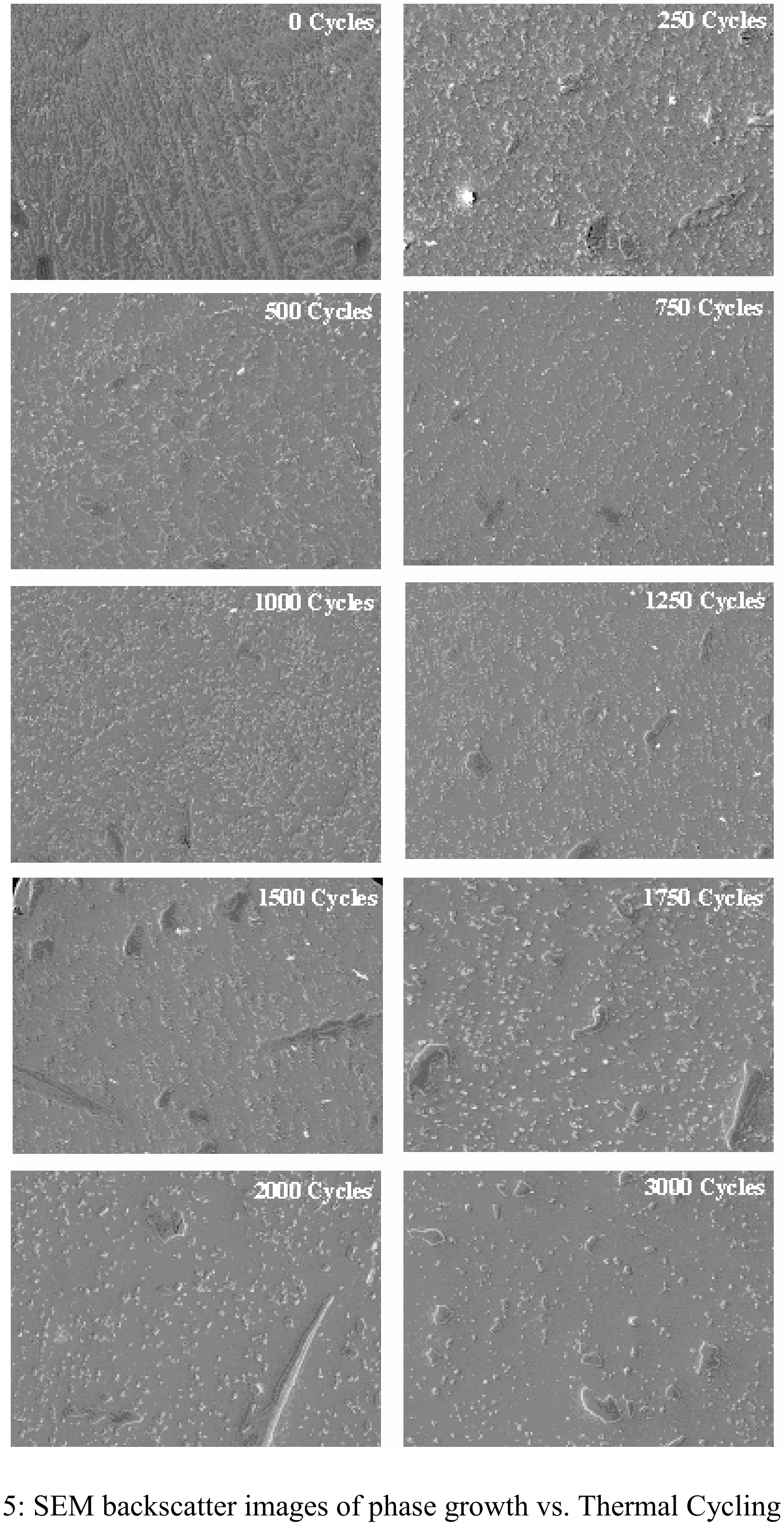

Figure 4.5: SEM backscatter images of phase growth vs. Thermal Cycling (-40°C to 125°C 95.5Sn4Ag0.5Cu solder, 280 I/O tape-array BGA, magnification 750X)

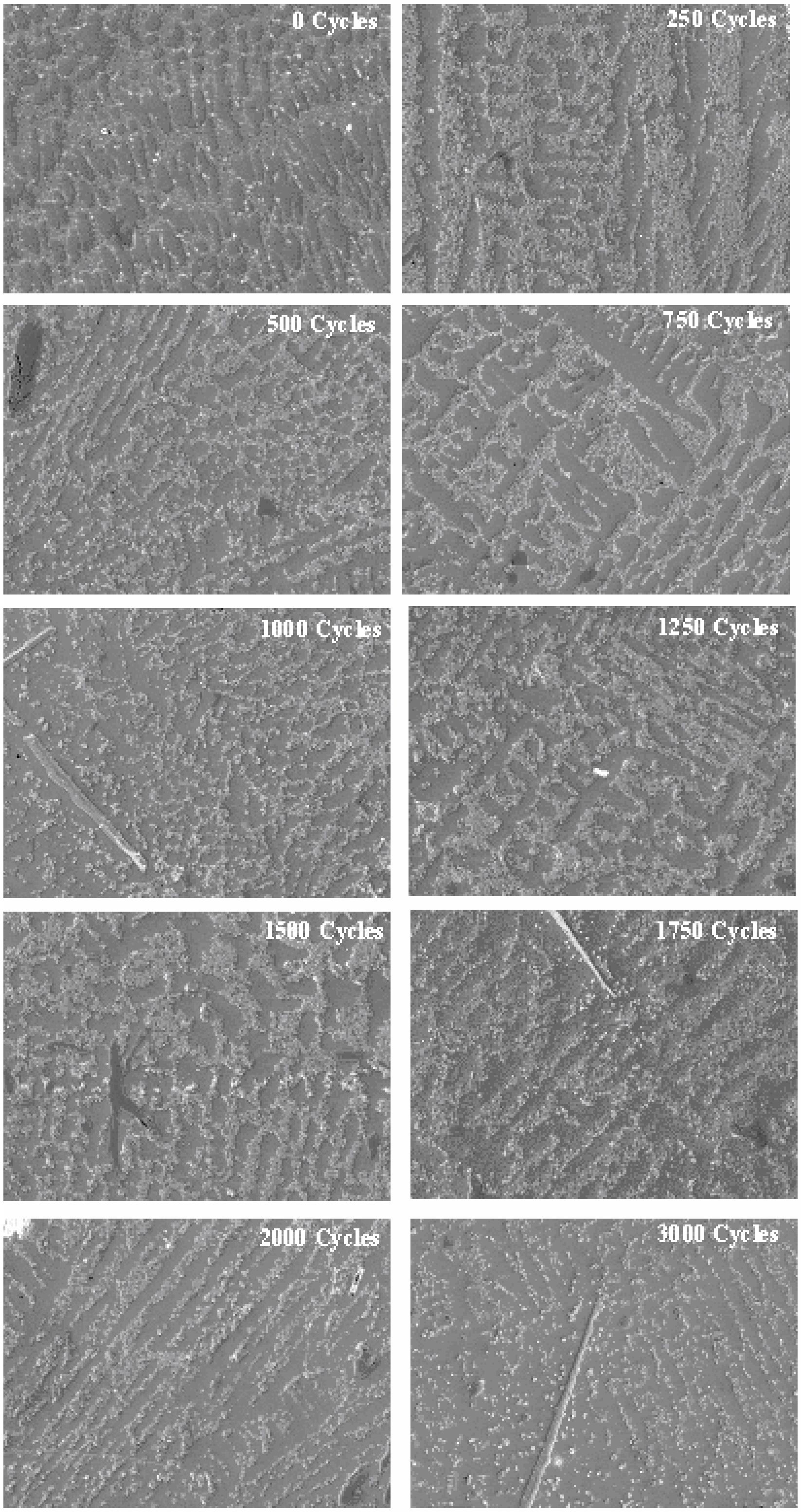

Figure 4.6: SEM backscatter images of phase growth vs. Thermal Cycling (-40°C to 125°C 95.5Sn4Ag0.5Cu solder, 676 I/O tape-array BGA, magnification 750X)

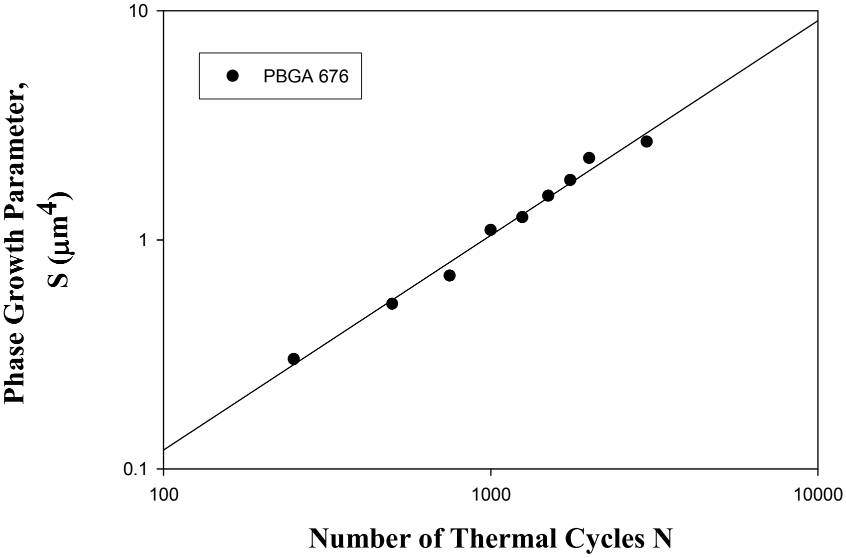

Figure 4.7: Phase Growth Parameter, at Various Levels of Cycles for PBGA 676 SnAgCu Solder Interconnect

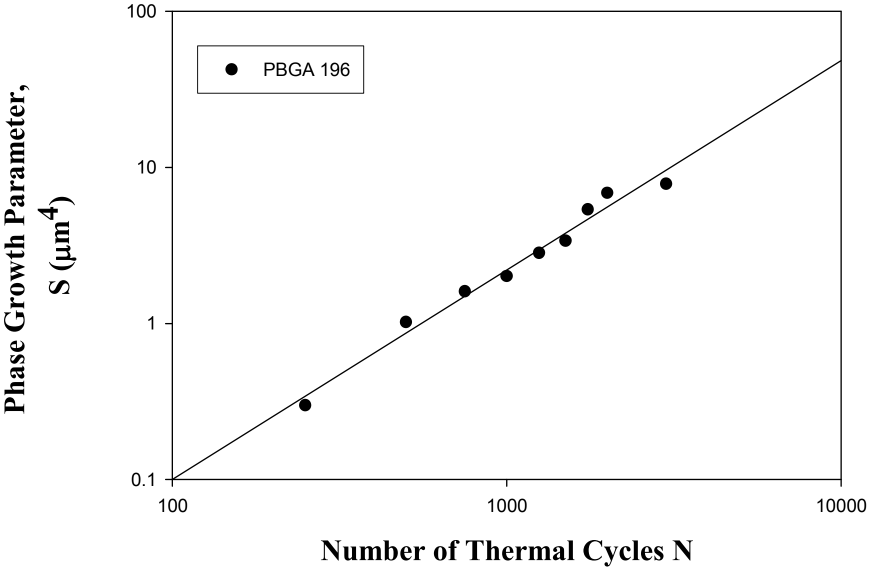

Figure 4.8: Phase Growth Parameter, at Various Levels of Cycles for PBGA 196 SnAgCu Solder Interconnect

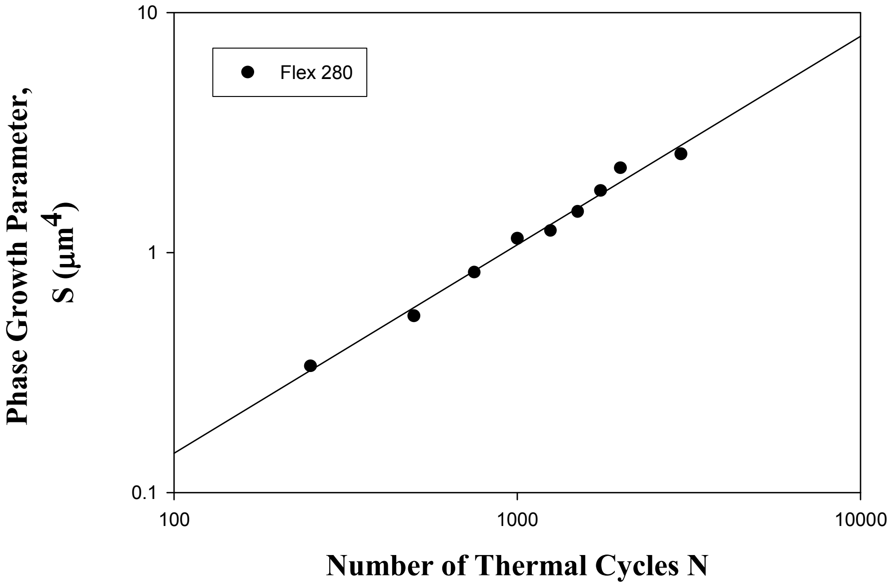

Figure 4.9: Phase Growth Parameter, at Various Levels of Cycles for FlexBGA 280 SnAgCu Solder Interconnect

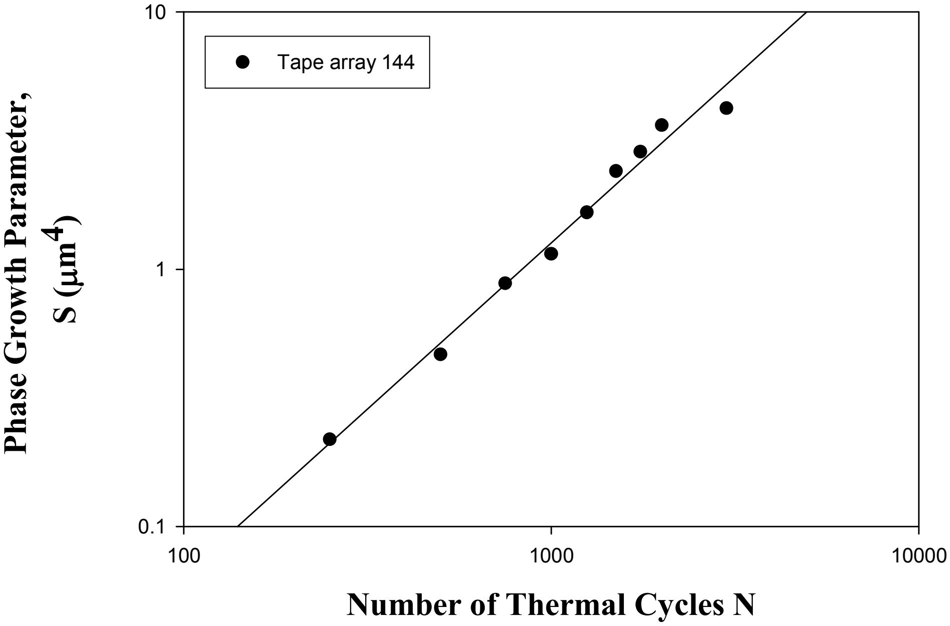

Figure 4.10: Phase Growth Parameter, at Various Levels of Cycles for TA BGA 144 SnAgCu Solder Interconnect

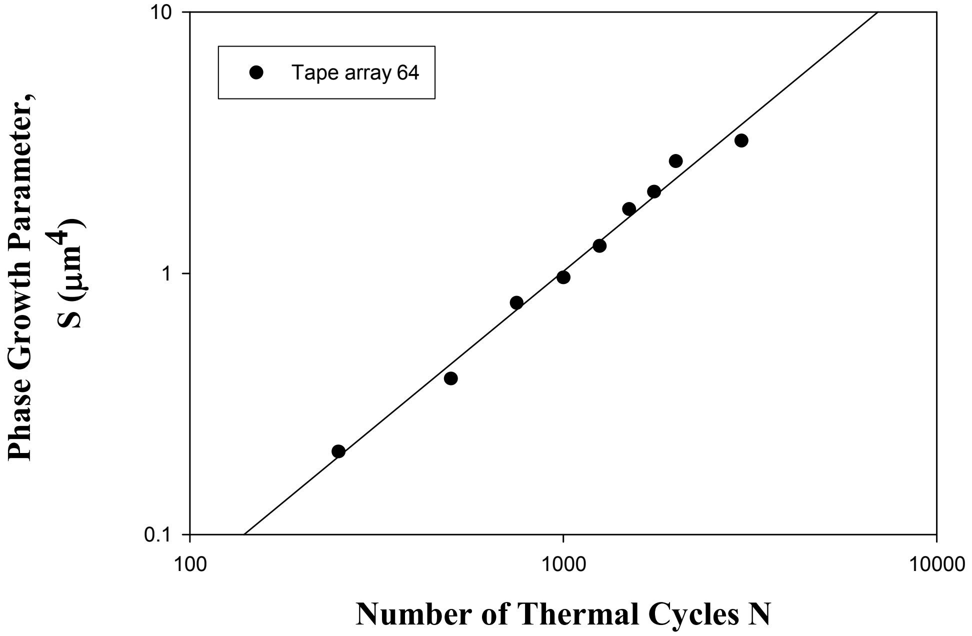

Figure 4.11: Phase Growth Parameter, at Various Levels of Cycles for CABGA 84 SnAgCu Solder Interconnect

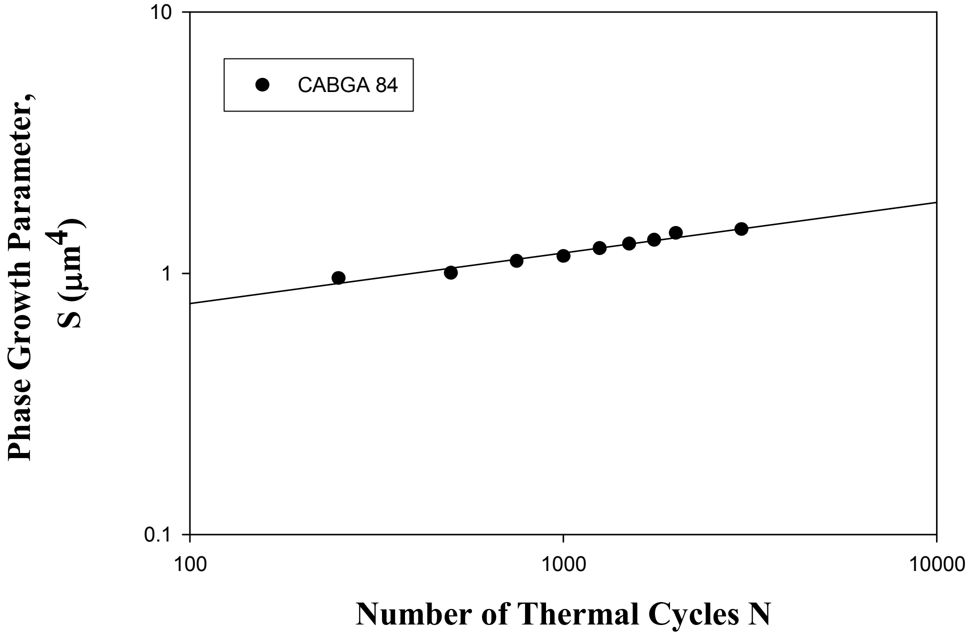

Figure 4.12: Phase Growth Parameter, at Various Levels of Cycles for TABGA 64 SnAgCu Solder Interconnect

Stabilization of the loop indicates that the damage is accumulated at more or less a constant rate. Previous studies have used products between derivatives of filed quantities such an inelastic strain energy density (ΔW) to quantify damage and shown that it is accumulated at a constant rate [Darveaux 1995, 1997, Lall 2004[b], 2005, 2006[a,b], 2007[a,b]]. Experimental data indicates that accumulation of damage in solder is accompanied with Ag_3Sn phase growth and grain coarsening. The damage manifests itself in ultimate appearance of cracks. In the case of SnAgCu alloy, Ag-Sn intermetallic is randomly distributed in the bulk Sn. The needles/spherical intermetallic precipitates are Ag_3Sn.

4.5 Crack Growth Measurements

Samples were cross-sectioned at various level of thermal cycling. Several sections were made per sample to study the crack initiation and propagation in various rows. The cross-sections were characterized by scanning electron microscopy (SEM). The primary and secondary crack lengths have been added [Islam 2005]. The primary crack, the crack initiated for the first time and in almost all cases it is initiated at the package interface. The secondary crack is the one initiated at later stage near the board surface. Multiple test boards were periodically removed from the chamber after every 250 cycles. Solder joint cracks have been measured at each temperature cycling data-interval. Figure 4.13 shows the crack length variation as we progress in number of thermal cycles as well as the grain coarsening around the crack. Figure 4.14-4.19 shows the characteristic crack length under thermo-mechanical stress for various package architectures and it is observed that slope varies for each package architecture as it is been observed during phase growth versus number of thermal cycle.

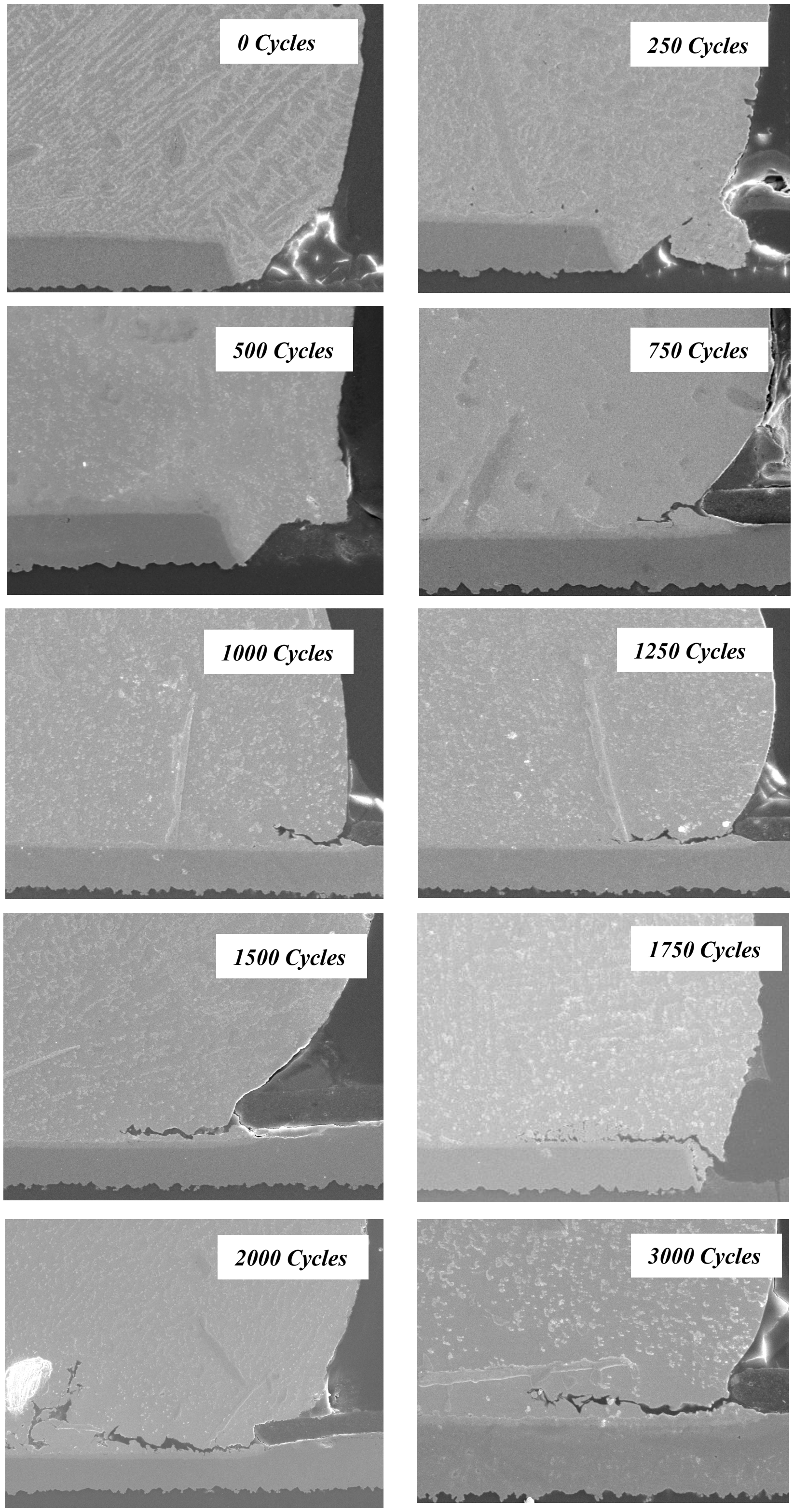

Figure 4.13: Correlation of Incipient crack growth with phase growth in ball-grid array package (95.5Sn4.0Ag0.5Cu solder, magnification: 250)

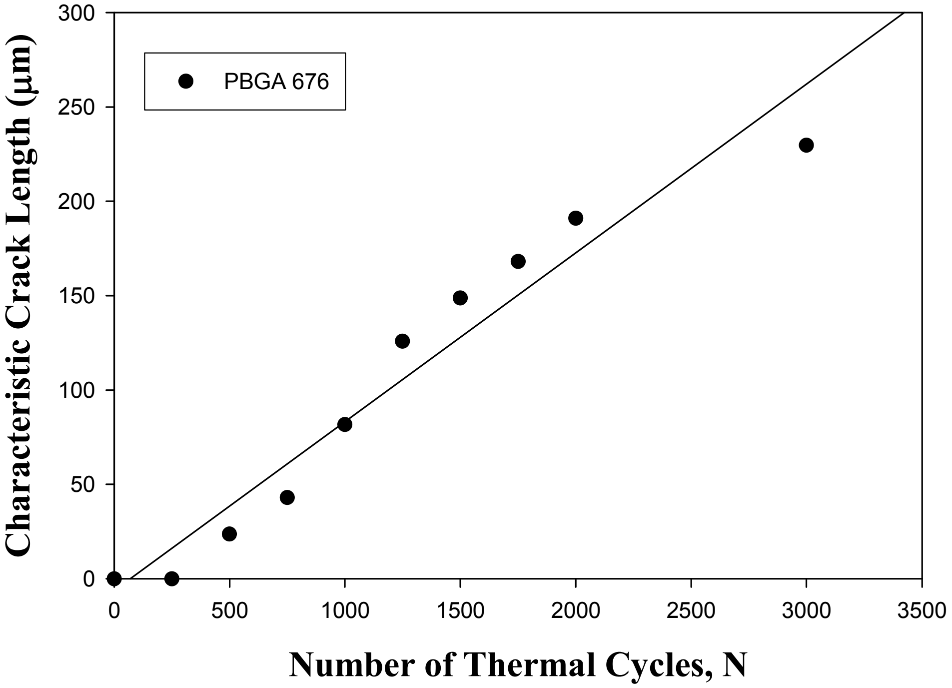

Figure 4.14: Characteristic crack length vs. Number of cycles for PBGA 676 package

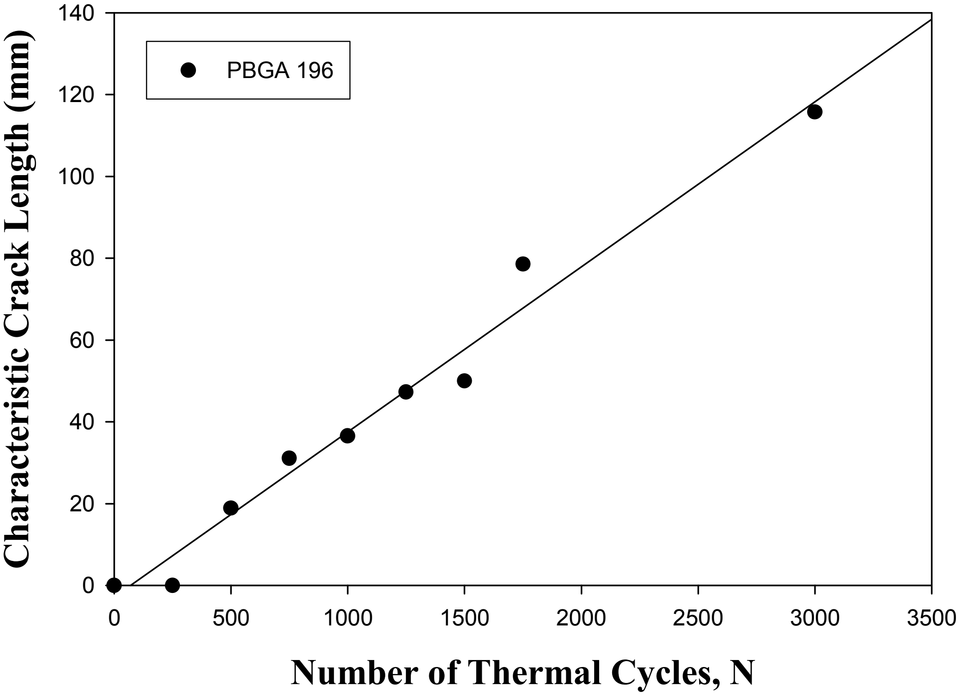

Figure 4.15: Characteristic crack length vs. Number of cycles for PBGA 196 package

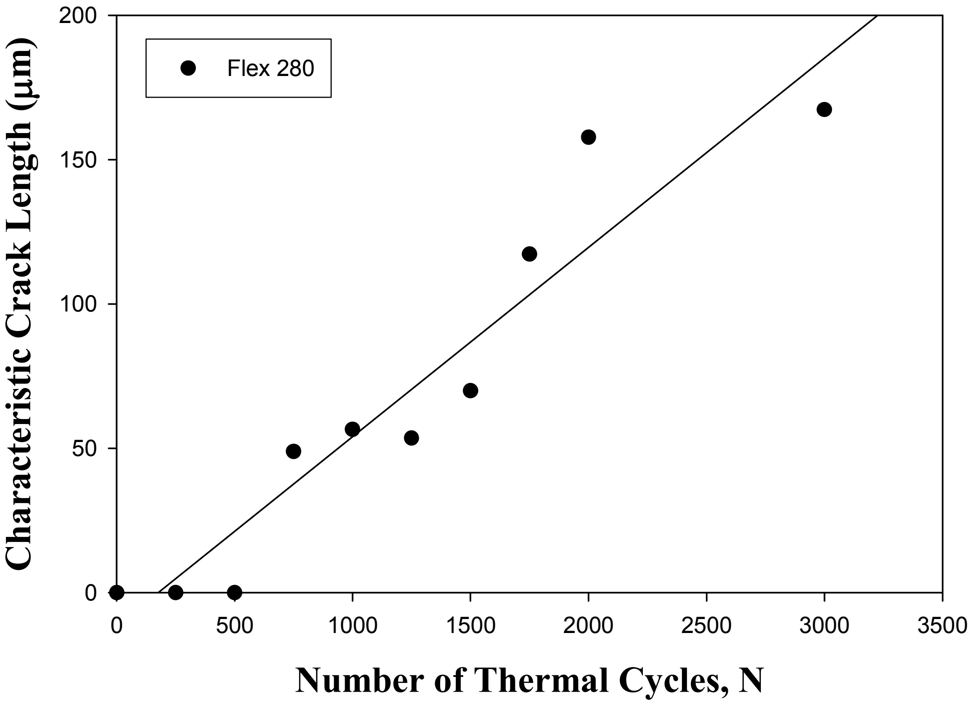

Figure 4.16: Characteristic crack length vs. Number of cycles for FlexBGA 280 package

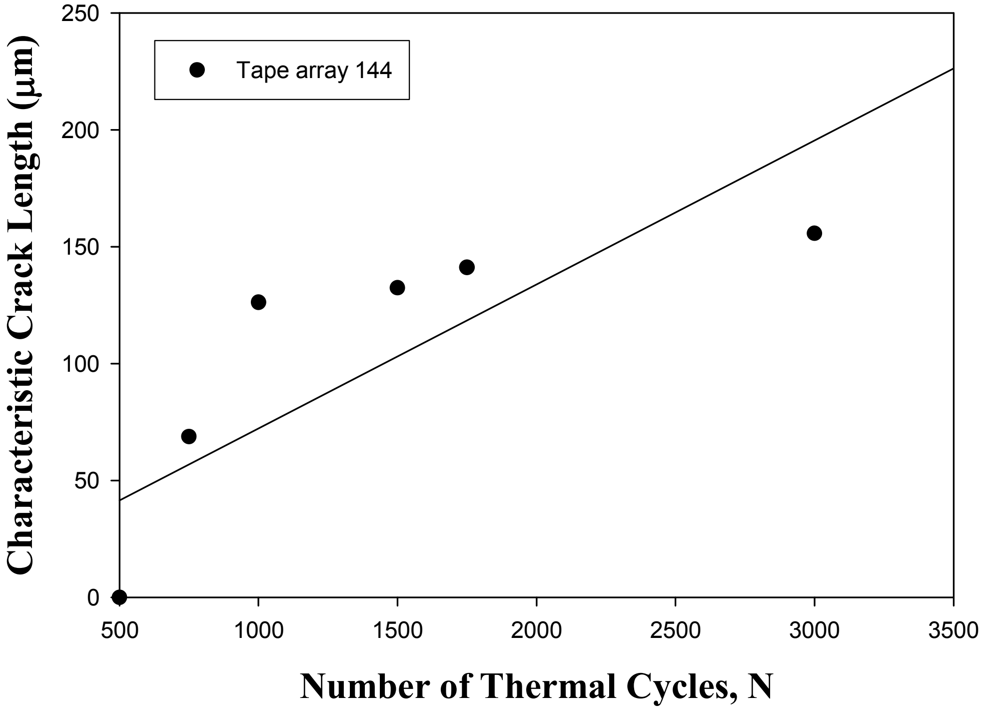

Figure 4.17: Characteristic crack length vs. Number of cycles for TABGA 144 package

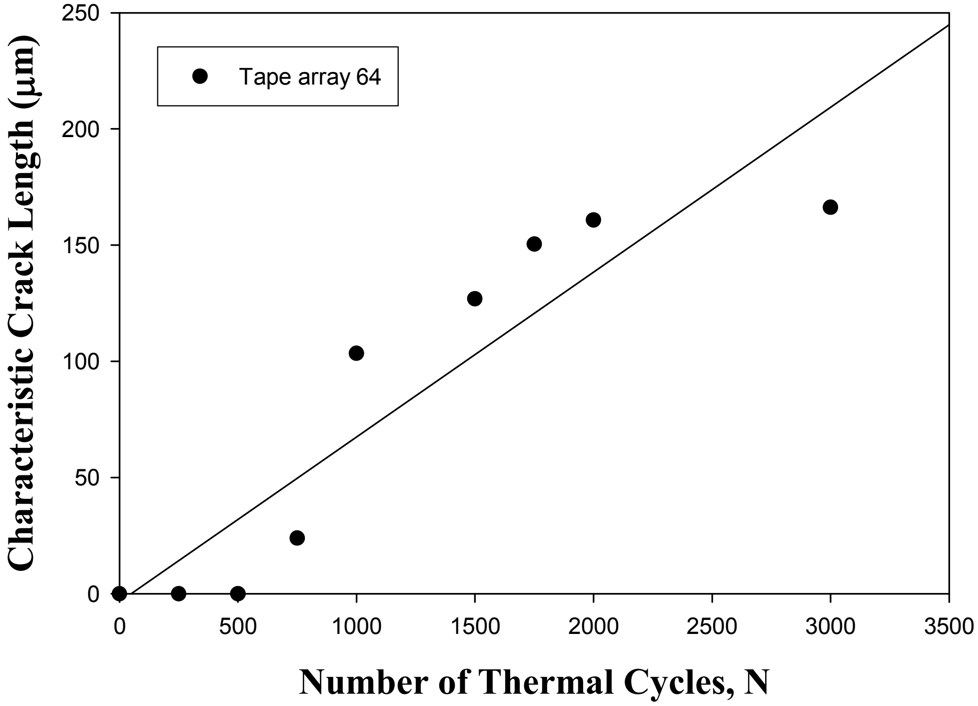

Figure 4.18: Characteristic crack length vs. Number of cycles for TABGA 64 package

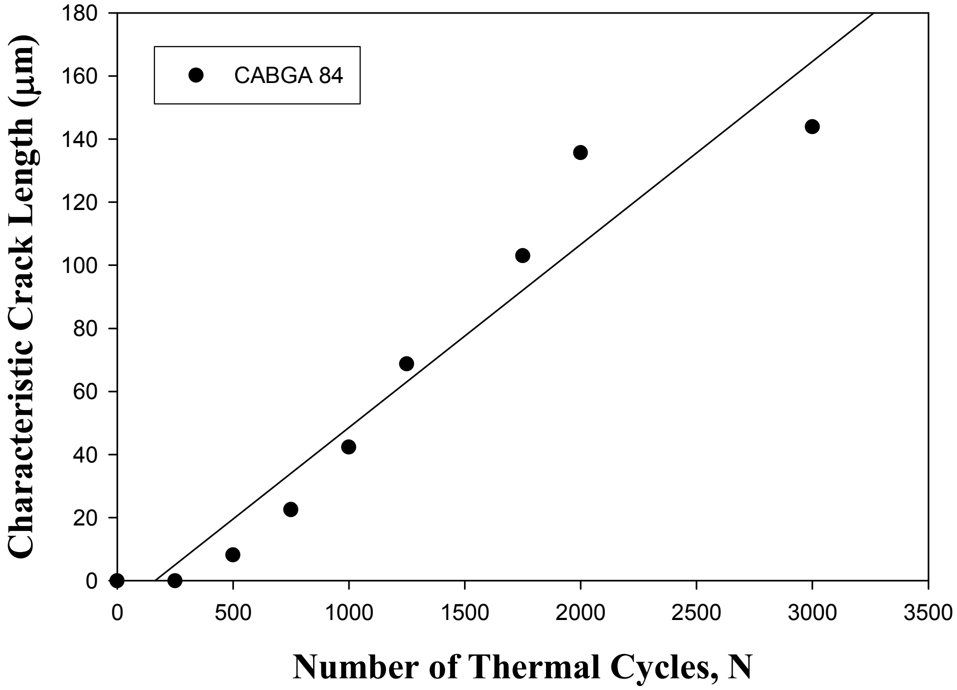

Figure 4.19: Characteristic crack length vs. Number of cycles for CABGA 84 package

4.6 Correlation of damage proxy with Inelastic Strain Energy density

The phase growth rate per cycle is closely related with the inelastic strain energy density per cycle. Prior studies have correlated the number of cycles to crack initiation and the crack propagation rate with the inelastic strain energy density [Darveaux 2000, Lall 2003, 2006]. Linear and non-linear, elastic, plastic, creep, temperature, time dependent and time-independent material properties have been incorporated in the finite element models. The thermal fatigue failure of electronic packages is associated with combined plastic-deformation and creep of solder joints. The Anand Viscoplasticity model for SnAgCu alloy, which was estimated earlier in chapter 3, is used in this study. Figure 4.20 shows the 3D diagonal symmetry finite element model for PBGA 196 I/O. Similarly for other package architecture the finite element model has been created in ANSYS^{TM} and temperature cycling has been simulated till the inelastic strain energy density for the critical solder ball stabilizes.

The damage proxy, phase growth parameter per cycle, has been correlated with time-to-failure (Figure 4.21), from non-linear finite element simulations using damage relationships of the form, $N = C_1(\Delta W)^{C_2}$ [Darveaux 1995, 1992, 1997, Zahn 2003]. Model predictions have been validated with experimental data. The corresponding damage accumulation rate is thus correlated to the inelastic strain energy density. Data indicates that phase growth parameter and its derivatives are valid proxies for use as leading indicators of failure. The correlation enables the evaluation of residual life in a deployed part based on rate of change of phase growth parameter under future intended use conditions.

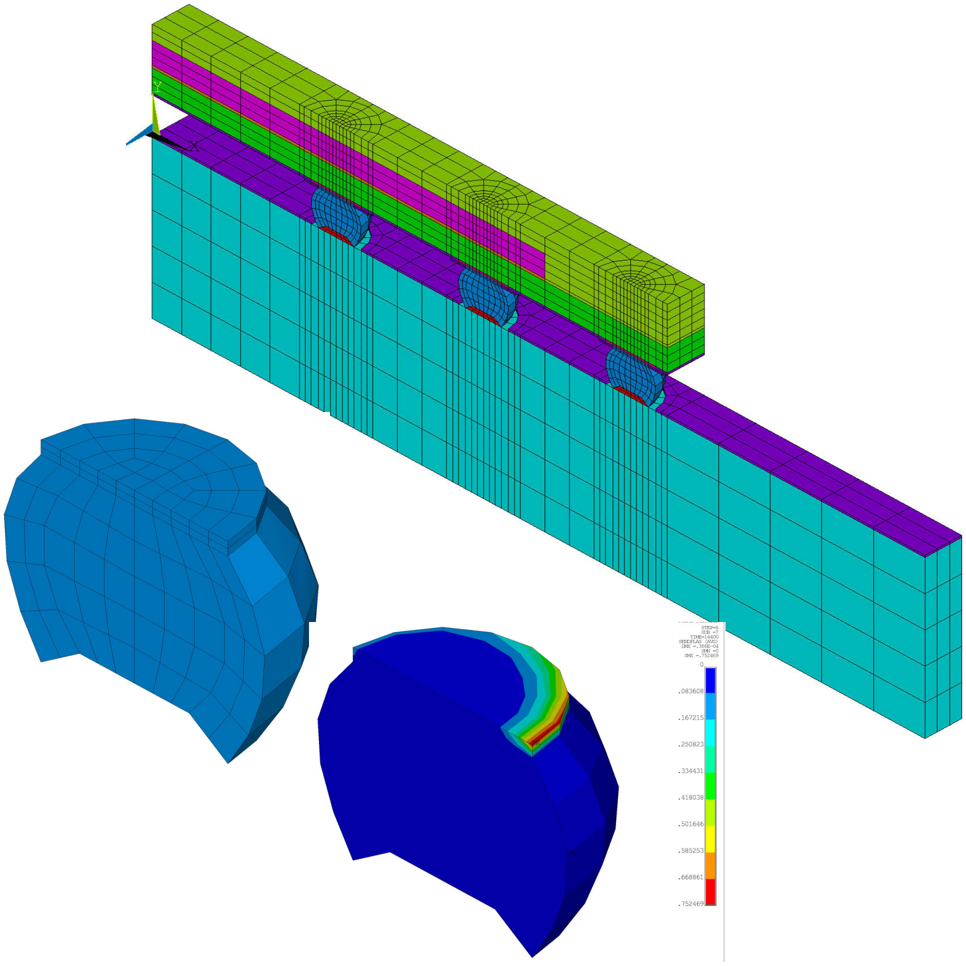

Figure 4.20: One of the example of Finite Element Model Pictures and Plastic work per volume for CABGA 84 Package

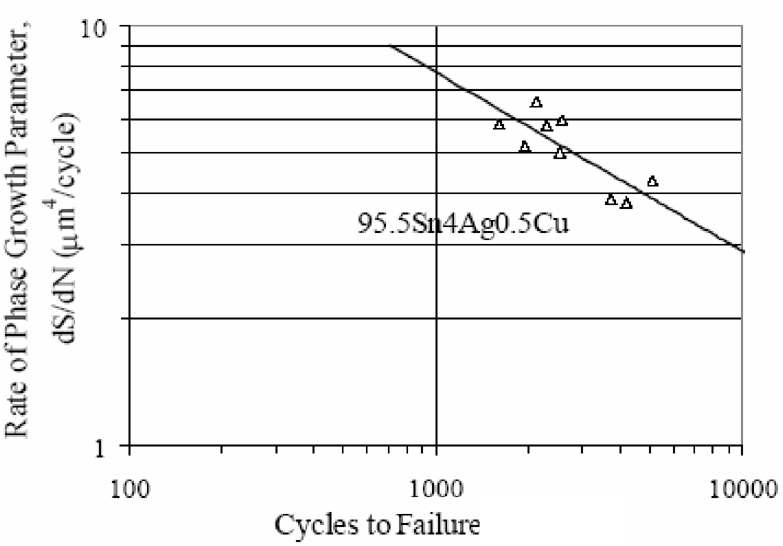

Figure 4.21: Relation between number of cycles to failure and phase-growth rate

The time-to-failure N_f of solder joints can be correlated with the rate of change of phase growth parameter per cycle, dS/dN. Since the rate of change of phase growth parameter has been correlated to the inelastic strain energy density, ΔW, therefore, it is hypothesized that the faster phase growth correlates with faster accumulation of inelastic work in the joint and lower cycles to failure. The following relationship has been developed for the solder interconnects,

$$N_f = C_2\left(\frac{dS}{dN}\right)^{-\gamma} \tag{4.8}$$

Where C_2, and γ are constants. The relationship enables the calculation of residual life. The phase growth rate in a deployed part can be monitored in the intended use-environment and the residual life evaluated (Figure 4.21).

4.7 Summary and Conclusions

A damage pre cursors based methodology for prognostication-of-electronics for assessment of residual-life has been developed and demonstrated under single stress of thermal cycling. The damage pre-cursors enable assessment of system damage-state significantly prior to appearance of any macro-indicators of damage. Phase growth rate has been identified as valid proxies for determination of residual life in electronic structures. The theoretical basis for the selection of prognostic parameters has been justified based on particle growth induced by volume diffusion. Mathematical relationships have been developed between phase growth, derivatives of phase growth for interrogation of residual life and damage state. Prognostics parameters have been validated versus macro-indicators including cracks initiation, crack propagation rates and inelastic strain energy density for 95.5Sn4Ag0.5Cu solder.

CHAPTER 5

ASSESMENT OF PRIOR DAMAGE USING NON-LINEAR LEAST SQUARE METHOD FOR PROGNOSTIC HEALTH MONITORING OF ELECTRONICS UNDER THERMAL CYCLING LOAD

5.1 Introduction

Methodologies for prognostication and health monitoring can significantly impact electronic reliability for applications in which even minimal risk of failure may be unbearable. In the previous chapter we have developed leading indicators of failure for prognostication of electronics. In this chapter a mathematical approach has been presented to calculate the prior damage in electronics subjected to cyclic thermo-mechanical loads. Health Monitoring (HM) refers to the broad concept of assessing the ongoing, in-service performance of a system using a variety of measurement techniques. HM application areas include fatigue crack damage in mechanical structures such as aircraft surface, ships, submarines, civil infrastructure, railway structures and power plants. Health Monitoring is aimed at the immediate detection and diagnosis of off-normal system operations and to take real-time corrective actions to avert the possibility of a system failure. The technical approach here relies on fusion of heterogeneous information derived from physics-based models of fatigue damage and real-time sensor data. HM can also provide the Operation and Maintenance (O&M) team with the information necessary to select and follow the optimum asset management path leading to substantial reduction in life cycle cost of the system. Prognostics refer to interrogation of material state of a system based on computation of certain proxies, stressors, and to predict the Remaining Useful Life (RUL) of the system for the intended environment.

PHM techniques have been well developed and established for mechanical structures. Since the wear and degradation in electronics is very difficult to detect compared to most of the other mechanical systems due to complex and tiny structures. But electronics have become the integral part of the system and reliability of these electronics effect the overall system reliability. Built-In-Self Test (BIST) circuit, Fuses and Canaries are the few of the existing PHM techniques in electronics, but they are very reactive in nature and provide a very limited insight into the remaining useful life prior to failure. PHM approach presented in this thesis is different from state-of-the-art diagnostics and resides in the pre-failure-space of the electronic system, in which no macro indicators such as crack or delamination exists. The presented approach enables the estimation of prior damage in deployed electronics by interrogation of the system state.

An electronic component operating in a harsh environment is subjected to temperature variations during its use-life. Therefore, a time-temperature history of the electronic system ambient would be extremely helpful in using life prediction models and computing life. Continuous capture of time-temperature history would put immense demands on existing system functions. In this paper, a mathematical approach has been presented to calculate the prior damage in electronics subjected to cyclic and isothermal thermo-mechanical loads. This methodology obviates the need to capture the prior stress history and helps in accurate prediction of remaining useful life. Previously, [Lall 2004[b], 2005, 2006[a,b], 2007[a,b]] have developed leading indicators of failure. In this thesis, proxies like the phase growth rate of solder interconnects have been experimentally identified as indicators to failure. Mathematical relationships have been developed for computation of residual life based on these damage proxies. This methodology eliminates the need for knowledge of prior stress histories and enables interrogation of system state using the identified damage pre-cursors. This health monitoring framework will facilitate quick assessment of system state and potential for failure of critical electronic systems. This approach of computing residual life for various package elements, to prognosticate electronic systems can be implemented prior to appearance of any macro-indicators of damage.

5.2 Test Vehicle

Area-array packages with 95.5Sn4.0Ag0.5Cu solder balls assembled on FR4-06 laminates and immersion Ag finish have been studied under thermo-mechanical loads in the range of -40°C to 125°C and isothermal aging at 125˚C. Phase growth data has been gathered and analyzed using image processing. Components analyzed include plastic, flex, tape-array and ceramic ball grid arrays with I/O counts are in the range of 64 to 676, pitch sizes are in the range of 0.5 mm to 1mm, and package sizes are in the range of 6mm to 27mm. The boards contain six trace layers to simulate the thermal mass of a true production board, though all functional traces were run on the topmost layer. All pads on the board were non-solder mask defined (NSMD) and had an immersion silver finish. Table 5.1 has the package dimensions used for this study.

Body Size	Package	Ball Count	Ball Pitch (mm)	Die Thickness (mm)	BT Thickness (mm)	Die size (mm)	BT Pad Type	Ball Diameter (mm)
6 mm	TABGA	64	0.5	0.36	0.36	4	NSMD	0.32
7 mm	CABGA	84	0.5	0.36	0.36	5.4	NSMD	0.48
10 mm	TABGA	144	0.8	0.36	0.36	7	NSMD	0.48
15 mm	PBGA	196	1	0.36	0.36	6.35	SMD	0.5
16 mm	FlexBGA	280	0.8	0.36	0.36	10	NSMD	0.48
27 mm	PBGA	676	1	0.36	0.36	6.35	SMD	0.63

Table 5.1- Dimensions for all package architectures used in this study

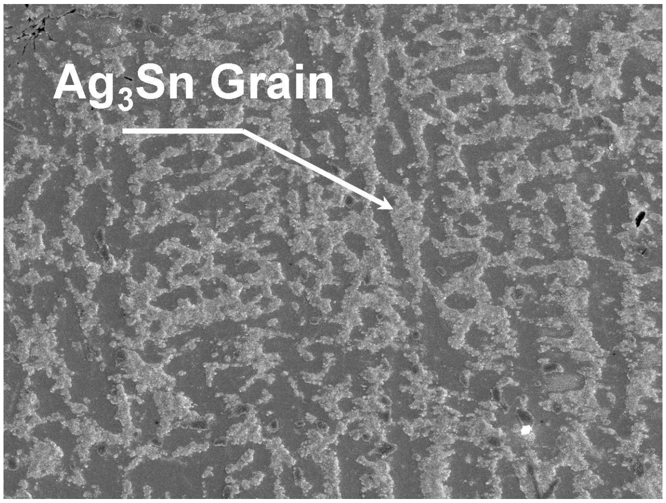

Figure 5.1- Ag_3Sn Phases in 95.5Sn4Ag0.5Cu (SAC 405) solder microstructure

5.3 Micro-structural Coarsening

Electronics deployed in underhood automotive applications is subjected to temperature variations in the neighborhood of -40°C to 125°C. These temperature excursions during operation of a circuit are due to both power-cycling and variations in ambient conditions resulting in thermo-mechanical cyclic stresses and strains induced primarily by thermal expansion mismatch between the package and the board assembly. Micro-structural coarsening during thermo-mechanical deformation is attributed to the generation of excess vacancies caused by the combined effect of local hydrostatic state of stress and the instantaneous inelastic strain rate [Dutta 2003[a], 2004, 2003[b], Jung 2001]. Evolution of solder microstructure and the growth of intermetallic due to thermal fatigue have been reported previously by several researchers.

In previous chapter the phase growth parameter variation with time for a polycrystalline material has been discussed. It is found that the following relationship best fits the experimental data if the boundary motion is dominant.

$$S = g^4 - g_0^{\ 4} = Kt \tag{5.1}$$

where g is average grain size at time t, g_0 is the average grain sizes of solder after reflow.

In this study, changes in solder microstructure and its derivatives have been investigated as the leading indicators of failure and interrogation of system state for assessment of damage from prior stress histories. Quantitative metrics of changes in microstructure have been identified and relationships have been developed to represent damage progression. Data presented covers a wide range of Sn4Ag0.5Cu lead-free packaging architectures and discrete devices in extreme temperature cycling environments. Figure 5.1 shows Ag_3Sn Phases in Sn4Ag0.5Cu solder alloy microstructure.

5.4 Correlation between Interconnect Damage and Leading-Indicators of Failure

Measurements of progression of phase growth parameter with time in thermal aging and thermal cycling has been used to evaluate (a) the time duration for which the component had been deployed, (b) the initial grain size (g_0), and (c) the remaining useful life from the experimental data extracted for field variables like grain size at different intervals of time. This methodology would be immensely helpful in deciding if the electronic component could be re-deployed for another mission without any impending failure, with a reasonable amount of confidence. The approach presented will be implemented using sacrificial (non-functional) devices placed near the actual component so that they are subjected to similar operating environment as the functional electronic assembly.

Previously it has been shown that [Lall 2004^{b}, 2005, 2006^{a,b}, 2007^{a,b}] damage progression within the solder joint can be assessed based on damage proxies including phase growth, IMC growth for a variety of packaging architectures. Experimental data indicates a proportional relationship between rate of change of phase growth $\left(\frac{dS}{dN}\right)$ and plastic work per unit volume (ΔW) across all component types. Therefore, the computational proxy, plastic work per unit volume (ΔW) has been replaced by $\frac{dS}{dN}$ to get a relationship of the type

$$N = K_1(\Delta W)^{K_2} \tag{5.2}$$

$$N_f = C_2\left(\frac{dS}{dN}\right)^{-\gamma} \qquad 5.3$$

Where the constants C_2 & γ could be obtained from a statistical regression fit. The grain size was measured for various area array packages at different time intervals. The grain sizes (g) were calculated using pictures taken from Scanning Electron Microscope (SEM), JEOL JSM-7000F. All samples were imaged after polishing and etching to reveal grain structure. The quantitative measure of Ag_3Sn particle size was established from a 60 μm x 45 μm rectangular region selected from a backscattered SEM image of a solder ball which experiences the highest strain. The location of the examination region was identical for various samples. The grain size (g) was averaged from various samples for each package architecture and stress exposure. The phase growth parameter was then calculated and data fitted to get the rate of phase growth parameter. This correlation enables the evaluation of residual life in a deployed part. The corresponding damage accumulation rate can then be computed in terms of inelastic strain energy density for thermal cycling, which can be used to evaluate residual life.

5.5 Life History Prediction

In this section, a methodology for determining the prior damage by interrogating the damage proxies of test structures has been presented. Electronic assemblies have been subjected to thermal cycling load. The thermal environments are intended to simulate a field application environment. The parts are withdrawn from the application environment for re-deployment in a new field environment. The damage proxies have been interrogated to determine the extent of damage inflicted and also remaining useful life of that assembly if it is to be re-deployed. Following sections will explain the prediction of stress history using phase growth in thermal cycling environments.

5.6 Levenberg- Marquardt Algorithm

The relationship between the phase growth parameter vs time is highly non-linear due to the presence of terms with fourth power and also due to the fact that experimental data has been fitted using power fit. Levenberg-Marquardt (LM) algorithm is an iterative technique that computes the minimum of a non-linear function in multi-dimensional variable space [Madsen 2004, Nelsen 1999, Lourakis, 2005]. It has been used successfully for computation of nonlinear least-square solutions. The Levenberg-Marquardt method is a combination of the steepest descent and the Gauss-Newton method. It is comparatively more robust because it converges to the solution even if it starts very far off the final minimum.

Let f be an assumed functional relation which maps a parameter vector $p \in R_m$ to an estimated measurement vector $X=f(p)\ x \in R_n$. An initial parameter estimate p_0 and a measured vector x are provided and it is desired to find the vector p, that best satisfies the functional relation f i.e. minimizes the squared distance $\varepsilon^T\varepsilon$ with $\varepsilon = x - f(p)$. The basis of the LM algorithm is a linear approximation to f in the neighborhood of p. For a small δp, a Taylor series expansion leads to the approximation

$$f(p + \delta p) \approx f(p) + J\delta p \qquad 5.4$$

where, J is the Jacobian matrix $\partial f(p)/\partial p$. At each step the value of δp that minimizes the quantity $\varepsilon = x - Jf(p)$, has been computed. The minimum is attained when $J\delta p - \varepsilon$ is orthogonal to the column space of J. This leads to

$$(J^T J)\delta p = J^T \varepsilon \qquad \textbf{5.5}$$

$J^T J$ is the approximate Hessian i.e. an approximation to the matrix of second order derivatives. Since the Newton's method implicitly uses a quadratic assumption on *f*, the Hessian need not be evaluated exactly. Rather the approximation can be used for rapid convergence. The equation for LM Method is

$$N\delta p = J^T \varepsilon \qquad 5.6$$

where $J^T J$ is approximated for rapid convergence. Also, the off-diagonal terms of N are identical to corresponding elements of $J^T J$ and the diagonal elements are given by

$$N_{ii} = \lambda \mathrm{diag}(J^T J) + (J^T J)_{ii} \qquad 5.7$$

$$\lambda_0 = 0.001 \qquad 5.8$$

If $\lambda_{(i+1)} = \dfrac{\lambda_i}{10}$, then accept the solution, else $\lambda_i = 10\lambda_i$ and solved again. The process iterates until a value of δp that decreases the error is found. If λ is small, the Newton method is used; else steepest descent method is used. Algorithm is modified to take the equations of phase growth under thermal cycling loads to calculate the unknowns.

5.7 Phase Growth Prediction

It has been observed and proved that phase growth follows the linear pattern under thermal cycling loading and isothermal aging [Dutta 2003[a, b], 2004]. Also, it is been observed that the phase growth data versus number of thermal cycle fits very well using power fit regression as compared to linear regression. So the equation 5.1 takes the following form

$$g^4 - g_0^4 = a(t)^b \tag{5.9}$$

where *b* is the slope of the equation and *a* is a constant term, g_0 is the initial grain size, *g* is the grain size at time t or at the end of N thermal cycles. From the population devices subjected to thermal cycling, four condition monitoring devices have been withdrawn and sectioned for four-different thermal cycle durations in the neighborhood of prognostication time. The damage proxies have been measured for all the samples. The following equation represents each interval

$$g_1^4 = g_0^4 + a(N + \Delta N_1)^b \tag{5.10}$$

$$g_2^4 = g_0^4 + a(N + \Delta N_2)^b \tag{5.11}$$

$$g_3^4 = g_0^4 + a(N + \Delta N_3)^b \tag{5.12}$$

$$g_4^4 = g_0^4 + a(N + \Delta N_4)^b \tag{5.13}$$

Since the equations are non-linear in nature, a solution using simultaneous equation approach is very difficult to achieve. Therefore, non-linear least square method has been used for obtaining the solution. Variable Solutions differ widely in their magnitudes. In order to find the global minima of error, it is necessary to solve the equations for a bounded solution of the variables. Based on the accelerated test experimental data, acceptable ranges of solutions for the variables a, b, N and g_0 were developed. The variable upper bound and lower bound ranges are shown in Table 5.2 for each variable.

The equation used in LM algorithm for phase growth are of the form x = f(p)

$$g = \sqrt[4]{g_0^4 + a(N + \Delta N)^b} \tag{5.14}$$

where g is the grain size at different thermal cycle intervals ΔN, and g_0, a, N and b are the parameters to be found. Since the LM method does a linear approximation of the specified function in the neighborhood of the parameters to be found, it does so by using a Taylor series expansion for the next approximation. Therefore, it is necessary to give the Jacobian with respect to each unknown as follows:

$$\frac{\partial g}{\partial g_0} = \frac{g_0^{\,3}}{\left(g_0^{\,4} + a\left(N + \Delta N\right)^b\right)^{3/4}} \qquad 5.15$$

$$\frac{\partial g}{\partial a} = \frac{(N + \Delta N)^{\,b}}{4\left(g_0^{\,4} + a\left(N + \Delta N\right)^b\right)^{3/4}} \qquad 5.16$$

$$\frac{\partial g}{\partial N} = \frac{ab(N + \Delta N)^{\,b}}{4(N + \Delta N)\left(g_0^{\,4} + a\left(N + \Delta N\right)^b\right)^{3/4}} \qquad 5.17$$

$$\frac{\partial g}{\partial b} = \frac{a\log(N + \Delta N)(N + \Delta N)^{\,b}}{4\left(g_0^{\,4} + a\left(N + \Delta N\right)^b\right)^{3/4}} \qquad 5.18$$

Subsequently, initial guess values have been developed for the variables in the variable range (for each variable) as shown in Figure 5.2 , using uniform distribution of the points in the design space to form four arrays, i.e. one for each variable. Variables g_0, a, N, b, were varied at a time, while keeping the other variables constant and provided as input to the Levenberg-Marquardt algorithm. The outputs from the algorithm, g_0, a, N, b and minimization error has been computed for each iteration. Sample row-wise output are provided below (g_0, a, N, b and minimization error):

```
0.68026       0.001154379   228.8075      1.1418        0.006663792
0.68325       0.001133889   228.8143      1.1417        0.006304846
```

The row corresponding to the least minimization error was isolated, and the variables in that row were selected as the final values for g_0, a, N, b. After life consumed (N) has been estimated, remaining useful life of the component can be found by deducting the N from N_f in the intended use environment.

5.8 Model Validation – Computation of Cyclic Thermo-mechanical stresses

The average phase growth parameter S, changes with the cycles in thermal cycle environment. In order to calculate the damage and remaining useful life under thermo mechanical loading, the phase size data were taken for different packages under different cycle intervals. Figure 5.3-5.8 show the SEM back-scattered images exhibiting examples of Ag_3Sn phase growth process in 64 I/O, 84 I/O,144 I/O,196 I/O, 280 I/O and 676 I/O BGA solder balls at different levels of thermal cycling. Data points only till 1000 cycles have been considered to demonstrate the methodology. Figure 5.9-5.14 shows the phase growth parameter vs. number of thermal cycles for all the packages on the test board.

Variable	Coarse Range
N (cycles)	10-1000
Constant ‘a’	0.0002 – 0.005
Constant ‘b’	0.60 – 1.50
Initial grain size ‘ g_0 ’	0.60 – 1.0

Table 5.2 - Variable Range for Phase-Growth Calculation under Thermal Cycling Load (based on Experimental data)

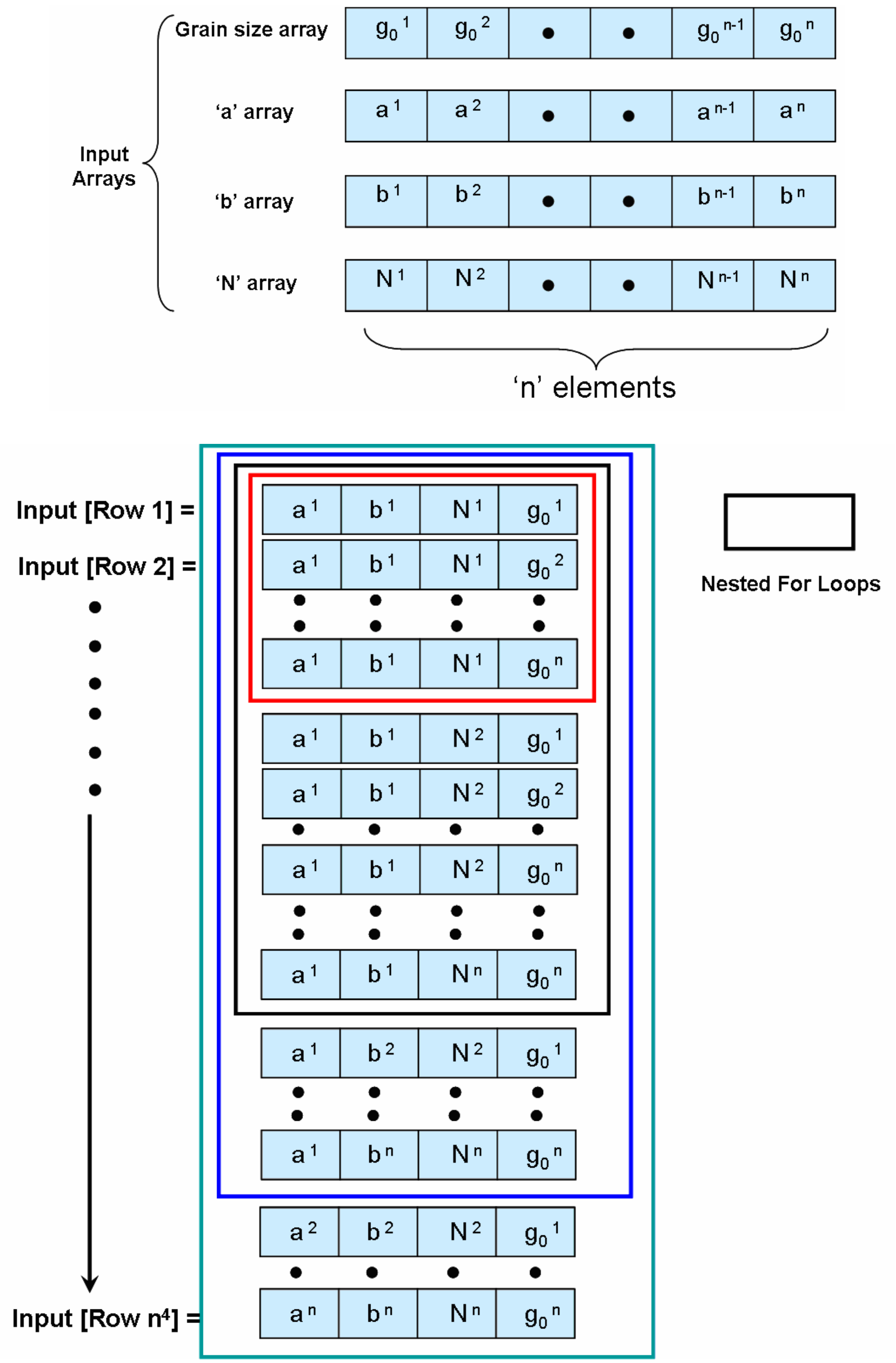

Figure 5.2 - Schematic illustration of input to the LM minimization code

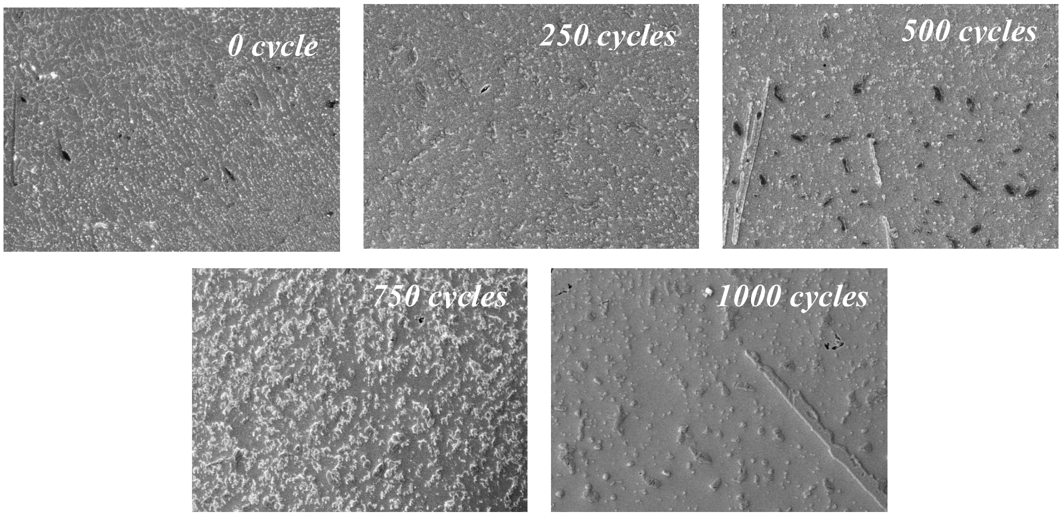

Figure 5.3 - SEM Back-scattered Images of Phase Growth versus Thermal Cycling (-40 to 125°C, 95.5Sn4Ag0.5Cu solder, 64 I/O Tape Array BGA, Magnification: 750x

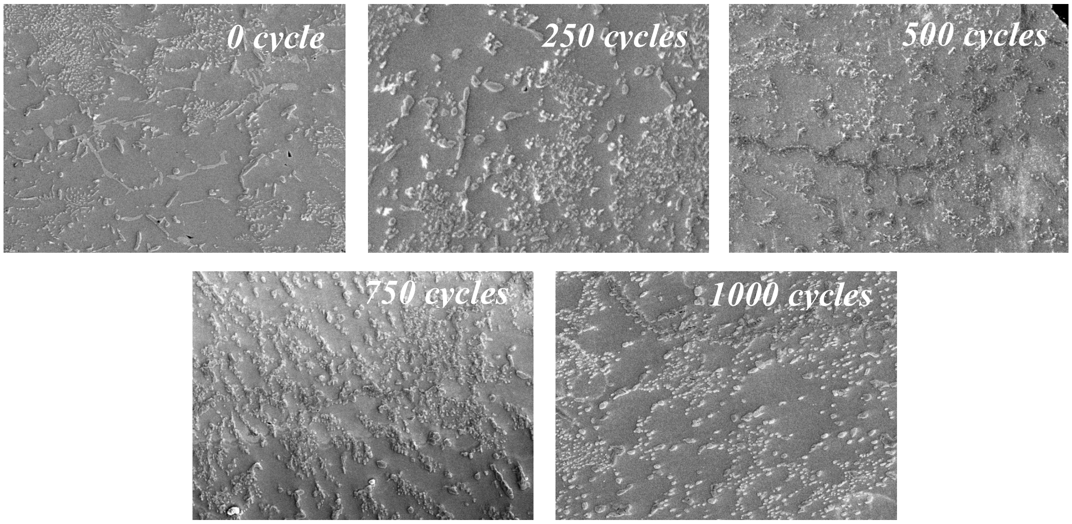

Figure 5.4 - SEM Back-scattered Images of Phase Growth versus Thermal Cycling (-40 to 125°C, 95.5Sn4Ag0.5Cu solder, 84 I/O Tape Array BGA, Magnification: 750x

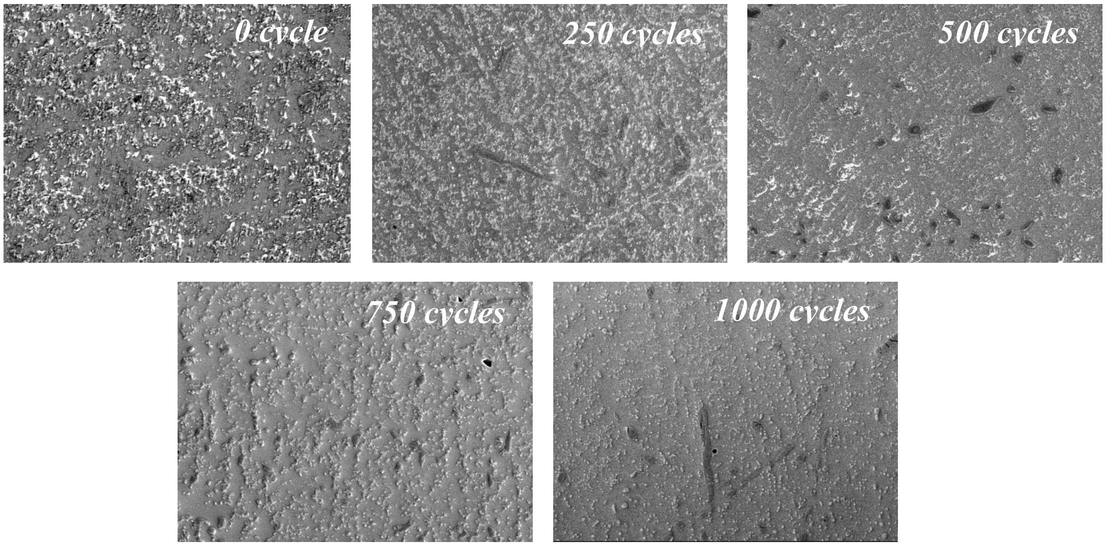

Figure 5.5 - SEM Back-scattered Images of Phase Growth versus Thermal Cycling (-40 to 125°C, 95.5Sn4Ag0.5Cu solder, 144 I/O Tape Array BGA, Magnification: 750x)

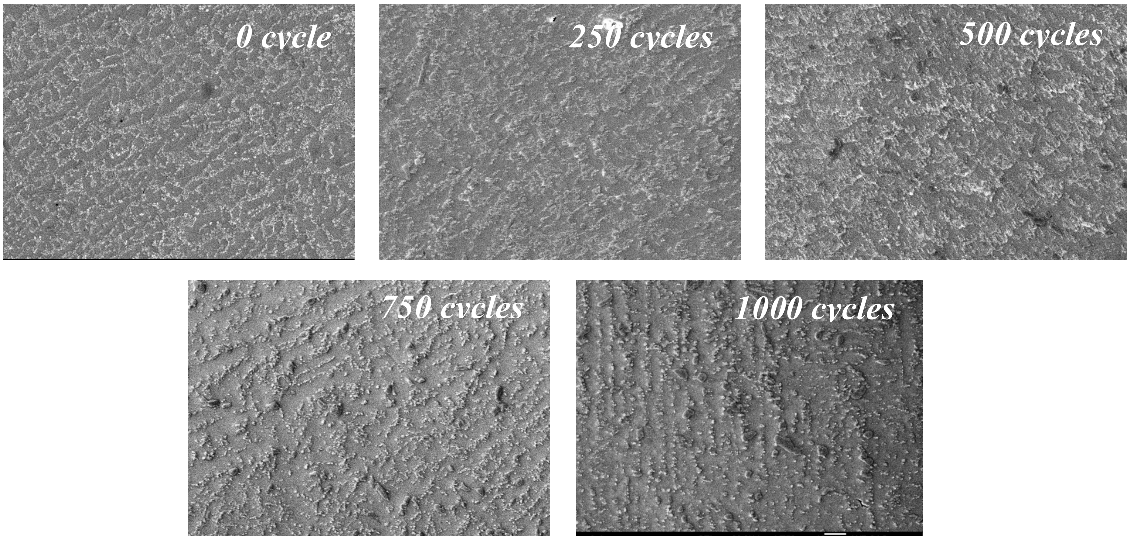

Figure 5.6 - SEM Back-scattered Images of Phase Growth versus Thermal Cycling (-40 to 125°C, 95.5Sn4Ag0.5Cu solder, 196 I/O Tape Array BGA, Magnification: 750x)

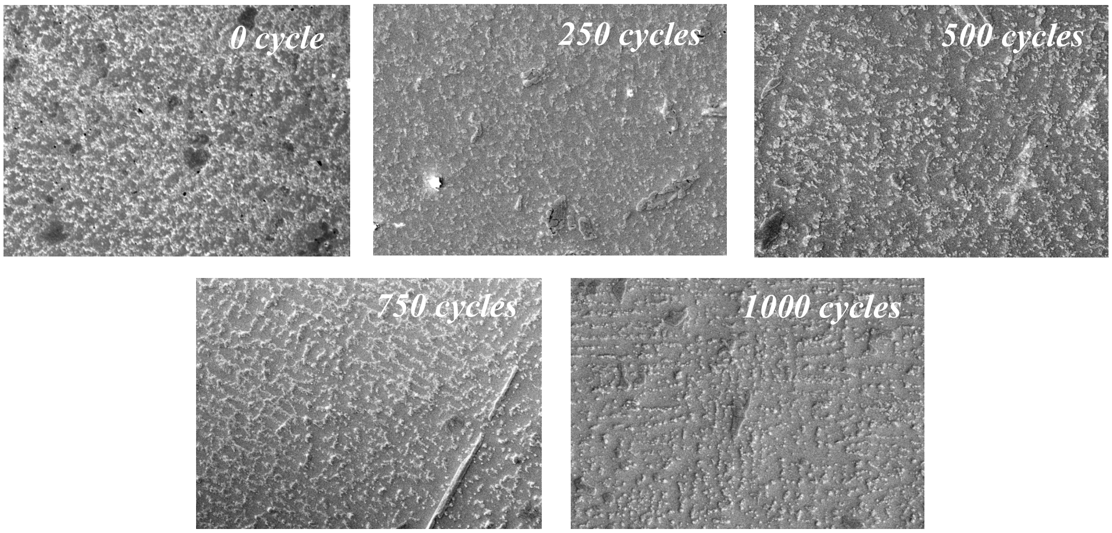

Figure 5.7- SEM Back-scattered Images of Phase Growth versus Thermal Cycling (-40 to 125°C, 95.5Sn4Ag0.5Cu solder, 280 I/O Plastic BGA, Magnification: 750x)

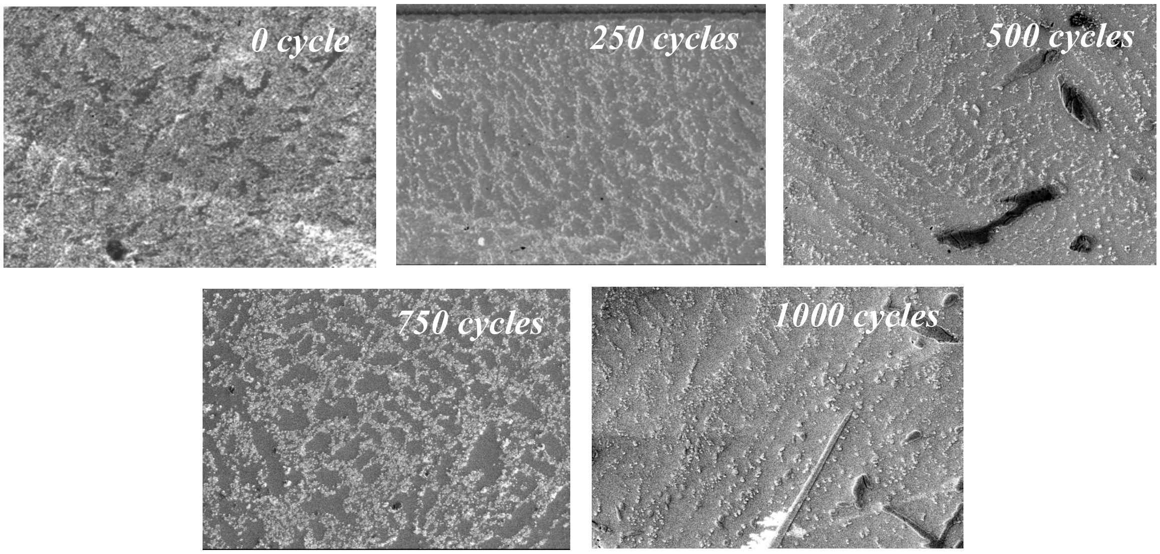

Figure 5.8 - SEM Back-scattered Images of Phase Growth versus Thermal Cycling (-40 to 125°C, 95.5Sn4Ag0.5Cu solder, 280 I/O Flex BGA, Magnification: 750x)

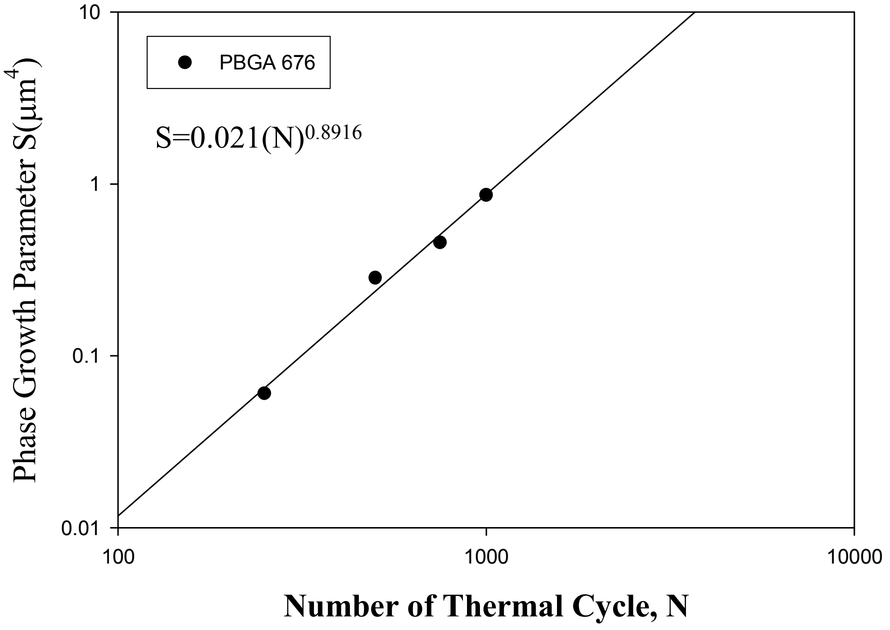

Figure 5.9 - Phase Growth Vs. Number of Thermal Cycles for PBGA 676

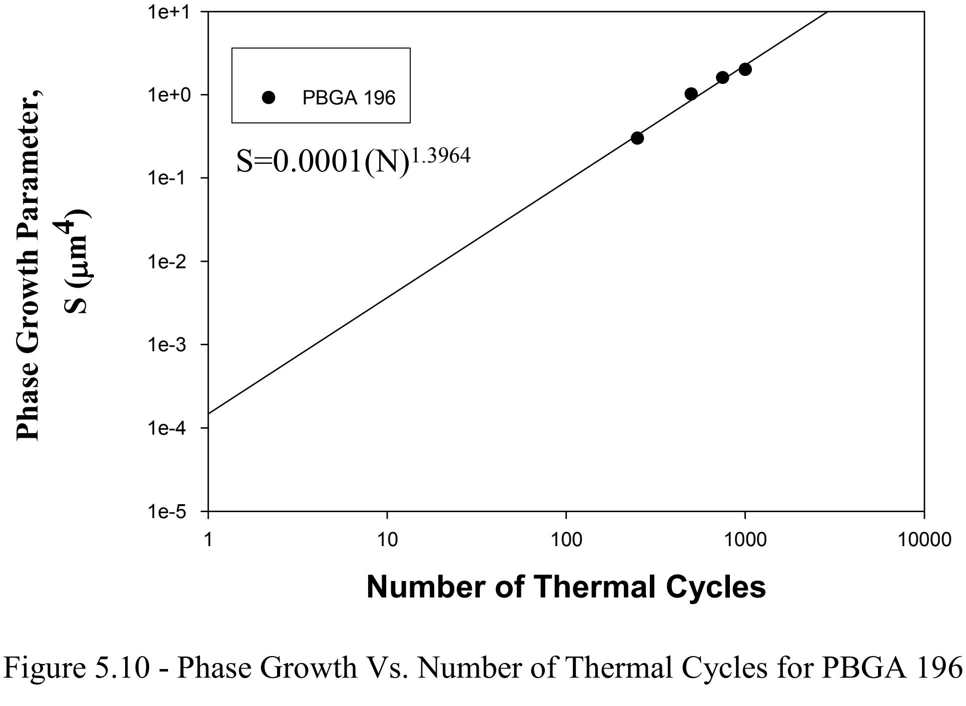

Figure 5.10 - Phase Growth Vs. Number of Thermal Cycles for PBGA 196

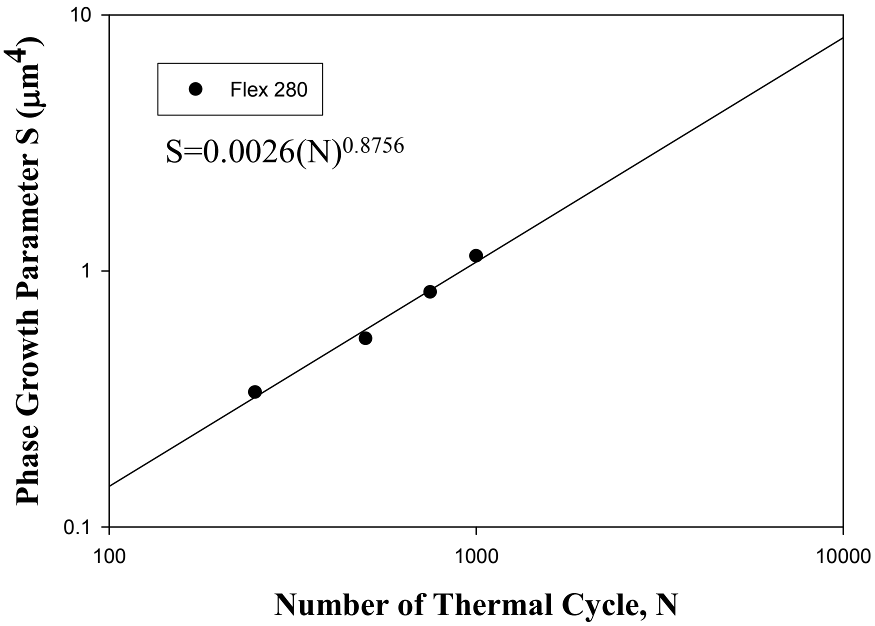

Figure 5.11 - Phase Growth Vs. Number of Thermal Cycles for Flex 280

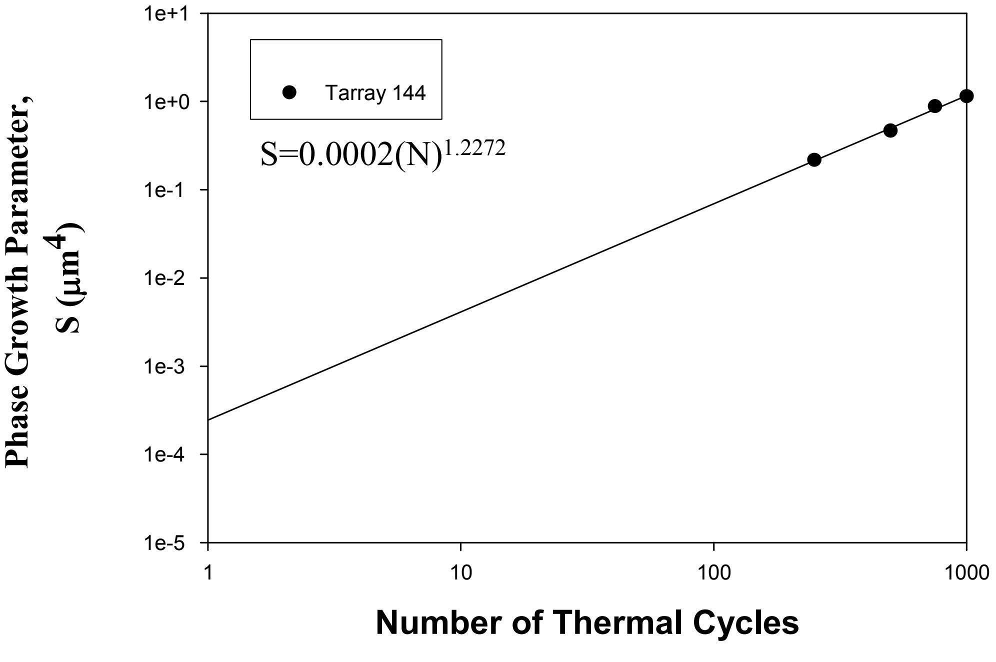

Figure 5.12 - Phase Growth Vs. Number of Thermal Cycles for Tape array 144

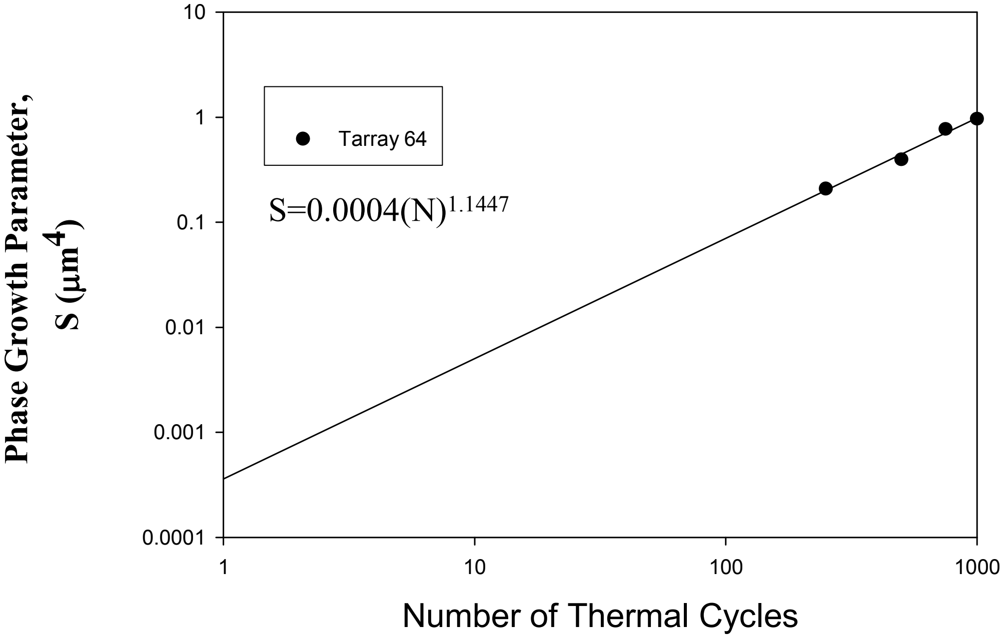

Figure 5.13 - Phase Growth Vs. Number of Thermal Cycles for Tape array 64

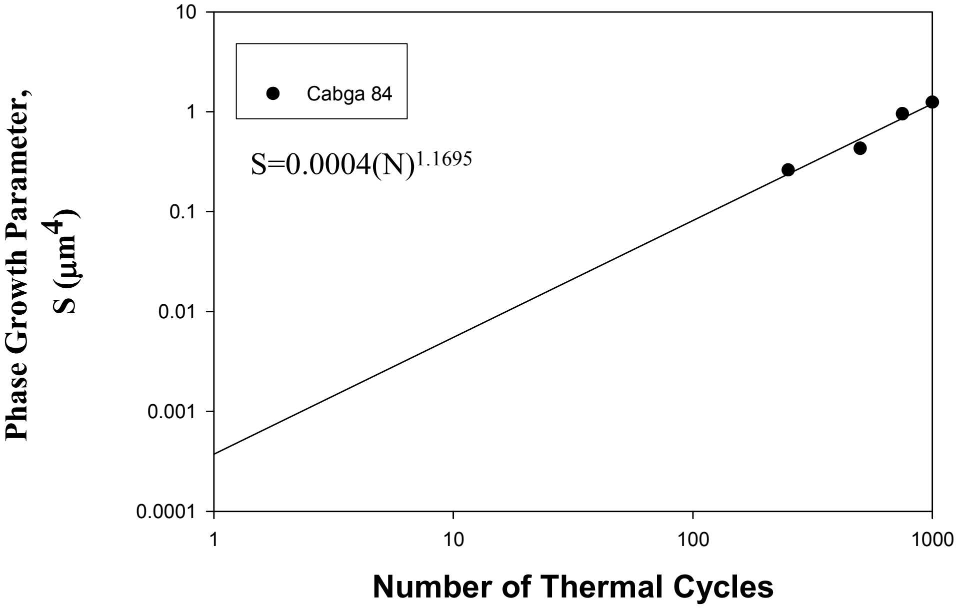

Figure 5.14 - Phase Growth Vs. Number of Thermal Cycles for CABGA 84

Most of the SnAgCu solder is comprised of Sn-phases, so that the growth rate of tin and Ag_3Sn intermetallic crystals are significant. Since Ag atoms have a higher diffusion rate in the molten solder, they can diffuse out, of the way and thus allowing the Sn dendrites to grow. Particles of Ag_3Sn grow either to spheres or to needles shape. In order to calculate the damage and remaining useful life under thermo mechanical loading, the grain size data were taken for different packages for four different thermal-cycle intervals in the time neighborhood of prognostication of the electronic package, at different thermal-cycle values. The measured grain-size values were given as input to the Levenberg-Marquardt Algorithm. For the problem being analyzed, it was found that the LM-solution will tend to converge to local minima, because it does not explore the whole design space.

In order to circumvent the problem, several initial guess values have been supplied within the trust-region. The solution has been identified as the one with minimum error (Figure 5.15). In the case of thermal cycling, the values of g_0, a, N, b have been computed. The computed values of g_0, a, N, b have been compared with the experimentally measured values for the same package. The error is minimized, in the neighborhood of 332 cycles, indicating that prior deployed life, N = 332 cycles is the solution for the 280 I/O BGA. This correlates well with the actual value of 250 cycles from experimental data. Table 4 and Table 5 shows the g_0, a, N, b values and their correlation of computed values with experimental values for the various packages including, 64 I/O Tape Array BGA, 84 I/O Chip Array BGA, 144 I/O Tape Array BGA, 196 I/O Plastic BGA, 280 I/O Flex BGA, and 676 I/O Plastic BGA.

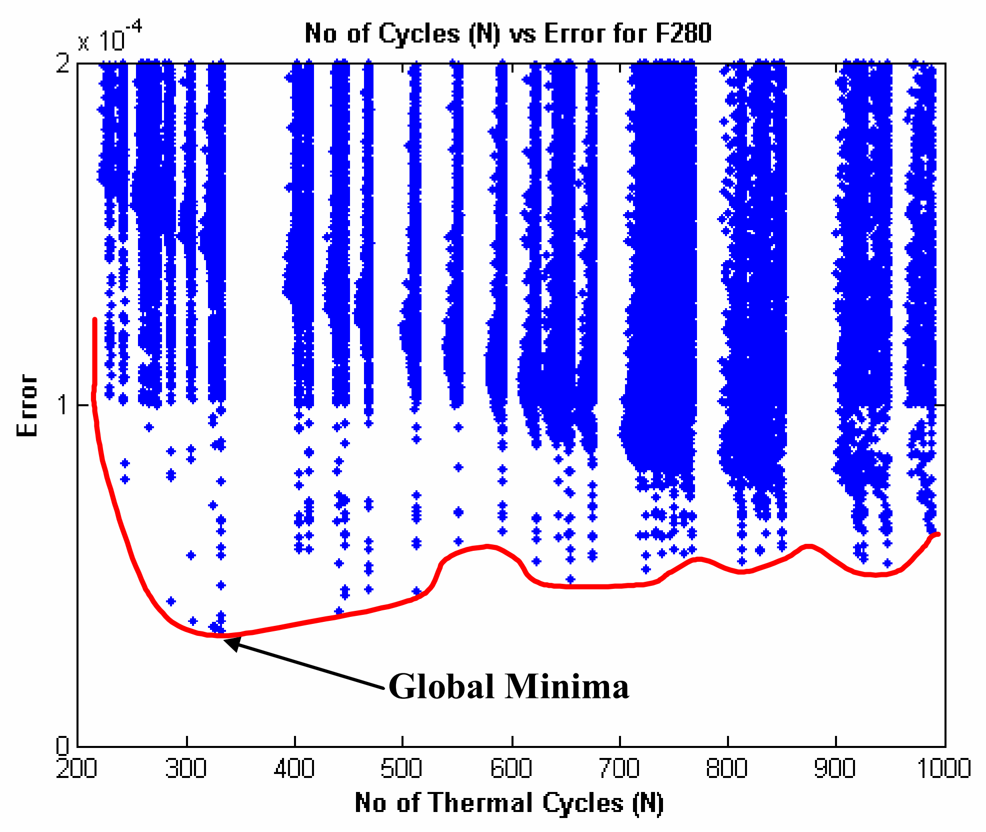

Figure 5.15 - Minimized Error vs. N (Thermal Cycles)

Package	Results			
	g		**N**	
	LM Algorithm	From Expt.	LM Algorithm	From Expt.
P676	0.9347	0.9021	230	250
P196	0.6018	0.8986	304	250
F280	0.9943	0.9882	332	250
T144	0.8401	0.8399	230	250
T64	0.8887	0.8665	231	250
C84	0.8965	0.8739	232	250

Table 5.3 - Comparison of LM result with experiment result

Package	Results			
	a		b	
	LM Algorithm	From Expt	LM Algorithm	From Expt
P676	0.0004278	0.0021000	1.1167060	0.8916
P196	0.0044294	0.0001000	0.9185924	1.3964
F280	0.0003734	0.0026000	1.1434259	0.8756
T144	0.0003325	0.0002000	1.1859530	1.2272
T64	0.0001000	0.0004000	1.3309870	1.1447
C84	0.0001000	0.0004000	1.3634911	1.1695

Table 5.4 - Comparison of LM result with experiment result

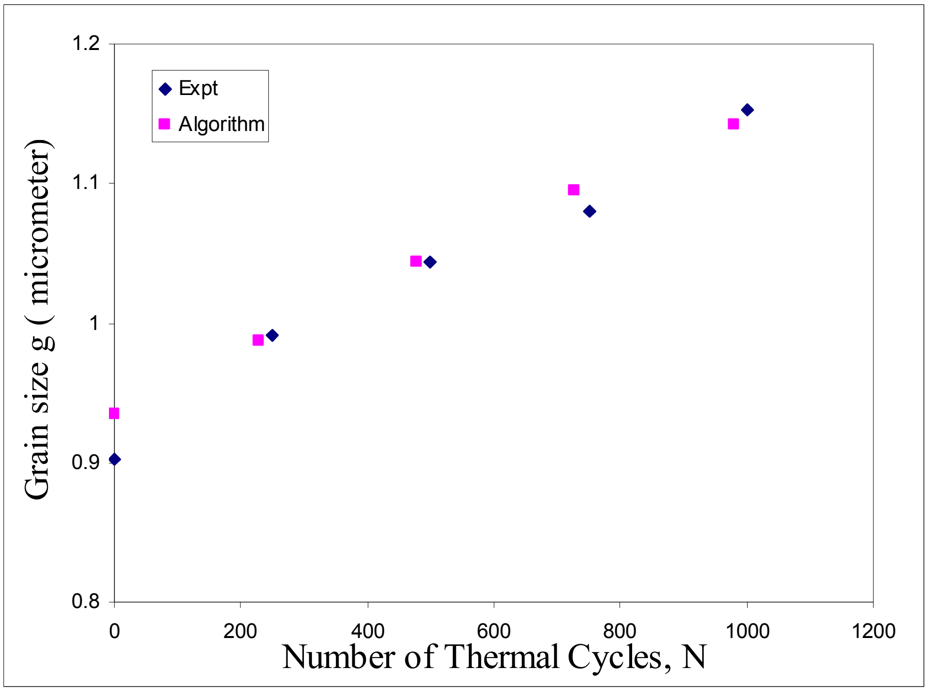

Figure 5.16 - Graphical comparison of grain size values obtained from prognostication model to experimental value for PBGA 676

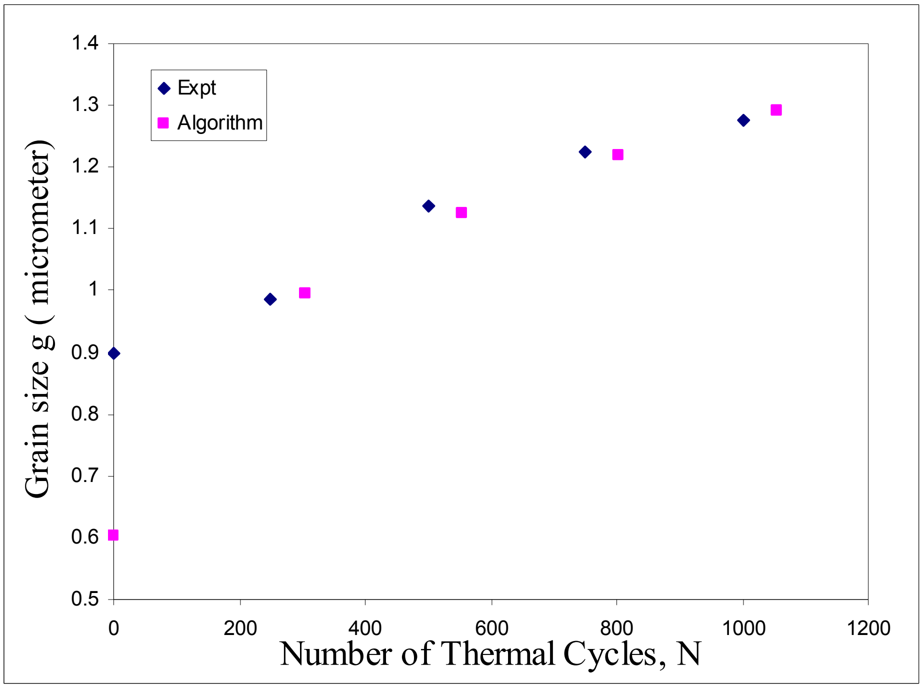

Figure 5.17 - Graphical comparison of grain size values obtained from prognostication model to experimental value for PBGA 196

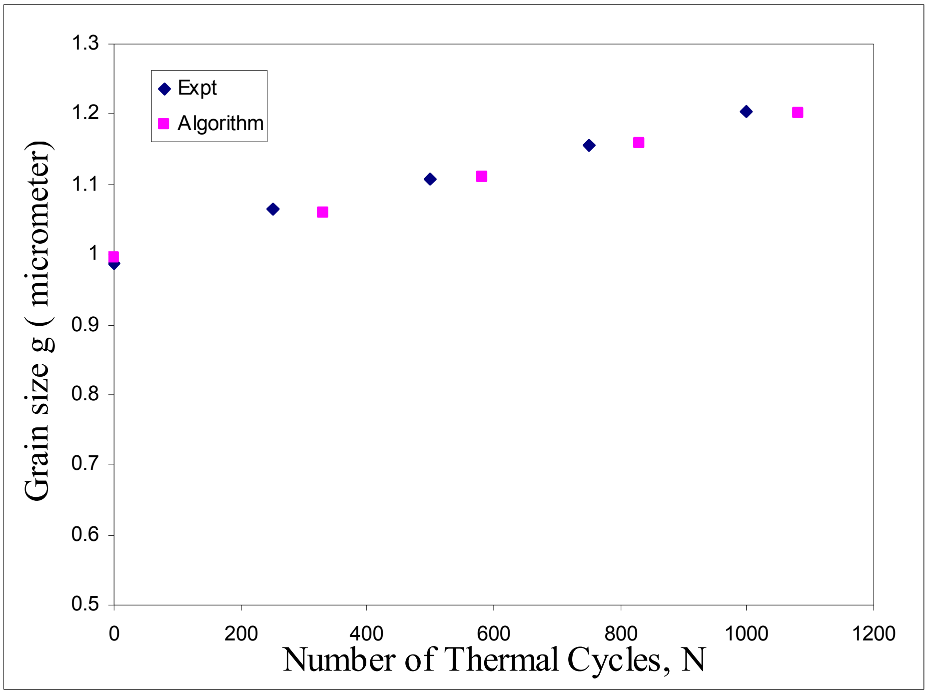

Figure 5.18 - Graphical comparison of grain size values obtained from prognostication model to experimental value for FlexBGA 280

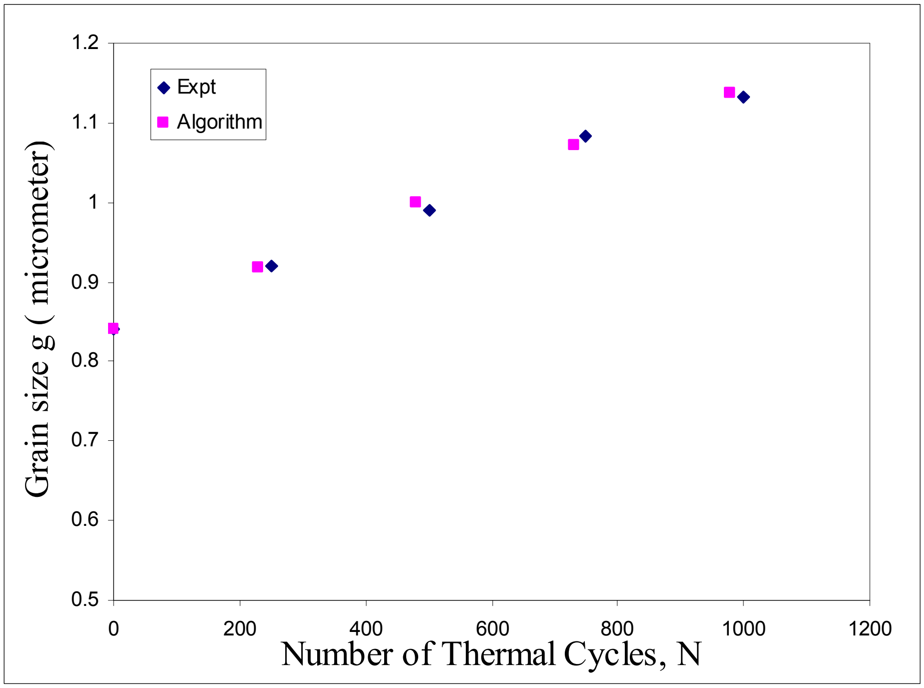

Figure 5.19 - Graphical comparison of grain size values obtained from prognostication model to experimental value for TABGA 144

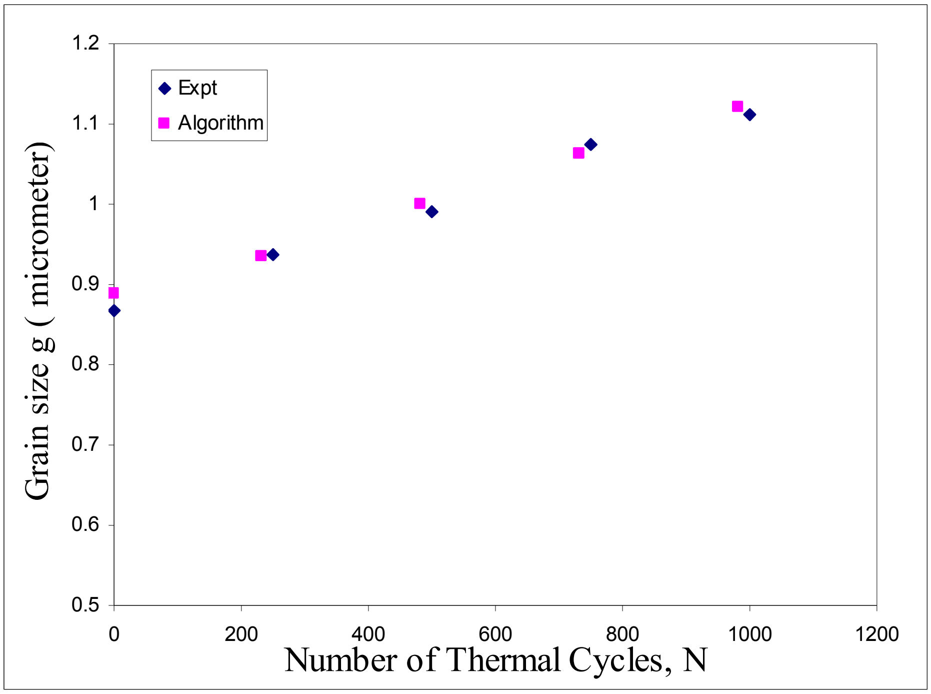

Figure 5.20 - Graphical comparison of grain size values obtained from prognostication model to experimental value for TABGA 64

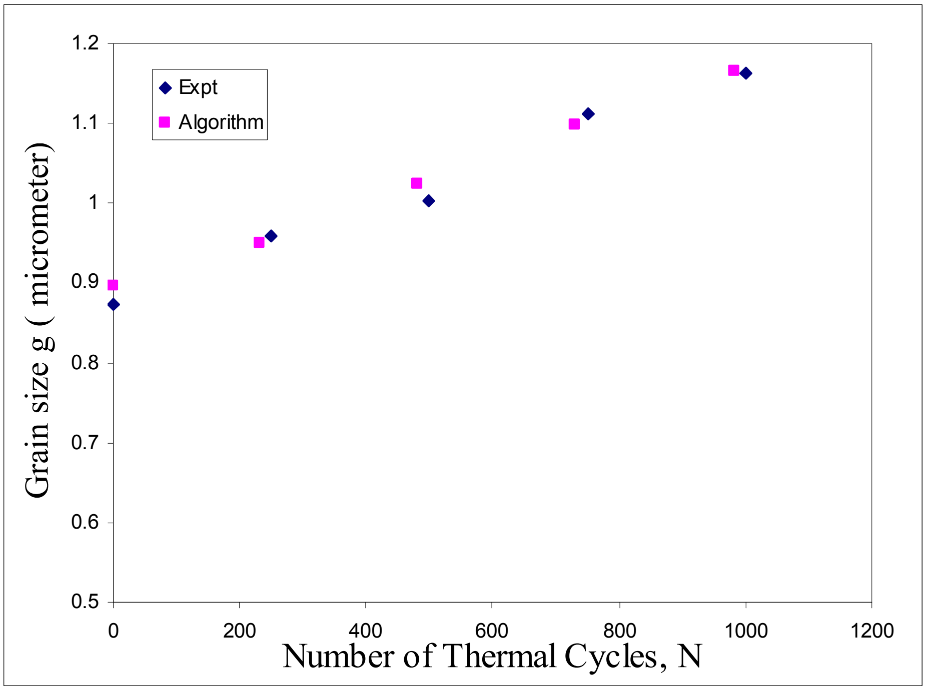

Figure 5.21 - Graphical comparison of grain size values obtained from prognostication model to experimental value for CABGA 84

The packages have been prognosticated in the neighborhood of four-experimental data-points including, 250, 500, 750, and 1000 cycles. The computed grain size and cycles have been plotted in Figure 5.16-5.21. The experimental data and the model predictions show good correlation.

5.9 Implementation of PHM Technique

The PHM technique presented in the paper may be implemented using condition monitoring devices, which can be cross-sectioned to interrogate the system state and determine the failure progression of the assembly. Consider an electronic assembly which has been deployed in the field application. The assembly needs to be redeployed in the same environment.

The condition monitoring devices in the system will then be withdrawn at periodic intervals in the deployed environment. The condition monitoring devices will be cross sectioned and their grain size data will be extracted. This data will be analyzed using Levenberg's-Marquardt Algorithm and methodologies discussed earlier, to find out the initial grain size (g0) and the prior time of deployment (N, or t) for which the component has been deployed. The rate of change of phase growth parameter, (dS/dN), will be computed using the computed values of damage proxies or leading indicators-of failure. The rate of change of phase growth parameter (dS/dN) can be correlated to time-to-failure [Lall 2004[b], 2005, 2006[a,b], 2007[a,b]]. Residual Life (RL) can be calculated using the following equation

$$RL = N_f - N \qquad 5.19$$

Table 5.5 shows the correlation of model predictions of remaining useful life, with experimental data. Model predictions show good correlation with experimental data.

Package	Algorithm				Experiment			
	dS/dN	Nf	N	RL	dS/dN	Nf	N	RL
PBGA 676	1.11671	2049	230	1819	0.8916	2566	250	2316
PBGA 196	0.91859	3968	304	3664	1.3964	2610	250	2360
FLEX 280	1.14343	2038	332	1706	0.8756	2662	250	2412
TARRAY 144	1.18595	2561	230	2331	1.2272	2475	250	2225
TARRAY 64	1.33099	1803	231	1572	1.1447	2096	250	1846
CABGA 84	1.36349	1664	232	1432	1.1695	1940	250	1690

Table 5.5 - Correlation of Computed Residual Life with Experimentally Measured Values

5.10 Summary and Conclusion

A methodology has been presented to calculate the prior damage in electronics subjected to cyclic and isothermal thermo-mechanical loads. The time duration for which the component has been deployed and initial grain size has been estimated using Levenberg-Marquardt Algorithm with Trust Regions. Methodology has been demonstrated using various leading-indicators of failure including, phase growth and intermetallic thickness. The presented approach uses nonlinear least square and gives an accurate method of estimating prior stress history of interrogating system-state before redeploying it in other missions. The prior stress histories have been calculated for both cyclic thermo-mechanical loads and isothermal loads. Computed results have been correlated with the experimental data for various aging times and thermal cycles for several packaging architectures. Model predictions of residual life correlate well with experimental data. The correlations indicate that the leading indicators based PHM technique can be used to interrogate the system state and thus estimate the Residual-Life of a component. The presented approach of computing residual life can be implemented prior to appearance of any macro-indicators of damage like crack. The methodology presented using condition monitoring components to find out the residual life, is promising because these components experience the same environment as actual component.

CHAPTER 6

PROGNOSTIC HEALTH MANAGEMENT METHODOLOGY FOR DAMAGE ASSESSMENT OF ELECTRONICS FOR VARIOUS LEAD FREE ALLOYS

6.1 Introduction

Various types of Pb-free alloys have been invented after the legislation to ban all the Pb products in the electronic industry. The most common Pb-free alloy used is Sn-Ag-Cu (SAC) because it offers several advantages over the other Pb-free alloys such as relatively low melting point (217 °C) with an operating range of 250°C - 280°C and it is ideally suited for the assembly of printed circuit boards due to its reasonable cost. The issue of solder joint reliability is of great concern while implementing an alloy for production which is dealt by demonstrating the thermal and mechanical reliability of this solder alloys. Silver is not only an expensive element in SAC alloys but it also plays a vital role in thermal and shock resistance of solders. The improvement of drop/shock reliability with lead free solder has been the key focus for many electronic products as Pb-free solders typically show increased brittle solder joint failures than that of Pb-Sn solder. Since lead-free solders have lower drop performance compared with Pb-Sn solders, many efforts have been reported to improve solder joint reliability with various lead free solders. The effect of lead free solder composition on drop reliability was studied by considering two of the most extensively used SAC formulations e.g. SAC 105 (Sn1.0Ag0.5 Cu) and SAC 405 (Sn4.0Ag0.5 Cu). The experimental study confirmed that the use of lead free solders with low Ag content like SAC105 significantly improved board level reliability during drop test when compared with SAC 405 alloys [Henshall 2007]. But on the contrary, it is been observed previously by researchers that the increase in the Ag and Cu content in the alloy will decrease the steady state creep rate [Dutta 2007]. Therefore, several researches are going on to investigate the best alloy which can be used in thermal cycling and also in the drop/shock environment.

Previously Lall, et al. [2004^{b}, 2005, $2006^{a,b}$, $2007^{a,b}$] have developed a methodology for Health Management of electronic systems based on leading indicators of failure like grain size coarsening, inter-metallic thickening, etc for eutectic Sn-Pb and SAC 405 alloy systems. Methodology presented resides in the pre-failure space of the system in which no macro-indicators such as cracks or delamination exists. These methodologies will trigger repair or replacement significantly prior to failure. The approach involves the use of condition monitoring devices which can be interrogated for damage proxies at finite time-intervals. In this thesis, the same methodology has been extended to other lead-free alloys like Sn1.0Ag0.5Cu, Sn3.0Ag0.5Cu and Sn0.3Ag0.7Cu under thermal cycling environment from -55°C to 125°C.

6.2 Experimental Approach

The solder alloys used in this study are Sn1.0Ag0.5Cu, Sn3.0Ag0.5Cu and Sn0.3Ag0.7Cu. The solder balls are attached to a Chip-array Ball Grid Array (CABGA) substrate with Cu bond pads. There are 15 packages on each board as shown in Figure 6.1. The package is of 10 mm body size, 0.5 mm pitch and has 100 I/O count. The Package is mounted on a printed wiring board made up of FR4 laminate. The package has been put in a thermal cycling chamber having -55°C to 125°C thermal profile. At an interval of 250 cycles, boards have been removed from the chamber and cross-sectioned. The cross-sections were studied under a scanning electron microscopy (SEM), JEOL JSM-7000F operated at an accelerating voltage of 20 kV. The pictures were taken at a magnification of 750x. All samples were imaged after polishing and etching to reveal the grain structure. The quantitative measure of precipitants particle size was established from a 60μm x 45 μm rectangular region selected from back scattered SEM image of the highest strain corner solder ball. The location of the examination region was identical for all the samples. Grain size was averaged from the various samples for each package architecture and stress exposure.

6.3 Methodology

The damage proxy has been identified as explained in Chapter 4 for all three alloys in the test matrix. The phase growth parameter S is then calculated at every thermal cycle interval using the following formula

$$S = g^4 - g_0^{\ 4} \qquad 6.1$$

where g is the grain size at time t and g_0 is the grain size after the reflow. The Phase growth data in this study indicates that the phase growth rate stays fairly uniform during the thermal cycling test. SEM backscattered images of grain size for three different alloys at various levels of thermal cycling have been shown in Figure 6.2 to 6.4. Figure 6.5 to 6.7 shows the plot of phase growth parameter vs. number of thermal cycles. The slope of the curve varies for each alloy i.e. the damage accumulation rate varies for different alloys. But the linearity of the microstructural evolution depicts the validity of phase growth as a proxy for damage progression. Once we have the phase size data, it has been used to interrogate the system state to investigate the prior damage and also to know the remaining useful life.

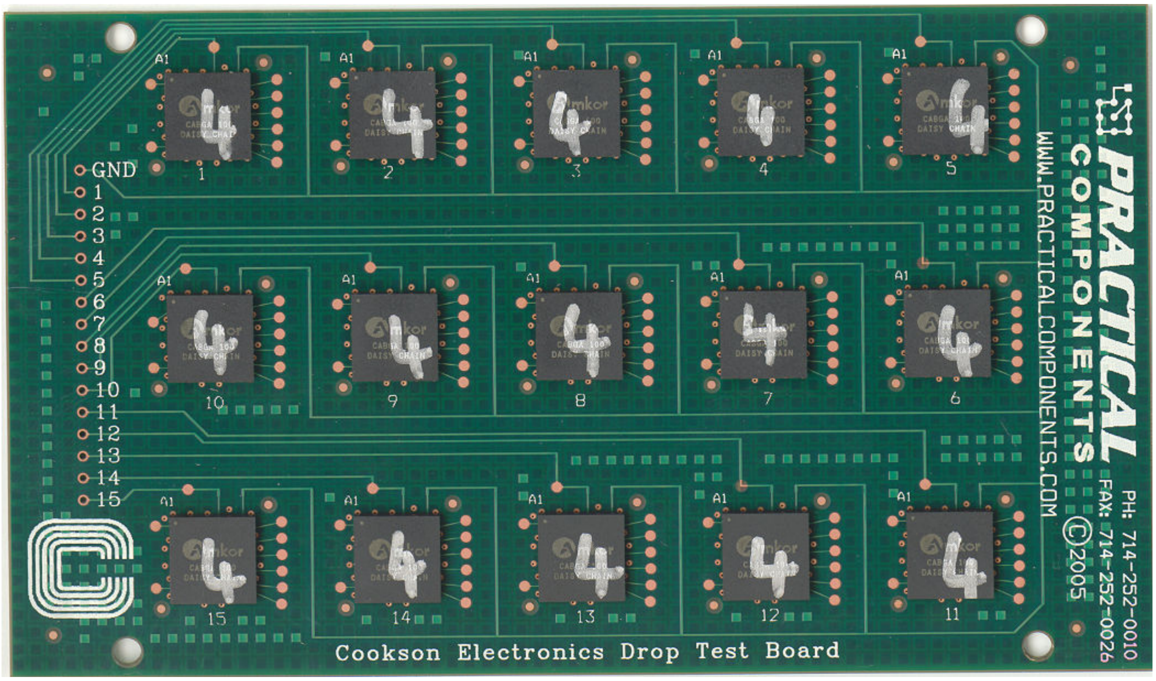

Figure 6.1- Cookson Test board used in the prognostication study of various lead-free alloys

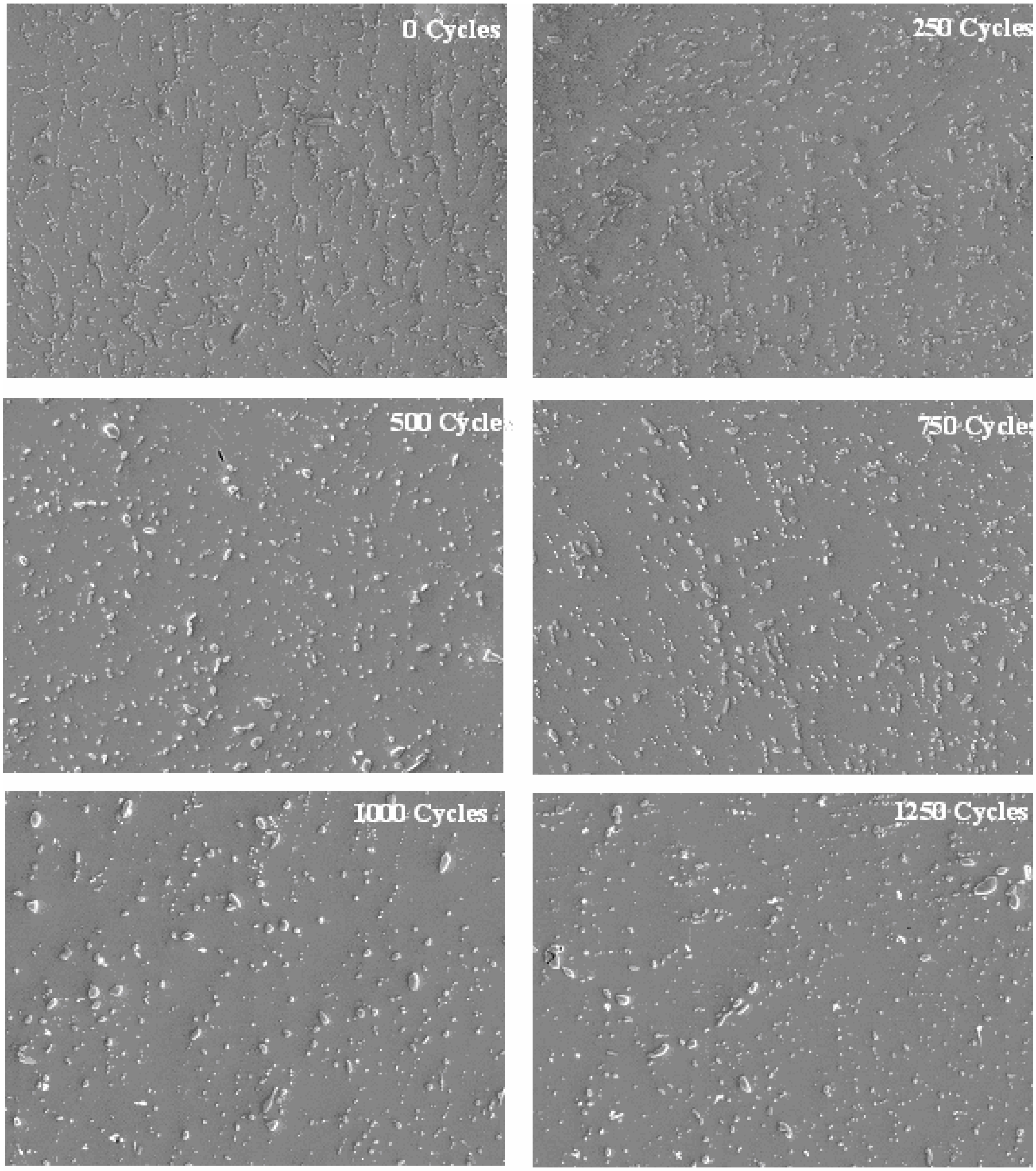

Figure 6.2- SEM Backscatter Pictures showing Phase size vs. Number of thermal cycles for SAC105 alloy

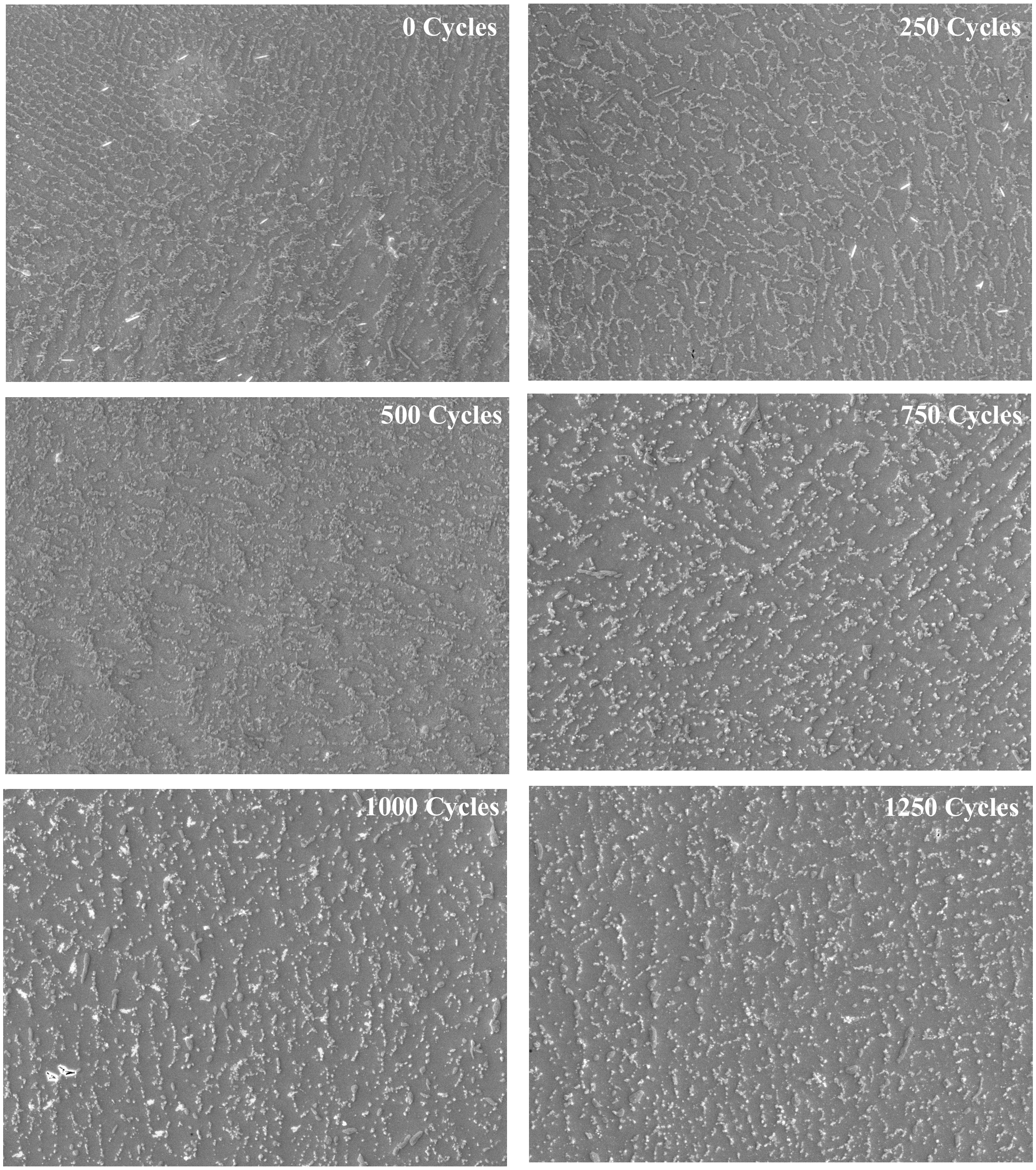

Figure 6.3- SEM Backscatter Pictures showing Phase size vs. Number of thermal cycles for SAC305 alloy

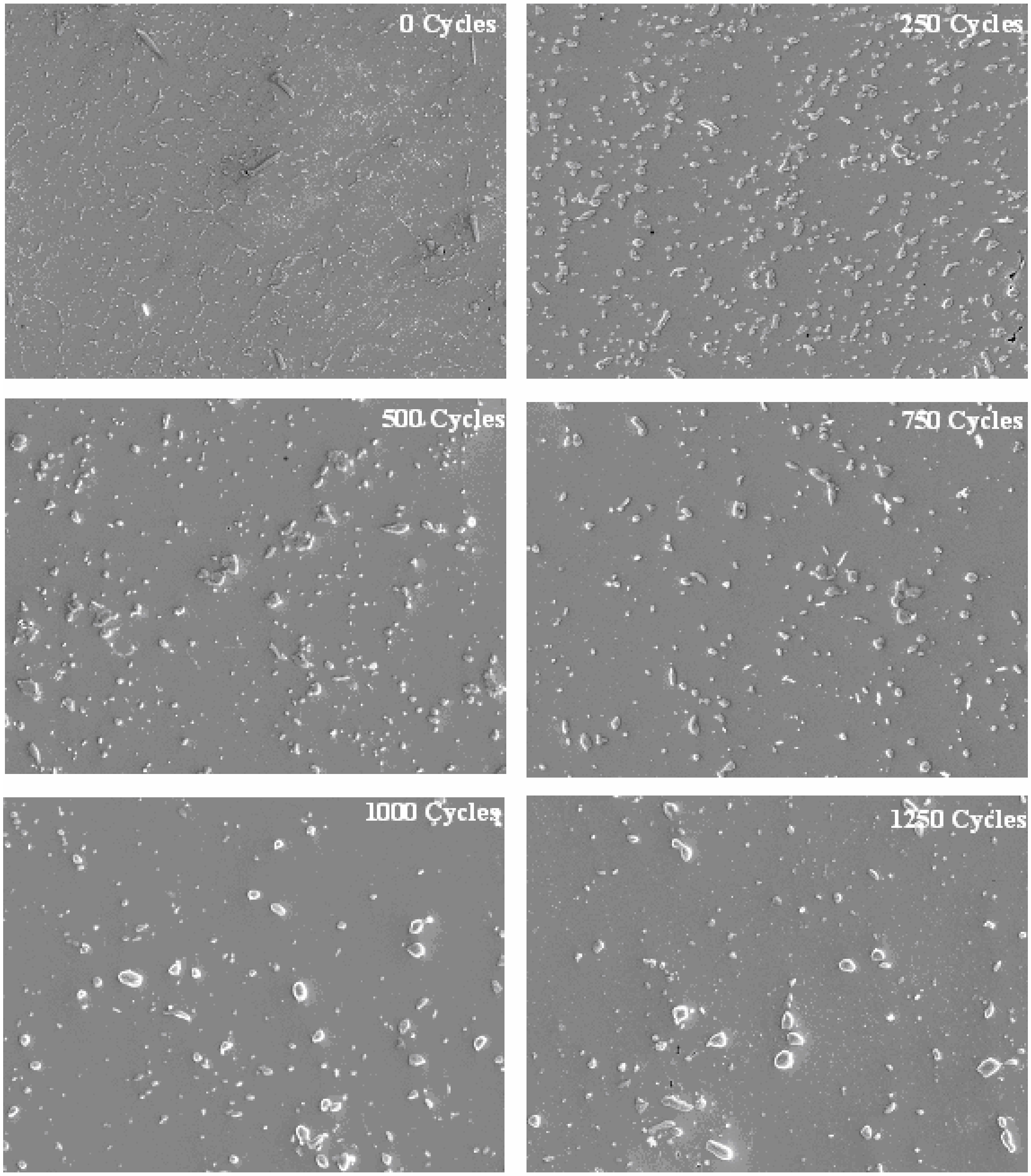

Figure 6.4- SEM Backscatter Pictures showing Phase size vs. Number of thermal cycles for SAC0307 alloy

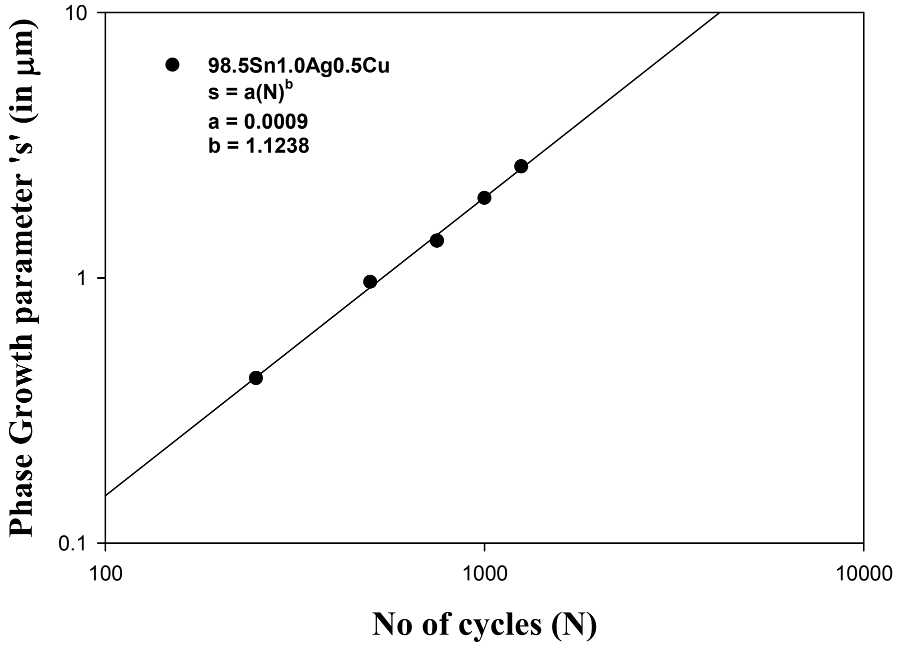

Figure 6.5- Phase Growth Parameter vs. Number of Cycles for SAC 105

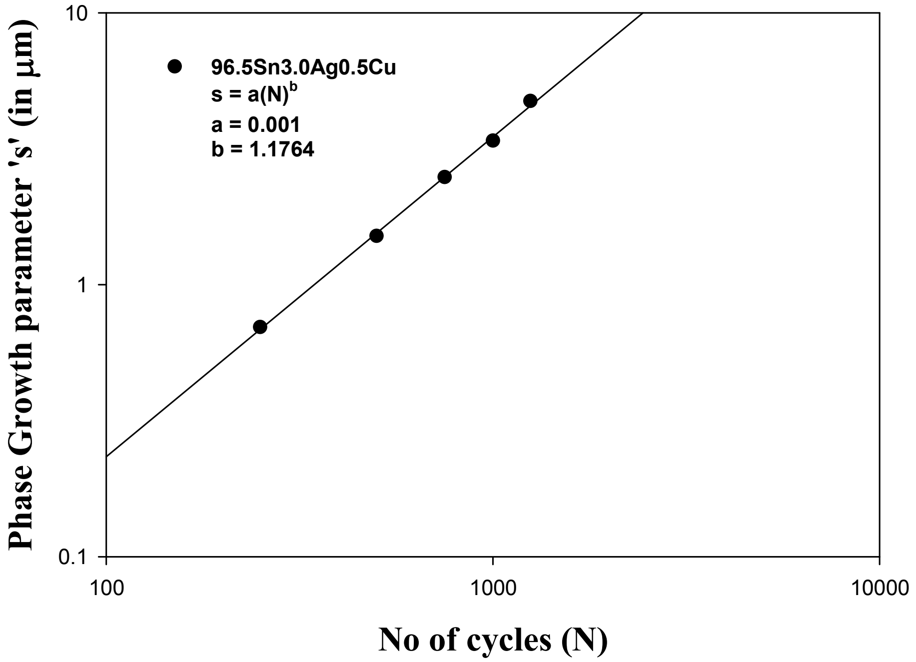

Figure 6.6- Phase Growth Parameter vs. Number of Cycles for SAC 305

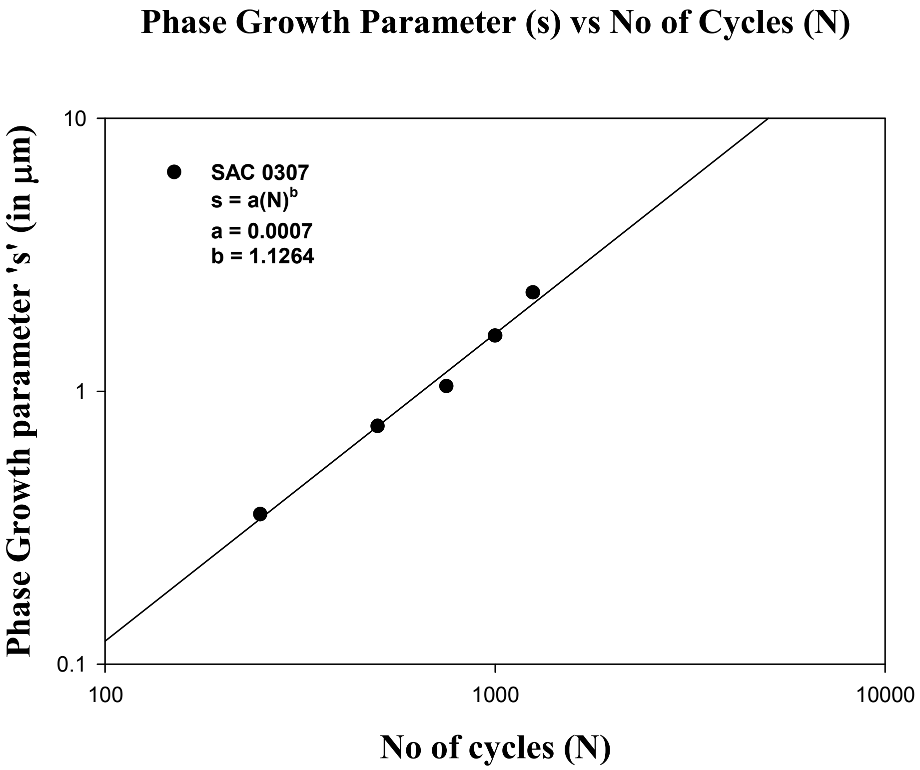

Figure 6.7- Phase Growth Parameter vs. Number of Cycles for SAC 0307

An energy dispersive X-ray (EDX) has been used to examine the morphology and composition of the precipitants in the Sn-matrix. Figure 6.6-6.8 shows the EDX analysis of the precipitants for SAC105, SAC305 and SAC0307 solder alloys. It is found that the Sn-matrix has the Ag_3Sn and Cu_6Sn component dispersed everywhere and also the size of these components varies after thermal cycling. Table 6.1 shows the composition of Sn, Ag and Cu composition of the precipitants in the Sn-matrix for all the three alloys. This analysis is qualitative and not quantitative. Therefore the expected composition of the elements may not match the actual values exactly.

Alloy	Weight %		
	Sn	Ag	Cu
SAC 105	91.01	7.79	1.20
SAC 305	83.17	10.61	6.22
SAC 0307	95.69	1.28	3.02

Table 6.1 - Weight percentage of metals in the precipitants of various solders alloys

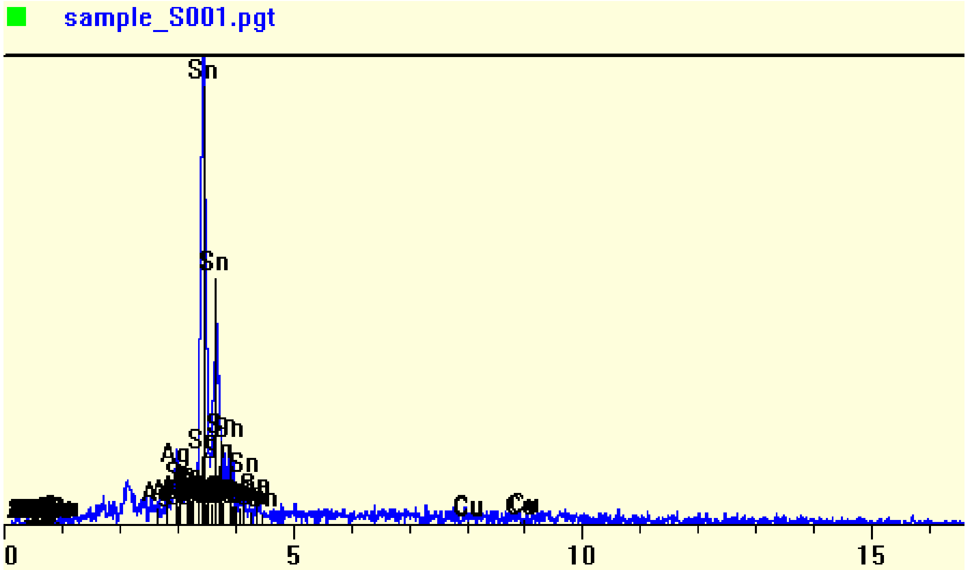

Figure 6.8 - EDX Analysis spectrum for SAC 105 precipitants

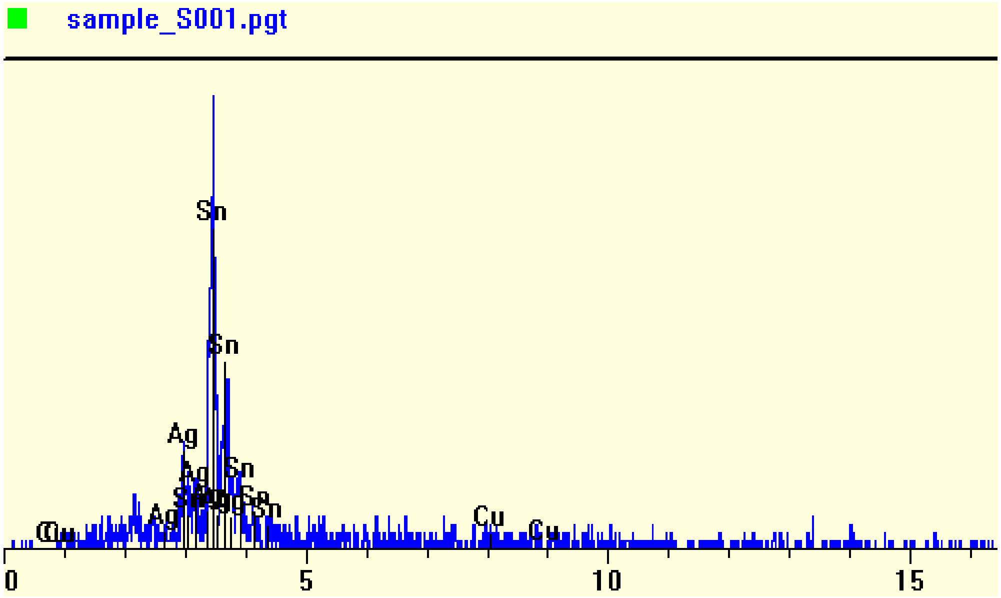

Figure 6.9 - EDX Analysis spectrum for SAC 305 precipitants

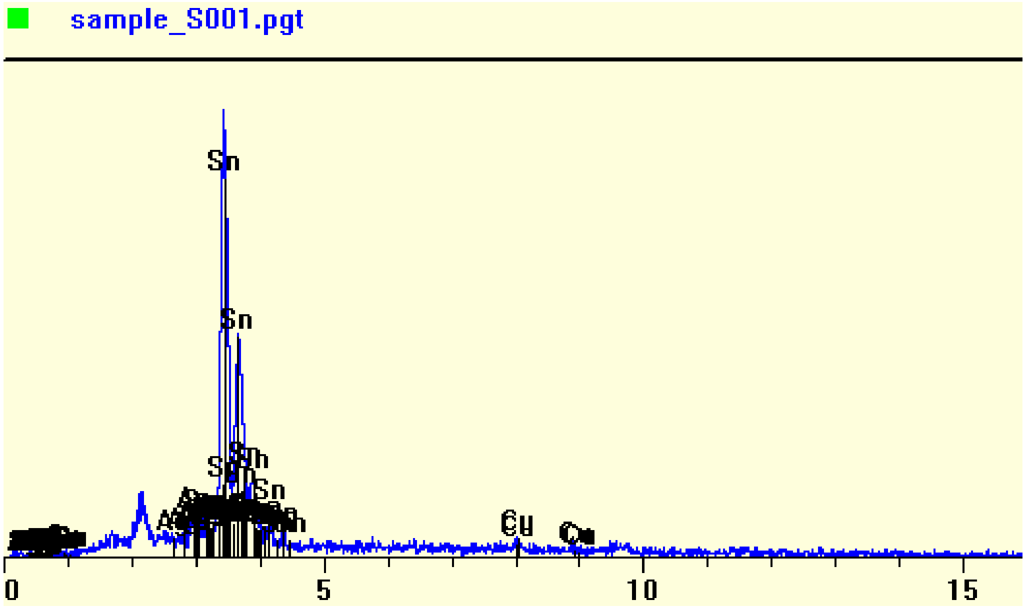

Figure 6.10 - EDX Analysis spectrum for SAC 0307 precipitants

6.4 Non-linear Finite Element Models

Linear, nonlinear, elastic, plastic, creep, temperature, time-dependent and time-independent material properties have been incorporated in the finite-element models. It is well known that time-dependent creep phenomena dominate solder joint fatigue because solder is above half its melting point at room temperature. The thermal fatigue failure of electronic packages is associated with combined plastic-deformation and creep of solder joints. The Anand Viscoplasticity model has been used by several researchers to model the constitutive behavior of solder. It is a standard material model in ANSYS to model the Viscoplastic behavior of metal.

Anand's model has been used by many researcher to quantify the interconnect damage during thermal fatigue analysis [Darveaux 2000]. In this study, the finite element model has been created only for two alloys, SAC105 and SAC305, to quantify the interconnect damage because material constants were not available for other alloys. Table 6.2 and Table 6.3 show the material properties used for finite element simulation [Amagai 2002, Chang 2006]. Thermo-mechanical analysis was performed on these models for thermal cycle ranging from -55°C to 125°C. Inelastic work per volume per thermal cycle was calculated for the elements at the interface of the solder interconnect with package pad for maximum strained solder ball. Volumetric average of inelastic strain-energy density accumulated per cycle for the critical ball where the crack propagates is given by the following equation.

$$\Delta W_{avg} = \frac{\sum_{k=1}^{N} \Delta W_k V_k}{\sum_{k=1}^{N} V_k} \qquad 6.2$$

where ΔW_k is the plastic work per volume for each element and V_k is the volume of each element. Figures 6.9 and 6.10 show the diagonal symmetry finite-element models and plastic work per volume results for SAC105 and SAC305 respectively.

The phase growth rate per cycle is closely related with the inelastic strain energy density per cycle. Prior studies have correlated the number of cycles to crack initiation and the crack propagation rate to the inelastic strain energy density [Darveaux 2000, Lall 2003]. Figure 6.11 shows the relationship between rate of change of phase growth parameter and inelastic strain energy density. Inelastic strain energy density for SAC 405 and Sn3.5Ag alloys has been computed from nonlinear finite element models. The time-to- failure N_f of solder joints can be correlated with the rate of change of phase growth parameter per cycle, dS/dN. Since the rate of change of phase growth parameter has been correlated to the inelastic strain energy density, ΔW, therefore, it is hypothesized that the faster phase growth correlates with faster accumulation of inelastic work in the joint and lower cycles to failure. The following relationship has been developed for the solder interconnects [Lall 2004[b], 2005, 2006[a,b], 2007[a,b]]

$$N_f = C_2\left(\frac{dS}{dN}\right)^{-\gamma} \tag{6.3}$$

where C_2, and γ are constants. The relation enables the calculation of residual life. The phase growth rate in a deployed part can be monitored in the intended use-environment and the residual life can be evaluated.

Material	Elasticity E(Mpa)	CTE(ppm/°C)	Poisson's ratio
Copper Pad	128,932	16.3	0.34
Solder Mask	3,100	16.3	0.3
Solder-Sn3.5Ag	47,572	25	0.35
Solder -SAC 305	38700-0.176T	25	0.35
Solder -SAC 105	47,000	25	0.35
Silicon	162716	25.4	0.28
Die Adhesive	6769	52.5	0.25
Mold	23,520	15	0.3
Substrate	17,890	12.4(X)	0.39
	(X & Z)	57 (Y)	(XY YZ)
	7846 (Y)	12.4(Z)	0.11 (XZ)
PCB	16,898	14.5	0.39
	(X & Z)	(X & Z)	(XY YZ)
	7,436 (Y)	67.20 (Y)	0.11 (XZ)

Table 6.2 - Material Properties used for finite element modeling

Definition	Parameter	SAC105	SAC305
Resistance	S_o (MPa)	30	45.9
Activation Energy / Boltzmann's Constant	Q/R(1/K)	8400	7460
Pre-Exponential Factor	A (1/sec)	24200000	5870000
Multiplier of Stress	ξ	0.043	2
Strain Rate Sensitivity of Stress	m	0.168	0.0942
Hardening Constant	h_o (MPa)	3162	9350
Coefficient of Deformation Resistance Saturation Value	s^ (MPa)	1.005	58.3
Strain Rate Sensitivity of Saturation Value	n	0.00081	0.015
Strain Rate Sensistivity of Hardening	a	1.59	1.5

Table 6.3 - Anand’s Constant for SAC105 and SAC305

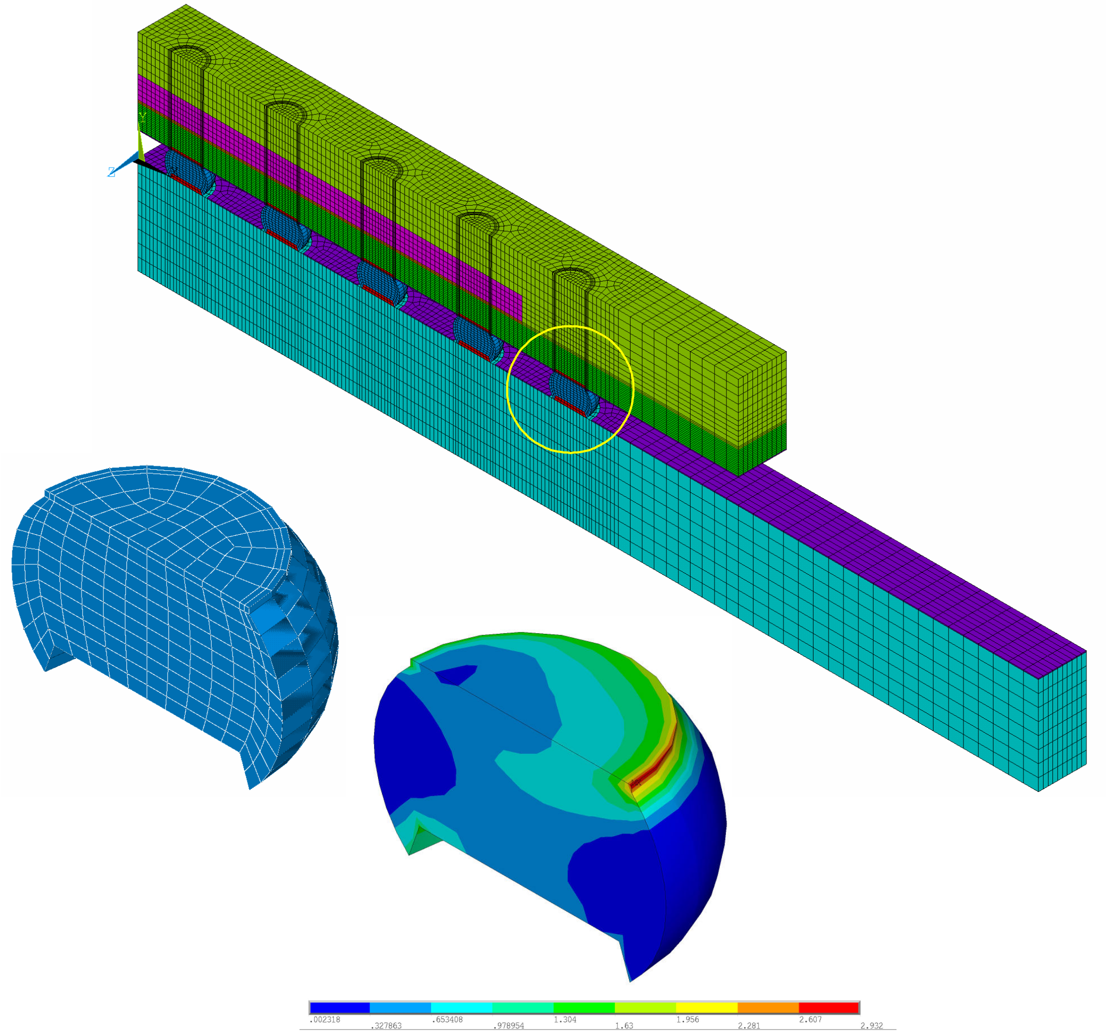

Figure 6.11 - CABGA 100 finite element model and plastic work per volume plot with SAC105 interconnects

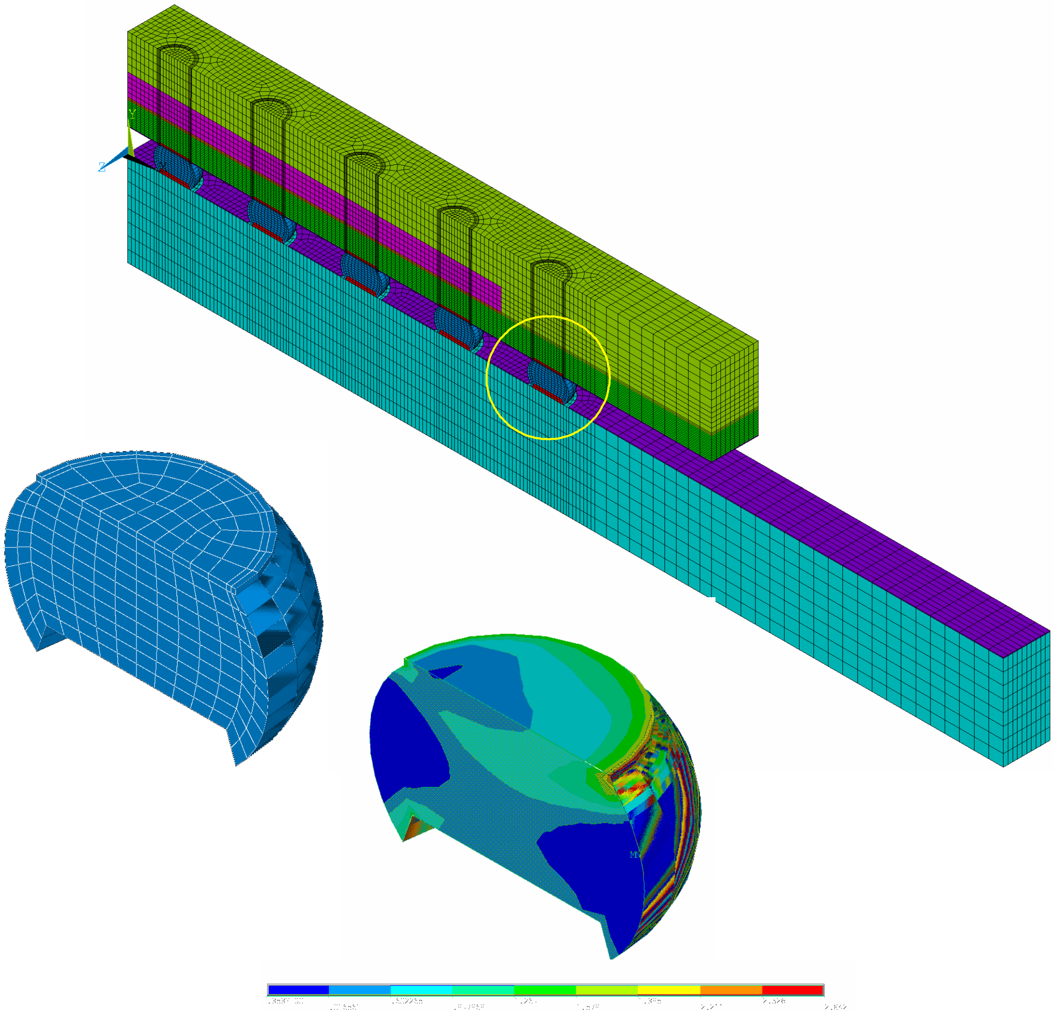

Figure 6.12 - CABGA 100 finite element model and plastic work per volume plot with SAC305 interconnects

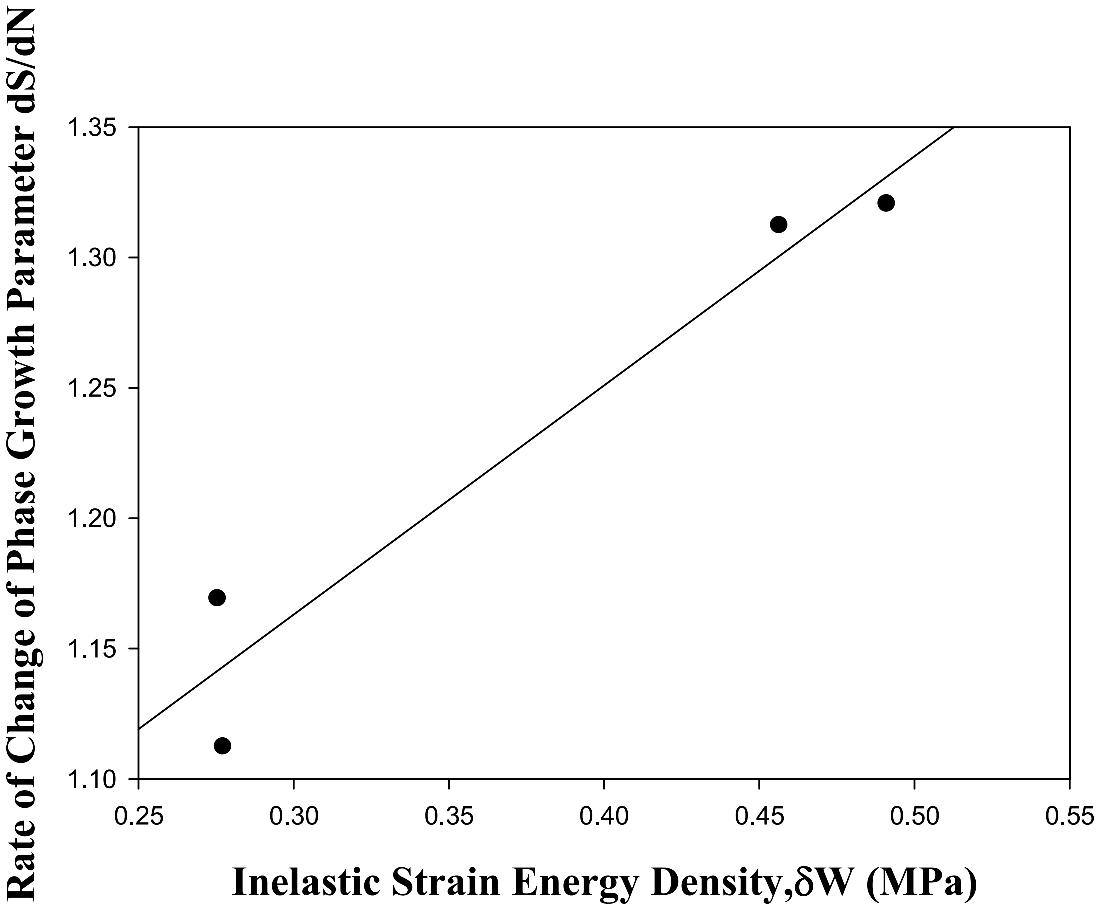

Figure 6.13 - Phase Growth Rate vs. Inelastic Strain Energy Density

6.5 Interrogation of system state

An approach, similar to the one presented in Chapter 5 has been used to interrogate the system state in order to quantify damage and remaining useful life under thermo mechanical load for the various lead free solder alloys. The grain size (g) data were taken for different packages for four different thermal-cycle intervals in the neighborhood of prognostication time of the electronic package. Equation 6.4 shows the set of four equations from four measured grain size values.

$$\begin{aligned} g_1^{4} &= g_0^{4} + a(N + \Delta N_1)^{b} \\ g_2^{4} &= g_0^{4} + a(N + \Delta N_2)^{b} \\ g_3^{4} &= g_0^{4} + a(N + \Delta N_3)^{b} \\ g_4^{4} &= g_0^{4} + a(N + \Delta N_4)^{b} \end{aligned} \tag{6.4}$$

where g_0, a, N and b are the unknowns and have been computed by inputting the measured grain size values (g_1, g_2, g_3, g_4) in to the Levenberg-Marquardt(LM) algorithm. The approach has been explained in detail in Chapter 5. For the problem being analyzed, it was found that the LM solution will tend to converge to local minima, because it does not explore the whole design space. Also, the rate of convergence of LM algorithm is sensitive to the starting location (or more precisely, the linearity around the starting location) [Ranganathan 2004]. In order to circumvent the problem, several initial guess values have been supplied within the trust-region. The solution has been identified as the one with minimum error. Bounded solution of the variables is based on accelerated test experimental data and acceptable ranges of solutions for the variables a, b, N and g_0 were developed. The variable upper bounds and lower bounds range for each variable, for each alloy system are shown in Table 6.4. The initial guess values have been varied uniformly in the range shown in the Table 6.4 to form four arrays, i.e. one for each variable. Variables g_0, a, N, b, were varied one at a time, while keeping the other three variables constant and were provided as input to the Levenberg-Marquardt algorithm. Schematic illustration of the operation is shown in Figure 6.14. For each row in the matrix, the algorithm has been solved. About 900,000 iterations have been solved and the answer has been written to a file. Amongst these iterations, the one with least error has been isolated for the final answer. This method has been was adopted to prognosticate in the vicinity of 250 & 500 cycles. Figure 6.14 to 6.19 shows the plot of minimization error vs. number of thermal cycles for SAC105, SAC305 and SAC0307 alloys for both 250 and 500 cycles prognostication. The computed values of g_0, a, N and b have been compared with the experimentally measured values and it has been shown in Table 6.5. The computed and measured grain size and cycles have been plotted in Figures 6.20 to 6.25. The experimental data and the model predictions show good correlation.

Alloy System	Constant 'a'	Constant 'b'	Initial Grain size 'g0'(μm)	N
SAC 105	0.0004 – 0.0013	1.10 – 1.20	0.92 – 1.02	0-1000
SAC 305	0.0005 – 0.0015	1.12 – 1.22	0.97 – 1.07	0-1000
SAC 0307	0.0001 – 0.001	1.10 – 1.20	0.85 – 0.95	0-1000

Table 6.4 - Variable Range for Phase-Growth Calculation under Thermal Cycling Load (based on Expt. data)

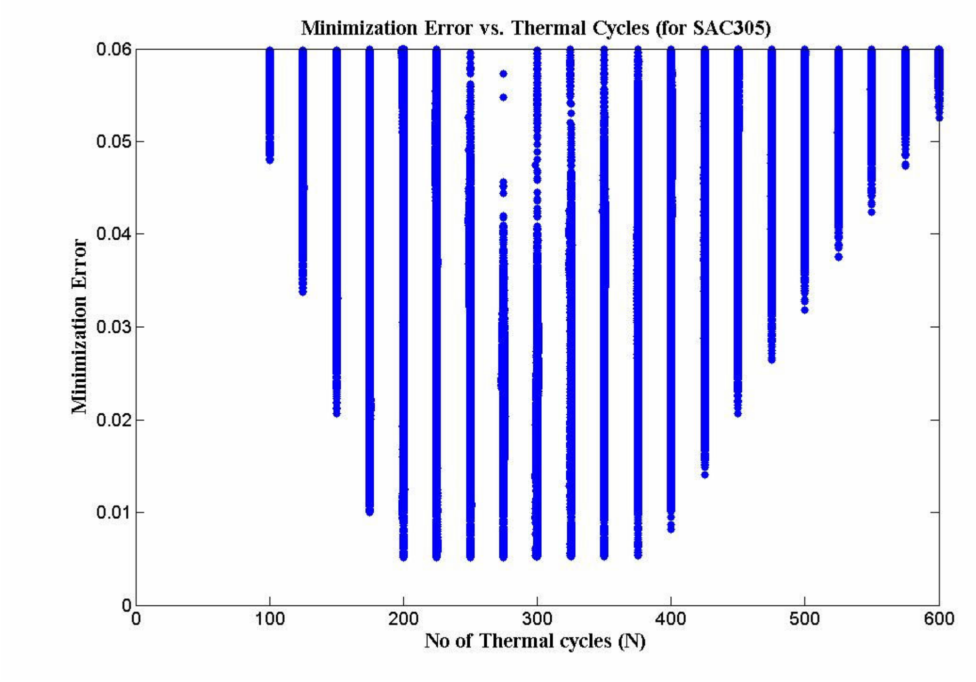

Figure 6.14 - Minimized error vs. N (Thermal Cycles) for SAC 105 Alloy system for prognostication at the vicinity of N=250 cycles

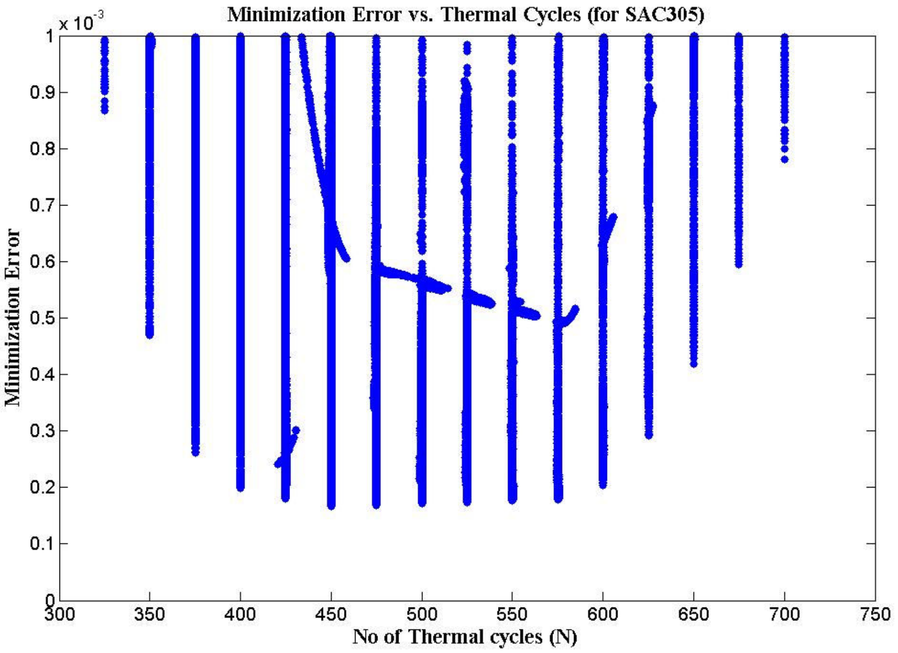

Figure 6.15 - Minimized error vs. N (Thermal Cycles) for SAC 105 Alloy system for prognostication at the vicinity of N=500 cycles

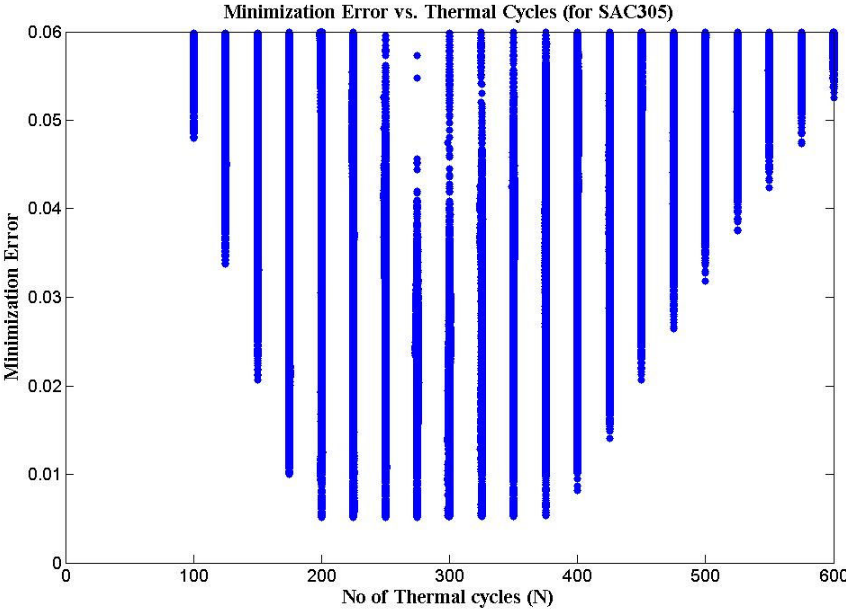

Figure 6.16 - Minimized error vs. N (Thermal Cycles) for SAC 305 Alloy system for prognostication at the vicinity of N=250 cycles

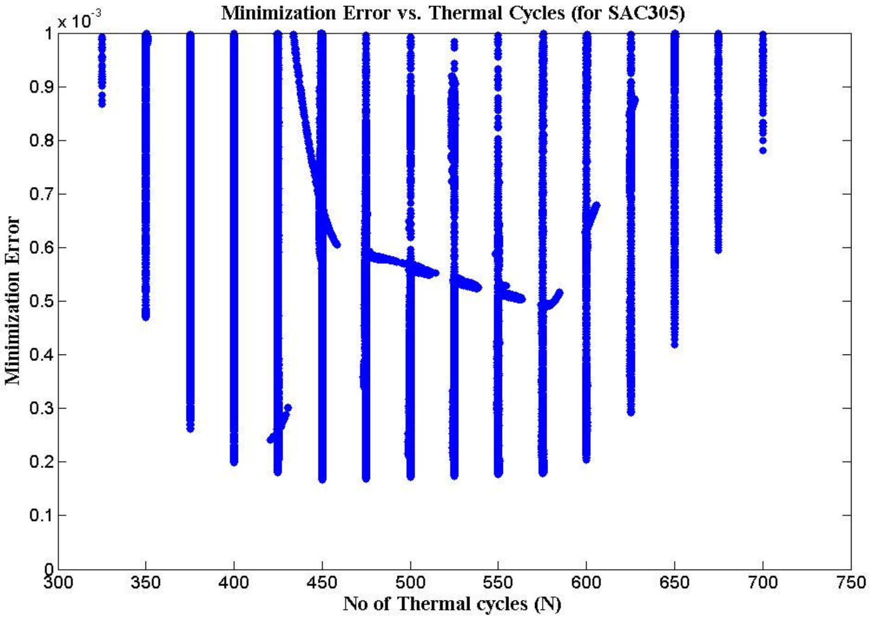

Figure 6.17 - Minimized error vs. N (Thermal Cycles) for SAC 305 Alloy system for prognostication at the vicinity of N=500 cycles

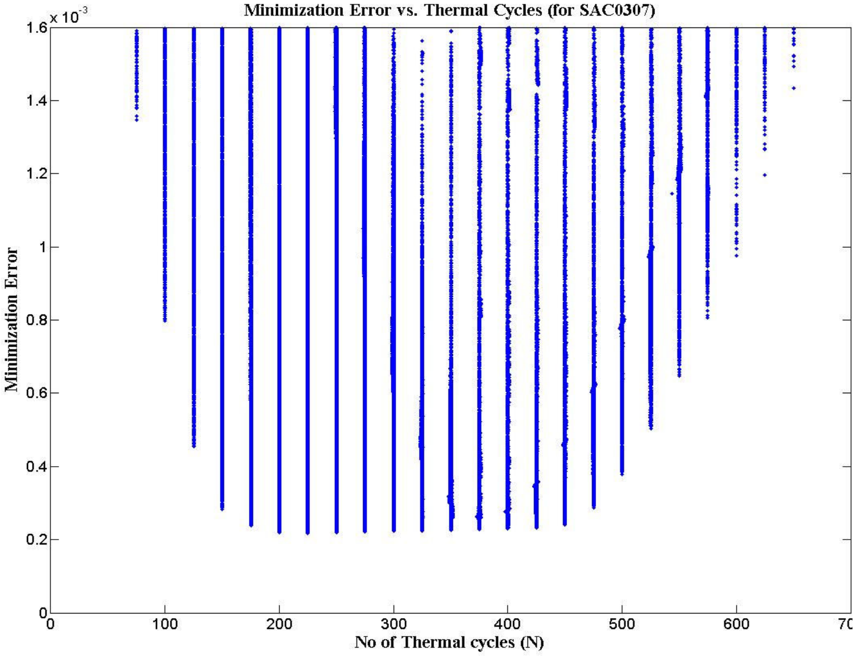

Figure 6.18 - Minimized error vs. N (Thermal Cycles) for SAC 0307 Alloy system for prognostication at the vicinity of N=250 cycles

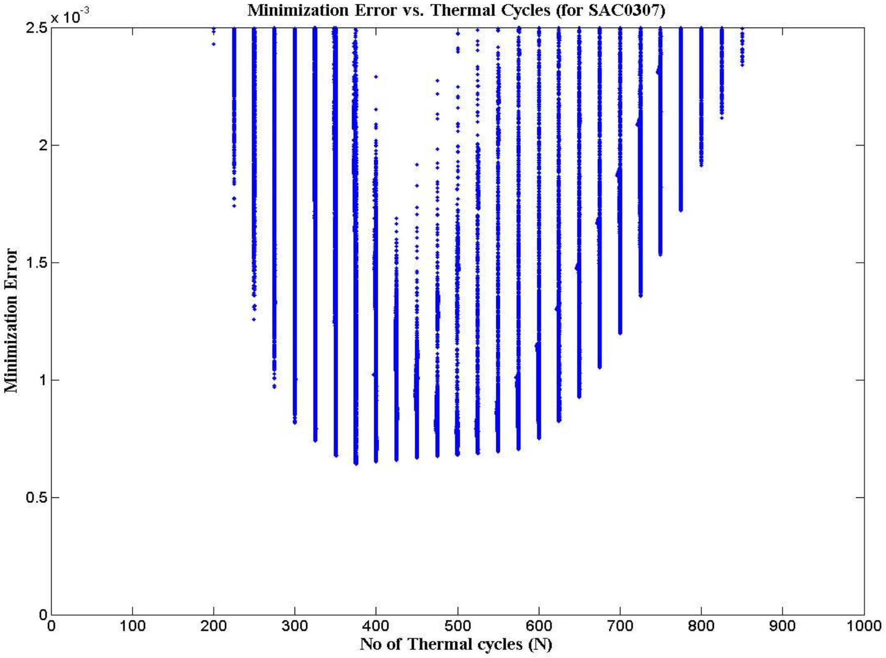

Figure 6.19 - Minimized error vs. N (Thermal Cycles) for SAC 0307 Alloy system for prognostication at the vicinity of N=500 cycles

Alloy System	Cycles ‘N’		Grain Size ‘g_0’ (in μm)		Constant ‘a’		Constant ‘b’	
	Expt. Data	LM Algo	Expt. Data	LM Algo	Expt. Data	LM Algo	Expt. Data	LM Algo
SAC 105	250	200	0.977535	1.0120	0.0008	0.00049	1.1349	1.1995
SAC 305	250	200	1.039139	1.0689	0.001	0.0013	1.1764	1.1383
SAC 0307	250	225	0.909137	0.9496	0.0007	0.0005	1.1264	1.20

Table 6.5 - Comparison of computed values of N, g_0, a & b from prognostication model (N=250) and experimental data

Alloy System	Cycles ‘N’		Grain Size ‘g_0’ (in μm)		Constant ‘a’		Constant ‘b’	
	Expt. Data	LM Algo	Expt. Data	LM Algo	Expt. Data	LM Algo	Expt. Data	LM Algo
SAC 105	500	425	0.977535	1.0155	0.0008	0.00051	1.1349	1.20
SAC 305	500	450	1.039139	1.0690	0.001	0.0008	1.1764	1.2197
SAC 0307	500	375	0.909137	0.9432	0.0007	0.00036	1.1264	1.20

Table 6.6 - Comparison of computed values of N, g_0, a & b from prognostication model (N=500) and experimental data

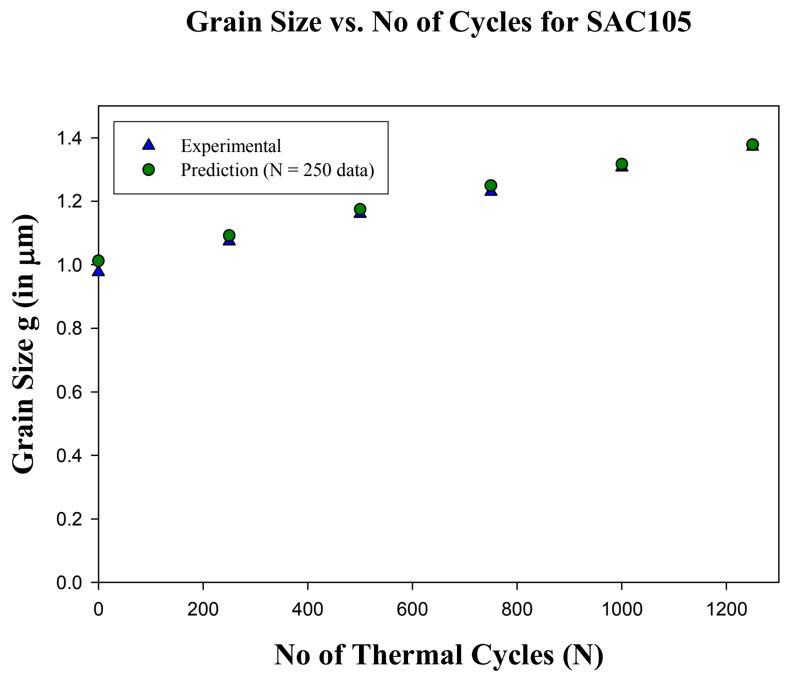

Figure 6.20 – Graphical comparison of computed grain size for prognostication model (N=250 cycle) with measured grain size for SAC 105

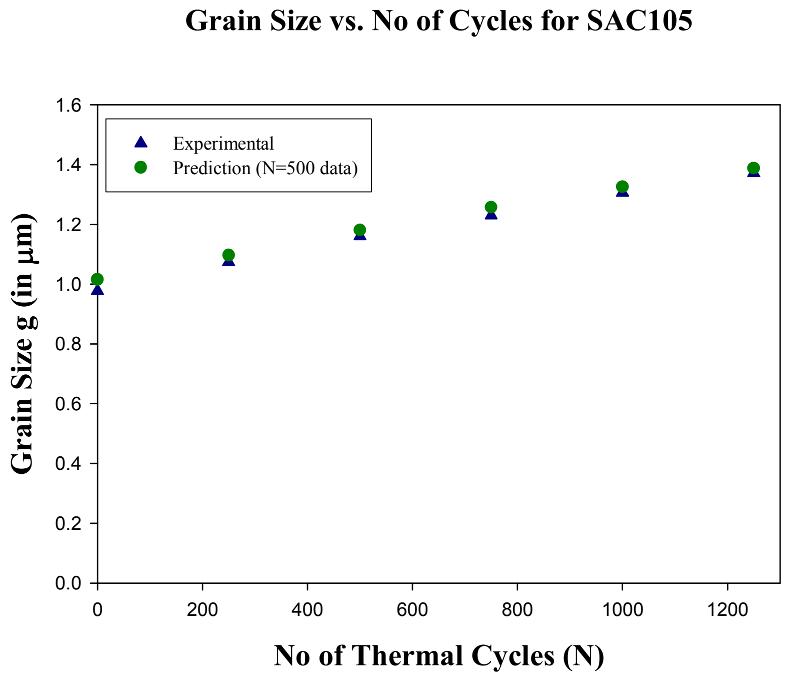

Figure 6.21 – Graphical comparison of computed grain size for prognostication model (N=500 cycle) with measured grain size for SAC 105

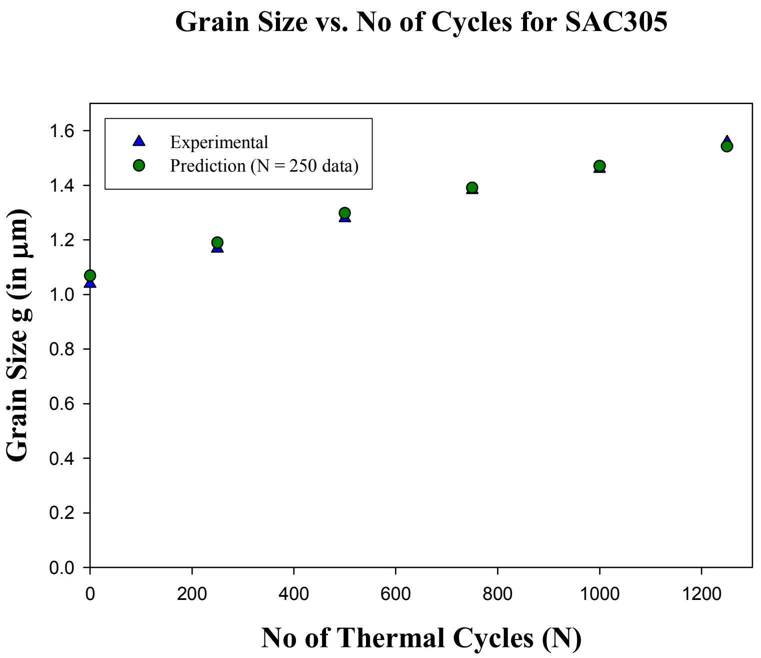

Figure 6.22 – Graphical comparison of computed grain size for prognostication model (N=250 cycle) with measured grain size for SAC 305

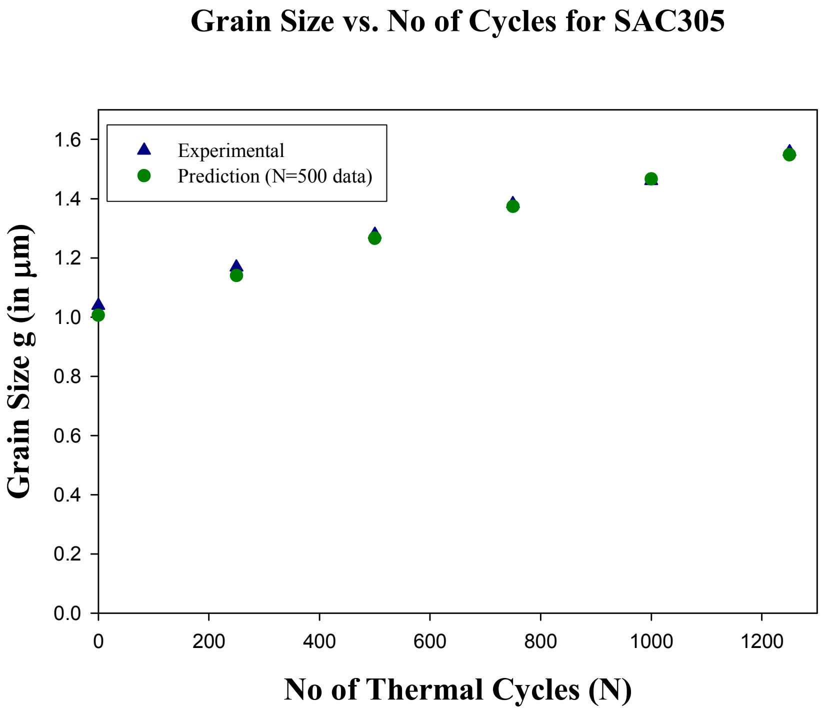

Figure 6.23 – Graphical comparison of computed grain size for prognostication model (N=500 cycle) with measured grain size for SAC 305

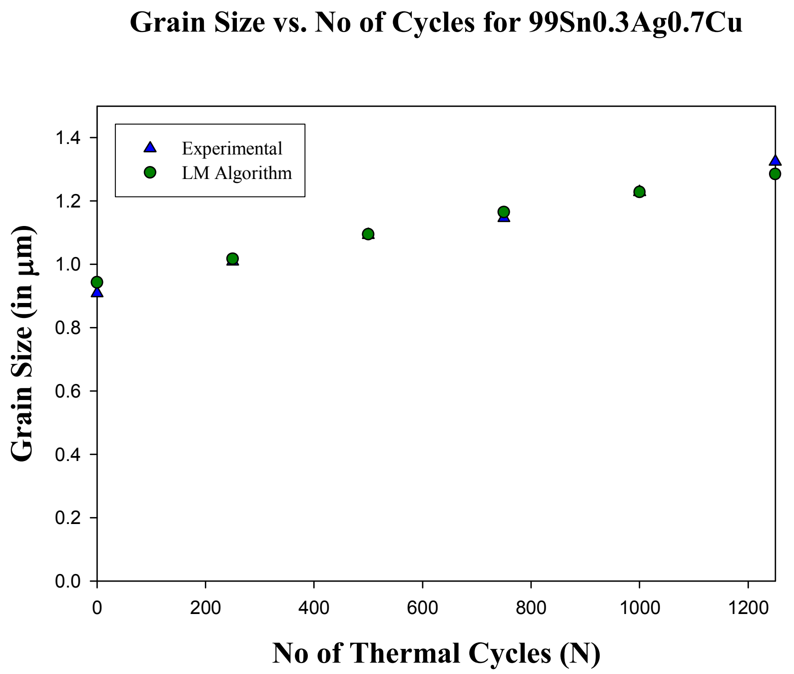

Figure 6.24 – Graphical comparison of computed grain size for prognostication model (N=250 cycle) with measured grain size for SAC 0307

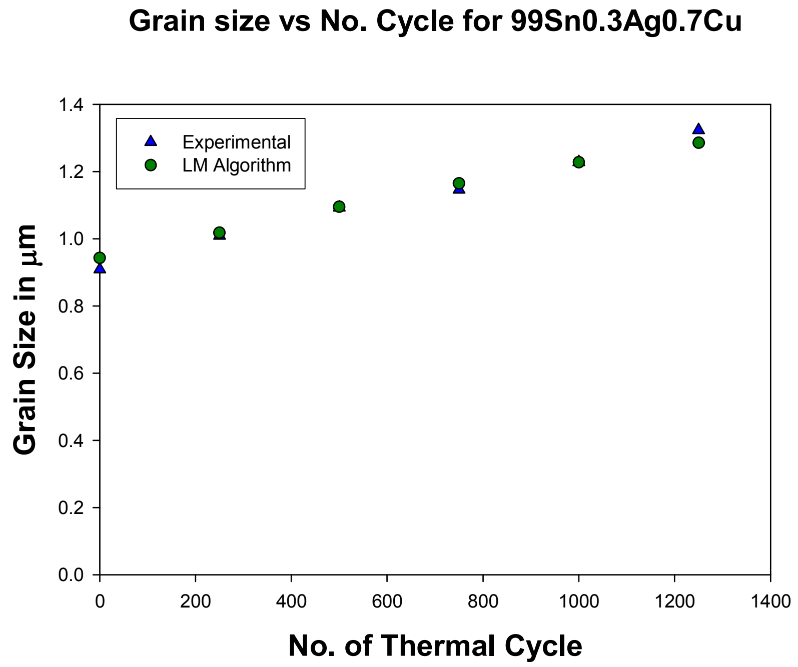

Figure 6.25 – Graphical comparison of computed grain size for prognostication model (N=500 cycle) with measured grain size for SAC 0307

6.6 Summary and Conclusion

The presented methodology for prognosticating the electronic packages has been leveraged to three different alloy systems like SAC 105, SAC 305 and SAC 0307. It has been found that computed values from the algorithm predicts well in comparison with the measured values. Methodology has been validated using various alloy systems, therefore, the algorithm developed to estimate the prior damage sounds promising. The developed technique can be implemented using the conditional monitoring devices. The comparison of residual life with the one obtained in the algorithm has not been discussed in this study as the reliability data is not available for these packages. The correlations indicate that the leading indicators based PHM technique can be used to interrogate the system state and thus estimate the Residual-Life of a component. The presented approach of computing residual life can be implemented prior to appearance of any macro-indicators of damage like cracks. The methodology presented using condition monitoring devices to find out the residual life is promising because these components experience the same environment as actual components.

CHAPTER 7

SUMMARY AND CONCLUSION

The reliability of Plastic Ball Grid Array, Flex-substrate Ball Grid Array, Tape-array Ball Grid Array and Chip-array Ball Grid Array with 95.5Sn4.0Ag0.5Cu solder alloy, under thermal cycling environment from -40°C to 125°C has been studied using experimental and finite-element approach. The study showed a good correlation between the experimental and finite-element method of calculating the fatigue life. The fatigue life obtained in this study has been used as a benchmark for life estimated in prognostication model. There is a difference in the fatigue life estimated by experiment and finite element models due to the approximations used in finite element models. The approximations are diagonal symmetry model to reduce the computation time, solder ball is assumed to be of same shape throughout, intermetallic compound has been ignored in the finite element model and the constitutive relationship is based on bulk solder material rather than the actual solder joint. Also, the non-linear least square method algorithm has been developed to estimate the material parameters to represent the Anand Viscoplastic model in ANSYS for solder using their material characterization data. As lead free solder alloys are still evolving, this algorithm can be used for any alloy system to estimate the material parameters using their material characterization data.

In this study, the reliability of various types of second level interconnections like Ceramic Ball Grid Array, Ceramic Ball Grid Array with Microperl SOL^{TM} (Polymer core solder ball), Ceramic Column Grid Array with copper reinforced columns, Plastic ball grid array packages with Microperl SOL using finite element models. Also comparison of the plastic work per volume and hysteresis loop for the maximum strained solder ball has been done for all the packages. It has been found that the copper reinforced column grid array has less plastic work per volume and a smaller area under the hysteresis loop as compared to other packages. Therefore, it has been concluded to be more reliable than the other packages. Amongst Plastic packages with Microperl and conventional solder ball, Microperl SOL showed significantly higher reliability than the normal solder ball architecture. But in ceramic packages, the difference is very small. However, the result could have been justified if we have the experimental results.

A damage pre-cursor based methodology for prognostication-of-electronics for assessment of residual-life has been developed and demonstrated under single stress of thermal cycling. The damage pre-cursors enable assessment of system damage-state significantly prior to appearance of any macro-indicators of damage. The phase growth rate has been identified as a valid proxy for determination of residual life in electronic structures. The theoretical basis for the selection of prognostic parameters has been justified based on particle growth induced by volume diffusion. A mathematical relationship has been developed between phase growth, derivatives of phase growth for interrogation of residual life and damage state. Prognostic parameters have been validated versus macro-indicators including cracks initiation, crack propagation rates and inelastic strain energy density for 95.5Sn4Ag0.5Cu solder.

A methodology has been presented to calculate the prior damage in electronics subjected to cyclic thermo-mechanical loads. The time duration for which the component has been deployed as well as the initial grain size has been estimated using Levenberg-Marquardt Algorithm with Trust Regions. The procedure has been demonstrated using leading-indicators of failure like phase growth. The presented approach uses the nonlinear least square method and gives an accurate method of estimating prior stress history of interrogating system-state before redeploying it in other missions. The computed results have been correlated with the experimental data for various packaging architectures. The residual life predicted using the model predictions correlate well with experimental data. The correlations indicate that the leading indicators based PHM technique can be used to interrogate the system state and thus estimate the Residual-Life of a component and also it can be implemented prior to appearance of any macro-indicators of damage like crack. The methodology presented using condition monitoring components to find out the residual life is promising because these components experience the same environment as actual component.

The presented PHM methodology has been leveraged to various lead-free solder alloy systems like SAC105, SAC305 and SAC0307. The damage proxy has been identified and their alloy compositions have been studied using EDX analysis. It is found that the phase growth rate increases with number of thermal cycles. The identified damage proxy and mathematical relationships developed in earlier studies for SAC405 has been justified for these lead-free solder alloy systems. Therefore, the mathematical relationships to compute the residual life using damage proxy can be applied to any of the lead-free alloy systems. Also, interrogating the system state using non-linear least square method has been applied to these alloy systems. It has been found that the algorithm predicts the prior-damage accurately for these alloy systems.

BIBLIOGRAPHY

Aguirre, G., and Movva, S., High reliability second level interconnects using polymer core BGAs, Proceedings of Electronic Component and Technology Conference, Vol, 2, pp. 1443-1448, 2004.

Allen, D., Probabilities Associated with a Built-in-Test System, Focus on False Alarms, Proceedings of AUTOTESTCON, IEEE Systems Readiness Technology Conference, pp. 643 – 645, September 22-25, 2003.

Amagai, M., Watanabe, M., Omiya, K. Kishimoto, & T., Shibuya, Mechanical Characterization of Sn-Ag Based Lead-free Solders, Microelectronics Reliability, vol 42, no 6, pp. 951-966, June 2002.

Anand, L., Constitutive Equation for the Rate-dependent Deformation of Metals at Elevated Temperatures, Transactions of ASME, Journal of Engineering Materials and Tech., Vol. 104, No 1, pp.12-17, 1982.

Anderson, N., and Wilcoxon, R., Framework for Prognostics of Electronic Systems, Proceedings of International Military and Aerospace/Avionics COTS Conference, Seattle, WA, Aug 3-5, 2004

Ardel, A. J., Acta Metallurgica, 16, pp.61-71, 1972

Bangs, E.R., and Beal, R.E., Wel.J.Res.Supp., 54, P.377, 1978

Barke, D., Chiu, W., K., Structural Health Monitoring in the Railway Industry: A Review, Structural Health Monitoring #4, pp. 81-93, 2005

Bartelo, J., Cain, S. R., Caleka, D., Darbha, K., Gosselin, T., Henderson, D.W., King, D., Knadle, K., Sarkhel, A., Thiel, G. and Woychik, C., Thermo mechanical fatigue behavior of selected lead-free solders, Proceedings IPC SMEMA Council APEX, 2001

Bradley, E., and Banerji, K., Effect of PCB Finish on the Reliability and Wettability of Ball Grid Array Packages, IEEE Transaction on Component Packaging and Manufacturing Technology Part B-Advanced Packaging, Vol. 19(2), pp.320-330, 1996.

Brown S.B., K.H. Kim & L., Anand, An Internal Variable Constitutive Model for Hot Working of Metals, International Journal of Plasticity, vol. 5,no. 2, pp. 95-130,1989

Callister, Jr., W., Materials Science and Engineering: An Introduction , Wiley, New York,1985

Chalo, P., and Blackshear, E., Reliability issues of BGA packages attached with lead-free solder, Proceedings InterPack01, The Pacific Rim/ASME International Electronic Packaging Technical Conference, Kauai, Hawaii, July 8-13, 2001

Chandramouli, R., Pateras, S., Testing systems on a chip, IEEE Spectrum, vol. 33, no. 11, pp. 42-47, Nov. 1996

Chang, J., Wang, L., Dirk, J., Xie, X., Finite Element Modeling Predicts the Effect of Voids on Thermal Shock Reliability and Thermal Resistance of Power Devices, Welding Journal, March 2006.

Chang, P., C., Flatau, A., and Liu, S., C., Review Paper: Health Monitoring of Civil Infrastructure, Structural Health Monitoring #2, pp. 257, 2003.

Cherian, G., Use of discrete Solder Columns to Mount LCCCs on Glass/Epoxy Printed Circuit Cards, Proceedings of International Electronics Packaging Conference, pp.701-710, 1984

Clifford, T., Final Report –Phase 1 T-Cycle Test, IP-Free Version, Lockheed Internal Document, July 25, 2004.

Coffin, Jr, L.F., Transactions of the ASME, Vol 76, pp.931,1954

Darveaux R. Solder Joint fatigue life model, ProcTMS, 1997

Darveaux, R., and Banerji, K., Constitutive Relations for Tin-Based Solder Joints, IEEE Trans-CPMT-A, Vol. 15, No. 6, pp.1013-1024, 1992.

Darveaux, R., Banerji, K., Mawer, A., and Dody, G., Reliability of Plastic Ball Grid Array Assembly, Ball Grid Array Technology, J.Lau, ed., McGraw-Hill, Inc. New York, pp.379-442, 1995

Darveaux, R., Effect of Simulation Methodology on Solder Joint Crack Growth Correlation, Proceedings of the 2000 Electronic Components and Technology Conference, pp.1048-1058, May 2000.

Dasgupta, A., Oyan, C., Barker, D., and Pecht, M., "Solder Creep-Fatigue Analysis by an Energy-Partitioning Approach," ASME Journal of Electronic Packaging, Vol 114, pp.152-160, June 1992

DeWolf, J., T., Robert, G., Lauzon, and Michael, P., Monitoring Bridge Performance, Structural Health Monitoring, pp. 129-138, 2002

Drees, R., and Young, N., Role of BIT in Support System Maintenance and Availability, IEEE A&E Systems Magazine, pp. 3-7, August 2004

Dutta I., Park, C., Choi, S., Creep and microstructural evolution in lead-free microelectronic solder joints, Proceedings of InterPACK '03, Paper Number IPACK2003-35209, Maui HI, July 6-11;2003, pp. 1-6, 2003

Dutta, I., A constitutive model for creep of lead-free solders undergoing strain-enhanced microstructural coarsening: a first report. J Electron Material;32(4):201-7, 2003

Dutta, I., A Constitutive Model for Creep of Lead-Free Solders Undergoing Strain-Enhanced Microstructural Coarsening: A First Report, Journal of Electronic Materials, Vol 32, No. 4, pp. 201-207, 2003a.

Dutta, I., Chen, T., Jadhav, S., Effect of Ag and Cu Concentrations on Creep of Sn-Based Solders, Proceeding of Interpack2007 July 8-12, Vancouver, British Columbia, Canada, 2007

Dutta, I., Impression creep testing and microstructurally adaptive creep modeling of lead free solder interconnects, TRC; 25-7, October 2004.

Dutta, I., Impression Creep Testing and Microstructurally Adaptive Creep Modeling of Lead Free Solder Interconnects, TRC, October 25-27, 2004.

Dutta, I., Park, C., and Choi, S., Creep and Microstructural Evolution in Lead-free Microelectronic Solder Joints, Proceedings of InterPACK '03, Paper Number IPACK2003-35209, pp. 1-6, Maui, HI, July 2003.

Engelmaier, W., Functional Cycling and Surface Mounting Attachment Reliability, ISHM Technical Monograph Series 6894-002, ISHM, pp. 87-114, 1984

Engelmaier, W., Solder attachment reliability, accelerated testing, and result evaluation, Solder Joint Reliability: Theory and Applications (Edited by J.H.Lau). Van Nostrand Reinhold, New York, 1991.

Englemaier, W., Reliability of leadfree solder joints revisited, Global SMT & Packaging, November 2003.

Fernando,G., F., Hameed, A., Winter, D., Tetlow, J., Leng, R., Barnes, G., Mays, G., Kister ,"Structural Integrity Monitoring of Concrete Structures via Optical Fiber Sensors: Sensor Protection Systems," Structural Health Monitoring, pp. 123-135, 2003.

Frear, DR., Microstructural evolution during thermo-mechanical fatigue of 62Sn36Pb2Ag and 60Sn40Pb solder joints, IEEE Trans Comp Hybrids Manufacturing Technolology;13(4):718-26, December 1990

Friswell, M., I., Penny, J., E.,T., Crack Modeling for Structural Health Monitoring, Structural Health Monitoring, Vol. 1, No. 2, pp. 139-148, 2002.

Galloway, J., Syed, A., Kang, W., Kim, J., Cannis, J., Ka, Y., Kin, S., Kin, T., Lee, G., and Ryu, S., Mechanical, Thermal and Electrical Analysis of a Compliant Interconnect, IEEE Transactions on Component and Packaging Technologies, pp. 1521-3331, 2005.

Gao, R., X., Suryavanshi, A., BIT for Intelligent System Design and Condition Monitoring, IEEE Transactions on Instrumentation and Measurement, Vol. 51, Issue: 5, pp. 1061-1067, October 2002.

Hassan, A., Agarwal, V. K., Nadeau-Dostie, B., Rajski, J., BIST of PCB Interconnects Using Boundary- Scan Architecture, IEEE Transactions on Computer-Aided Design, vol. 11, no. 10, pp. 1278-1288, October 1992

Henshall, G., Roesch, M., Troxel, K., Holder, H., Miremad, J., Manufacturability and Reliability Impacts of Alternate Pb-free BGA alloys, HP Global Engineering Services, June 2007.

Ingalls, E., M., Cole, M., Jozwiak, J., Milkovich, C., Stack, J., Improvement in Reliability with CCGA Column Density Increase to 1mm Pitch, Proceedings of Electronic Components and Technology Conferencce, pp. 1298-1304, 1998.

Islam, N., Investigations on Damage Mechanics and Life Prediction of fine pitch electronics in Harsh Environment, Dissertation, Mechanical Engineering Department Auburn University, August 2005

Jung, K., Conrad, H., Microstructure Coarsening During Static Annealing of 60Sn40Pb Solder Joints: I Stereology, Journal of Electronic Materials, Oct 2001.

Kim, Y., B., Noguchi, H., & Amagai, M., Vibration Fatigue Reliability of BGA-IC Package with Pb-Free Solder and Pb-Sn Solder, Proceedings of 53rd Electronic Components and Technology Conference, pp. 891-897, 2003

Kok, R., Furlong, C., Development and Characterization of MEMS Inertial System for Health Monitoring of structures, , Experimental Techniques, Vol. 29, No. 6, pp 46-53, November / December 2005.

Lall, P., Hande, M., Bhat, C., Islam, M., Suhling, J.C., Lee, J., Prognostics Health Monitoring (PHM) for Prior-Damage Assessment in Electronics Equipment under Thermo-Mechanical Loads, Electronic Components and Technology Conference, Reno, Nevada, pp. 1097-1111, 2007[a].

Lall, P., Hande, M., Bhat, C., Islam, M., Suhling, J.C., Lee, J., Feature Extraction and Damage-Precursors for Prognostication of Lead-Free Electronics, Microelectronics Reliability Journal, Volume 47, pp. 1907–1920, December 2007[b].

Lall, P., Hande, M., Bhat, C., Islam, M., Suhling, J.C., Lee, J., Feature Extraction and Damage-Precursors for Prognostication of Lead-Free Electronics, Electronic Components and Technology Conference, San Diego, California, pp. 718-727, 2006[a].

Lall, P., Islam, N., Rahim, K., Suhling, J. C., Prognostics and Health management of Electronic Packaging, IEEE Transactions on Components and Packaging Technologies, Vol. 29, No. 3, pp. 666-677, September 2006[b].

Lall, P., Islam, N., Suhling, J., Prognostication and Health Monitoring of Leaded and Lead Free Electronic and MEMS Packages in Harsh Environments, Proceedings of the 55th IEEE Electronic Components and Technology Conference, Orlando, FL, pp. 1305-1313, June 1-3, 2005.

Lall, P., Islam, M. N. , Singh, N., Suhling, J.C., Darveaux, R., Model for BGA and CSP Reliability in Automotive Underhood Applications, IEEE Transactions on Components and Packaging Technologies, Vol. 27, No. 3, pp. 585-593, September 2004[a].

Lall, P., Islam, N., Rahim, K., Suhling, J., Gale, S., Leading Indicators-of-Failure for Prognosis of Electronic and MEMS Packaging, Proceedings of the 54th IEEE Electronic Components and Technology Conference, Las Vegas, Nevada, pp. 1570-1578, June 1 - 4, 2004[b].

Langan, J., P., Solder Alternatives to HASL, Proceedings of the AESF Annual Technical Conference of American Electroplaters and Surface Finishers Society, pp.219-222, Orlando, FL, 1996.

Lifshitz, I.M., and Slyozov, V. V., Journal of Physical Chemistry Solids, 19, pp-35-50, 1961.

Lindley, T., R., BGA Solder Joint Reliability for Automotive Electronics, Proceedings of the 1995 International Conference on Multichip Modules, pp.126-133, Denver, CO, April 19-21, 1995.

Lourakis, M., A Brief Description of the Levenberg-Marquardt Algorithm Implement by levmar, Institute of Computer Science, Foundation for Research and Technology, 2005.

Ma, H., Characterization of Lead-free Solders for Electronic Packaging, PhD Dissertation, Electrical and Computer Engineering Department, Auburn University, May 2007.

Madsen, K., Nielsen, H.,B., Tingleff, O., Methods for Non-linear Least Squares Problems, Technical University of Denmark, 2004.

Master, R., N., Ceramic Column Grid Array for Flip Chip Applications, Proceedings 45th Electronic Components and Technology Conference, pp.925-929, 1995.

Mawer, A., Vo, N., Johnson, Z., and Lindsey, W., Board-Level Characterization of 1.0 and 1.27mm Pitch BGA for Automotive Under-Hood Applications, Proceedings of the 1999 Electronic Component and Technology Conference, pp.118-124, Sandieago, CA, June 1-4-1999.

Mishra, S., and Pecht, M., In-situ Sensors for Product Reliability Monitoring, Proceedings of SPIE, Vol. 4755, pp. 10-19, 2002.

Morris Jr., J., W., D., Tribula, T., S., E., Summers and D., Grivas, The Role of Microstructure in Thermal Fatigue Pb-Sn Solder Joint, Solder Joint Reliability; Theory and Applications, D.Lau, H. John, and R. Van Nostrand, Eds, New York: Van Nostrand, ch. 7, 1991.

Morris, J. W., Song, H.G., Hua, Fay., Creep Properties of Sn Rich Solder Joints, Proceedings of the 2003 Electronic Components and Technology Conference, New Orleans, Louisiana, pp 54-57., 2003.

Morrow, J., Cyclic plastic strain energy and fatigue of metals, internal friction, damping and cyclic plasticity, ASTM STP 378, p 73, 1965.

Morrow, J., Fatigue properties of metals, Division 4 of the SAE iron and steel technical committee, 1964.

Nielsen, H., B., Damping Parameter in Marquardt's Method. Technical Report IMM-REP-1999-05, Technical University of Denmark, 1999.

Pang, H., L., J., Patrick, T., H., Low, B., S., Xiong, Lead-free 95.5Sn3.8Ag0.7Cu Solder Joint Reliability Analysis For Micro-BGA Assembly, IEEE Inter Society Conference on Thermal Performance, pp. 131-135, 2000.

Pang, J., H., L., Kwang, Hong Tan, Xunqing, Shi. And Z., P., Wang Thermal Cycling Aging Effect on Microstructural and Mechanical Properties of a Single PBGA Solder Joint Specimen, IEEE Transaction on Components and Packaging Technologies, Vol. 24, No. 1, March 2001.

Pang, J., Xiong, B., S., Neo, C., Zhang, X., R., Lo, T., H., Bulk Solder and Solder Joint Properties for Lead Free 95.5Sn3.8Ag0.7Cu Solder Alloy, Proceedings of 53rd Electronic Components and Technology Conference, pp.673-679, New Orleans, LA, pp. 28-30, May 2003.

Paris, P., C., and Erdogan, F., A Critical Analysis of Crack Propagation Laws, Journal of Basic Engineering, Vol. 85, pp 528-534, 1960.

Paris, P., C., Gomez, M.P., and Anderson, W.P., A Rational Analytic Theory of Fatigue, The Trend in Engineering, Vol. 13, pp. 9-14,1961.

Prasad, R., Surface Mount Technology: Principles and Practice, p.804, 1997.

Ramakrishnan, A., Syrus, T., and M. Pecht, Electronic Hardware Reliability, Avionics Handbook, pp. 22-1 to 22-21, CRC Press, Boca Raton, Florida, December 2000.

Ranganathan, A., The Levenberg Marquardt Algorithm, College of Computing, Georgia Tech Website, June 2004.

Ridout, S., and Bailey, C., Review of methods to predict solder joint reliability under thermo-mechanical cycling, Fatigue Fracture Engineering Material Structure, Vol 30, pp. 400-412, July 2006.

Rodgers, B., Flood, B., Punch, J.,Waldron, F., Experimental Determination and Finite Element Model Validation of the Anand Viscoplasticity Model Constants for SnAgCu, IEEE 6th International Conference on Thermal, Mechanical and Multiphysics Simulation and Experiments in Micro-Electronics and Micro-Systems, pp. 490-496, August 2005.

Rosenthal, D., and Wadell, B., Predicting and Eliminating Built-in Test False Alarms, IEEE Transactions on Reliability, Vol. 39, No 4, pp. 500-505, October 1990.

Sayama, T., Takayanagi, T., and Mori, T., Analysis of Grain Growth Process in Sn/Pb Eutectic Solder Joint, EEP-Vol. 26-1, Advances in Electronic Packaging-1999, Volume 1, ASME, 1999.

Sayama, T., Takayanagi, T., Nagai, Y., Mori, T., and Yu, Q., Evaluation of Microstructural Evolution and Thermal fatigue Crack Initiation in Sn-Ag-Cu Solder Joints, Proceedings of InterPACK '03, Paper Number IPACK2003-35096, pp. 1-8, Maui, HI, July 2003.

Schubert, A., Dudek, R., Auerswald, E., Gollhardt, A., Michel, B., Reichi, H., Fatigue Life Models for SnAgCu and SnPb Solder Joints Evaluated by Experiments and Simulation, Proceedings of the 2003 Electronic Components and Technology Conference, New Orleans, pp 603-610, 2003.

Sekhar, A., S., Identification of a Crack in a Rotor System using a Model-based Wavelet Approach, Structural Health Monitoring, pp. 293-308, 2003.

Sekisui, Inc., Technical Data, Area Array Connection Material Microperl SOL, August 2005.

Senkov, O.N., and Myshlyaev, M.M., Acta Metallurgica, 34, pp. 97-106, 1986.

Sinha, A., Issacs, P., Tofil, T., Mechanical Reliability of CCGA Solder Joints, Proceedings of SMTA International, April 1997.

Speight, M.V., Acta Metallurgica, 16,pp.133-135, 1968.

Syed, A., R., Creep Crack Growth Prediction of Solder Joints During Temperature Cycling – An Engineering Approach, Transactions of the ASME, Vol. 117, pp. 116-122, June 1995.

Syed, A., R., Thermal Fatigue Reliability Enhancement of Plastic Ball Grid Array(PBGA) Packages, Proceedings of the 1996 Electronic Components and Technology Conference, pp.1211-1216, Orlando, FL, May 28-31, 1996.

Thompson, T., Carrasco, A., and Mawer, A., Reliability Assessment of a Thin (Flex) BGA Using Polyimide Tape Substrate, Proceedings of the IEEE/CPMT International Manufacturing Technology (IEMT) Symposium, pp.207-213, 1999.

Tribula, D.G., Grivas, D., Frear, D., and Morris, J., Journal of Electronic Packaging, 111, pp. 83-89, 1989.

Vandevelde, B., Beyne, E., Van Puymbroeck, J., V., and Heerman, M., Thermal fatigue analysis of the flip-chip assembly on the polymer stud grid array(PSGA) package, Proceedings of Electronic Component and Technology Conference, pp. 823-829, 1999.

Vichare, N.,M., Pecht, M.,G., Prognostics and Health Management of Electronics, IEEE Transaction on Component and Packaging Technologies,vol 29 no.1,March 2006.

Wiese, S., Microstructural Dependendence of Constitutive Properties of Eutectic SnAg and SnAgCu solders, Proceedings of the 2003 Electronic Components and Technology Conference, New Orleans, Louisiana, pp.197-206, 2003.

Williams, T., W., Parker, K. P., Design for Testability - A Survey, Proceedings of the IEEE, January 1983.

Winslow, T., R., Converting Ball Grid Array Components to Column Grid Array, Military, Aerospace, Space and Homeland Security: Packaging Issues and Application Workshop, 2005.

Wolverton, A., Brazing and Soldering, 13, pp. 33, 1987.

Yee, S., and Ladhar, H., Influence of Pad Geometry on Ceramic Ball Grid Array Solder Joint Reliability, Proceedings of the IEEE/CPMT International Electronic Manufacturing (IEMT) Symposium, pp.267-273, 1996.

Yoon, S., W., and Moon J., T., CSP board level reliability testing of Pb-free Sn-Ag-X (X=Cu, In) and polymer-core solder ball, Proceedings of Technical Program Pan Pacific Microelectronics Symposium, pp. 29-37, 2001.

Zahn, A., B., "Impact of Ball Via Configuration on Solder Joint Reliability in Tape Based Chip-Scale Packages", 52nd Proceedings of the 2002 Electronic Components and Technology Conference, pp. 1475- 1483, May 2002.

Zahn, B, Solder Joint Fatigue life model methodology for 63Sn37Pb and 95.5Sn4Ag0.5Cu materials, Proceedings of the electronics components and technology conference. New Orleans, Louisiana, pp. 83-94, 2003.

Zhang, Q., & Dasgupta, A., Constitutive Properties and Durability of Lead-Free Solders, Lead-Free Electronics, S. Ganesan & M.Pecht, eds., CALCE EPSC Press, Maryland, pp. 65-137, 2003.

Zhang, Q., Viscoplastic Constitutive Properties and Energy-Partioning Model of Lead-Free Sn3.9Ag0.6Cu Solder Alloy, Proceedings of the 2003 Electronic Components and Technology Conference, New Orleans, Louisiana, pp. 1862-1868, 2003.

Zorian, Y., A Structured Testability Approach for Multi Chip Boards Based on BIST and Boundary Scan, IEEE Transactions on Components, Packaging, and Manufacturing Technology-Part B, vol. 17, no. 3, pp. 283-290, August 1994.

APPENDIX

LIST OF SYMBOLS

β	Weibull Slope
$\acute{\eta}$	Characteristic Life
λ	Damping Parameter in LM Algorithm
ξ	Multiplier of Stress
$\hat{s}$	Coefficient of Deformation Resistance Saturation Value (MPa)
$\acute{\varepsilon}_p$	Inelastic strain rate
σ^*	Saturation Stress
Θ	Temperature
σ_0	Initial stress value
σ	Inelastic Stress
ε_p	Plastic Strain
α_w	Characteristic Life
σ_h	Local hydrostatic state of stress
ε	Instantaneous inelastic strain rate
γ	The free energy per unit area of the phase boundary,
Ω	Molar volume of the particle phase,
δ	Phase boundary width

τ_c	Time constant associated with the decay of a vacancy formation
γ	Average shear-strain rate
$N_{1\%}$	Number of cycles necessary to cause 1% of the parts
N	Number of thermal cycle
So	Initial Value of Deformation Resistance (MPa)
Q/R	Activation Energy / Boltzmann's Constant(1/K)
A	Pre-Exponential Factor(1/sec)
m	Strain Rate Sensitivity of Stress
ho	Hardening Constant (MPa)
n	Strain Rate Sensitivity of Saturation Value
a	Strain Rate Sensitivity of Hardening
S	Deformation resistance
ΔW_{avg}	Average In elastic strain energy density
ΔW_k	Plastic work per volume for each element
V_k	Volume of each element.
K_1	Fatigue Life Prediction constant
K_2	Fatigue Life Prediction constant
K_3	Fatigue Life Prediction constant
K_4	Fatigue Life Prediction constant
a	Solder joint diameter at the interface
N_0	Crack Initiation Life
da/dN	Crack Growth Rate

g	Grain size at time t
g_0	Initial grain size
K	Time-independent constants
n	Time-independent constants
r	Average particle radius
r_0	Initial radius of an average particle
B_1	Parameter related to the volume fraction of the particles,
C_0	Equilibrium solute concentration near the phase boundary
D_b	Coefficient of solute diffusion in the phase boundary
R	Gas constant
T	Absolute temperature
t	Time
B	Phase geometry parameter
$Q_{f,\, v}$	Enthalpy of formation of a vacancy
N	Constant that scales the vacancy concentration to ε
D_{sol}	Effective solute diffusivity in the matrix
D^{0}_{sol}	The associated frequency factor
Q_{sol}	Activation energy respectively
$T_{max} - T_{min}$	Temperature range of the cycle
$\mathrm{T}_{\mathrm{min}}$	Minimum Temperature
$\mathrm{T}_{\mathrm{max}}$	Maximum Temperature
S	Phase Growth Parameter

dS/dN	Rate of Change of Phase Growth Parameter
N_f	The number of Cycles to Failure
J	The Jacobian of the matrix
CTE	Coefficient of Thermal Expansion
BT	Bismaleimide Triazine
PCB	Printed Circuit Board
PBGA	Plastic Ball Grid Array
CBGA	Ceramic Ball Grid Array
CCGA	Ceramic Column Grid Array
SMT	Surface Mount Technology
PTH	Plated Through Hole
PHM	Prognostics Health Management
BIST	Built In Self Test
LCCC	Leadless Ceramic Chip Carriers
SOIC	Small Outline Integrated Circuits
HASL	Hot Air Solder Leveling
MPS	Metalized polymer spheres
PSGA	Polymer Stud Grid Array
RL	Residual Life
SEM	Scanning Electron Microscope
TABGA	Tape Array Ball Grid Array
CABGA	Chip-array Ball Grid Array

FlexBGA	Flex substrate Ball Grid Array
HM	Health Monitoring
RUL	Remaining Useful Life
NSMD	Non-Solder Mask Defined
SMD	Solder Mask Defined
EDX	Energy Dispersive X-rays